Assessment of the left ventricular systolic and diastolic function in rats using electrocardiogram-gated cardiac positron emission tomography

-

Bestimmung der linksventrikulären systolischen und diastolischen Funktion in Ratten durch Elektrokardiogramm-getriggerte kardiale Positronen-Emissions-Tomographie

Doctoral thesis for a medical doctoral degree

at the Graduate School of Life Sciences,

Julius-Maximilians-Universität Würzburg,

Section Intergrative Biology

submitted by

Christoph Marcel Eißler

from

Reutlingen

Würzburg **2020**

Submitted on:

……..……..

Office stamp

Members of the Thesis Committee:

Chairperson: **Prof. Dr. med. M. Prelog**

Primary Supervisor: **Prof. Dr. med. A. Buck**

Supervisor (Second): **Prof. Dr. med. T. Higuchi**

Supervisor (Third): **Prof. Dr. med. C. Lapa**

Supervisor (Fourth): **Prof. Dr. med. S. Störk**

Date of Public Defence: ……..……

Date of Receipt of Certificates: …….

Table of Contents

1 Introduction

Heart failure (HF) is a serious medical condition in Germany since it is still the leading cause of in-hospital deaths and the second leading cause for hospitalization [2]. Even if the treatment for HF has improved in the last years, the HF-related in-hospital deaths remained consistently high [2]. However, patients with symptomatic HF often present themselves with a normal left ventricular ejection fraction (LVEF) and symptoms and clinical signs mainly due to mechanical abnormalities of the myocardial tissue during diastole, defined as diastolic dysfunction (DD) [3-5]. Therefore, evaluation of the diastolic and the systolic function yields important data on the diagnosis of both systolic heart failure (SHF) and diastolic heart failure (DHF).

An early detection of a DD is crucial to identify risk patients and to improve their outcomes since DD is known as an independent risk factor for the occurrence of HF and cardiac death [6]. Epidemiological studies have revealed the importance of DD since it is quite prevalent and is predictive for all-cause mortality [6-8].

Despite the good availability of the established techniques for the assessment of DD, they provide barely information about the underlying pathophysiological conditions. In general, left ventricular (LV) function can be assessed by diverse modalities, including echography, magnetic resonance imaging (MRI) or single photon emission computed tomography (SPECT). Primarily, transthoracic echocardiography (TTE) is a widely available non-invasive technique, used for the evaluation of heart function in the clinical setup.

The introduction of the electrocardiogram (ECG)-gated positron emission tomography (PET) for the evaluation of LV function provides the advantage of a simultaneous evaluation of the dynamic performance and depending on the tracer, the assessment of myocardial perfusion, glucose metabolism or fatty-acid metabolism in clinical and preclinical studies. Although the PET offers the opportunity to assess biochemical processes on a subcellular level and to evaluate the cardiac function simultaneously, only few studies have investigated the utility of ECG-gated PET in the assessment of LV diastolic function parameters. However, the results of investigations of the LV volumes and ejection fraction (EF) in humans and animals using the ECG-gated Fluorine-18-2'-Fluoro-2'-deoxy-D-glucose (^{18}F-FDG) PET has shown good correlation with the results of MRI studies [9, 10]. But since the determination of entire LV function by using ECG-gated PET is not well established, the relation between

myocardial metabolism and/or perfusion and the cardiac function, had to be evaluated by different techniques (PET and ECHO or MRI). Therefore, it would be desirable to determine the LV systolic and diastolic function directly from the ECG-gated PET. Especially in the preclinical setup the evaluation of the LV function in different animal models is crucial to gain new insights into the pathophysiology of cardiac diseases and to monitor the effect of new treatment approaches.

Since the occurrence of DD is also high in diabetic subjects, which develop DD as an early sign of a special form of cardiomyopathy (diabetic cardiomyopathy), a diabetic rat model has been used to investigate the ability of the ECG-gated PET in the assessment of the LV systolic and diastolic function [11].

In conclusion, the aim of this thesis is to investigate the feasibility of the ECG-gated ^{18}F-FDG PET in the assessment of the LV function including diastolic parameters in a genetic rat model of type 2 diabetes mellitus (T2DM) and healthy control rats.

1.1 Electrocardiogram-gated cardiac ^{18}F-FDG positron emission tomography

The PET is a well-established non-invasive molecular imaging modality that enables the assessment of the in-vivo distribution of different imaging agents, which are labelled with positron-emitting radionuclides. This imaging modality enables among other things the investigation of tissue metabolism, protein expression and blood flow in both human patients and experimental animal models [12-18].

1.1.1 Principles of PET imaging

The PET enables the generation of tomographic images of the radionuclide-labelled tracer distribution, which has been injected in the object of study. The radionuclides, which are used for the PET are all positron emitters.

1.1.1.1 Positron decay

The positron is an elementary particle that is defined as antimatter. Since it is the antiparticle of the electron, they both have an identical mass and spin but an opposite electrical charge [19]. Positrons may be generated by positron decay of an unstable proton-rich radionuclide. Positrons are ejected from the nucleus with a kinetic energy which is characteristic for each radionuclide. Once emitted, the positron rapidly loses its kinetic energy due to electrostatic interactions with protons and electrons of the surrounding tissue. As the positron slows, it undergoes a special process with a nearby electron, which is known as positron annihilation. During this process the mass of the electron and the positron are converted into energy in form of a pair of gamma ray photons. Each of the two simultaneously generated photons has the energy of 511 kiloelectron volts (keV) (energy equivalent to the positron/electron mass). Due to the conservation of energy and momentum, the photos are emitted in opposite directions (see figure 1) [20, 21].

Figure 1 Positron Emission.

This scheme was generated using the program Powerpoint 2016 (Microsoft Office 365 ProPlus) (according to Kinehan P. et al. 2006 [1]). It shows the simplified four steps in the process of positron emission.

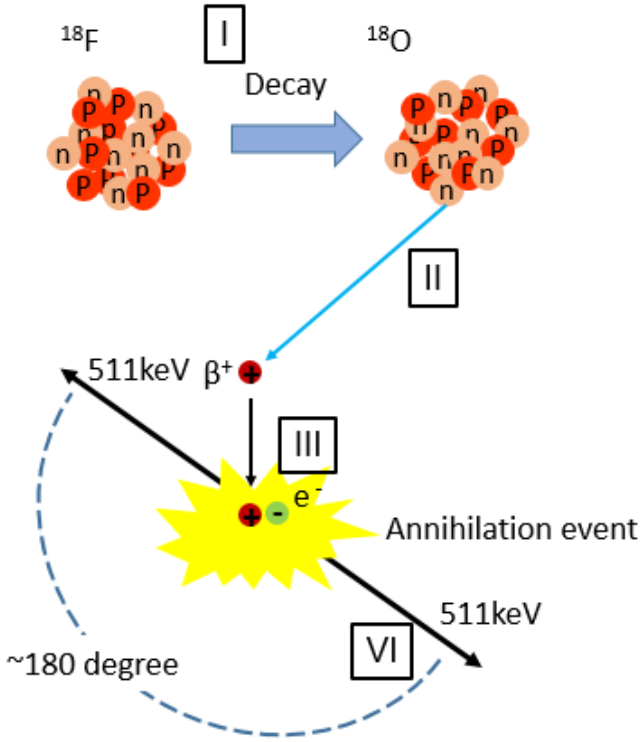

I.) An unstable proton-rich atomic nucleus (in this case 18-fluoride) decays to a stable form (in this case 18-oxygen) by converting a proton into a neutron and a positron.

II.) Because of its positive charge the positron is ejected from the positive charged nuclei with a specific kinetic energy.

III.) If the kinetic energy falls, the positron annihilates with a nearby electron.

IV.) The mass of the electron and proton is converted into two 511 keV photons (gamma rays), which travel in opposite direction [20].

1.1.1.2 Detection of annihilation events

The annihilation photons are emitted in a relative angle of nearly 180 degrees and travel at the speed of light. The PET scanner can detect these gamma rays, which reach the surrounding detectors nearly at the same time. The line that can be drawn between any two detectors of the PET scanner, which register a photon, is referred to as line of response (LOR) [20]. The PET detector blocks are usually arranged in a cylinder formed out of discrete rings, with a certain ring diameter and an axial field of view (FOV). Through this 360-degree arrangement of the detectors, the scanner can detect paired scintillation events referred to as “coincidence events”.

Figure 2 Schematic PET scanner setup.

This figure was generated using the program Powerpoint 2016 (Microsoft Office 365 ProPlus).

The blue ring represents the circular ordered detector units of the PET scanner and the dark grey prism the carrying system of the scanner. The light grey ellipsoid stands for an object of study (for example a patient or animal). The yellow ellipsoid represents a tissue which accumulates the radionuclide marked substance (for example the heart or a tumour mass). The red small explosions symbols stand for annihilation events, the origin of the two gamma rays, which are emitted in the direction of the black arrows and detected by the PET detectors. The black arrows show the LOR which connect the paired detectors.

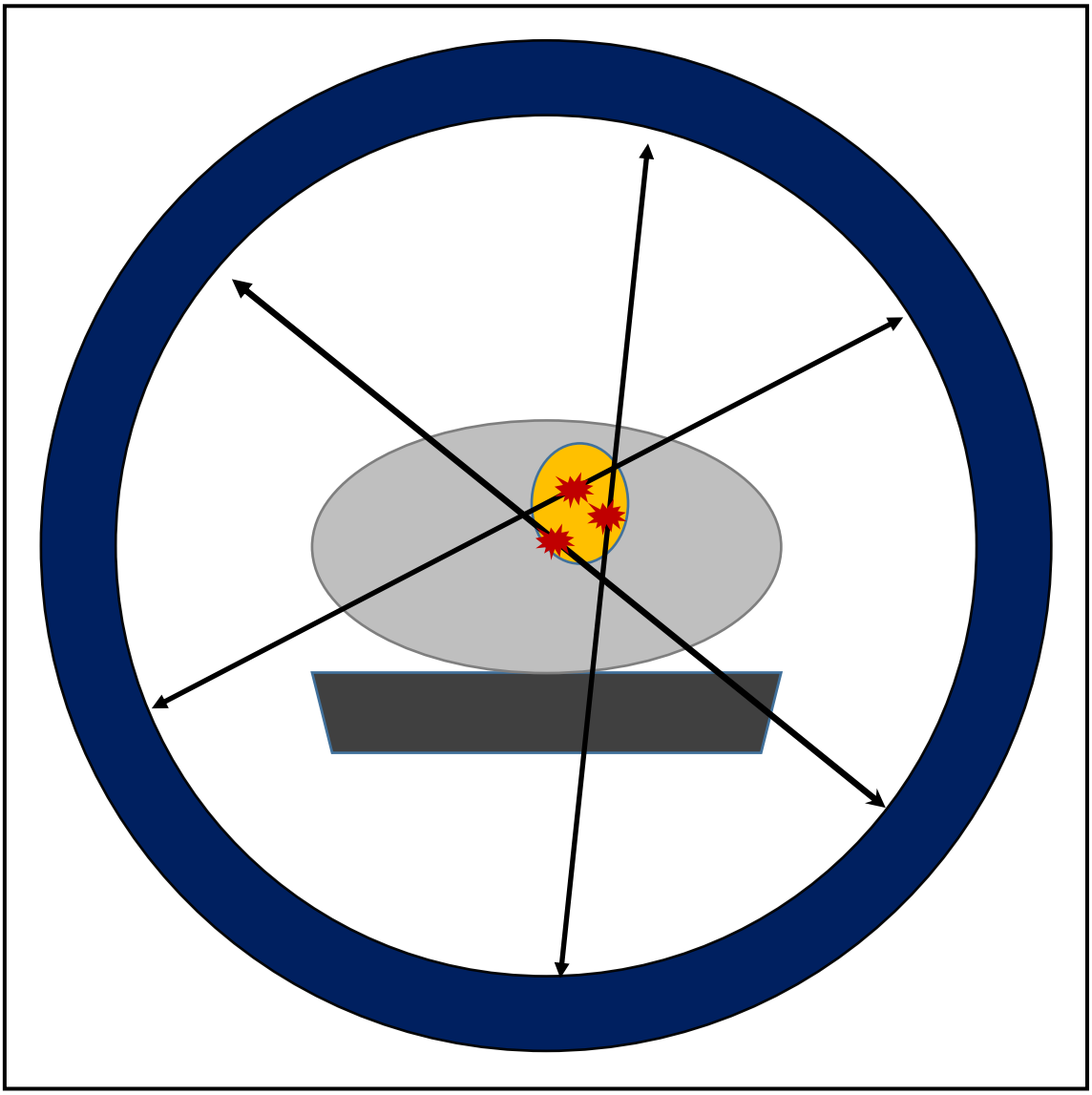

1.1.1.3 PET detectors and scanner design

In the past 30 years, different materials have been introduced to create an optimal detector for the detection of the 511 keV photons. The most often used detector material are inorganic scintillators [21, 22]. After a 511 keV photon has hit the detector-crystal, it causes the formation of photoelectric electrons, which further leads to electrons in excited states located in the crystal lattice. Through the return of the excited electrons to lower energy levels, a part of their energy is emitted in form of a flash of visible light. This flash of light can be detected by photon detectors such as a photomultiplier tube (PMT), which are linked to the detector crystal. The PMT convert the light signals into electronic pulse signals, which in turn are processed by further electronics. The signal of the PMT is proportional to the stored energy in the crystals. If the detected energies are outside of the range for 511 keV photons, the scintillation event is rejected. This setup helps to minimize the number of scatter events [20].

To detected simultaneously events, the signals from the PMT are processed by coincidence electronics, which sample the information of all detector units and further determine the time of every single detected event of each detector. Subsequently, the detected timing pulses are compared. Two events are considered to be simultaneously if their timing pulse overlap. A true coincident event is present if the two detected events are initiated by the two 511 keV gamma rays of the same annihilation event. When two 511 keV gamma rays are originated from different annihilation events, but both reach the detectors in the coincident timing window there are also registered as coincident event, even if they are randomly coincident [20, 21].

1.1.1.4 Data correction

To improve the quantitative accuracy of PET imaging, a correction for many different factors is needed, including scatter events, body attenuation, random events and dead time loss of which the most important ones are described briefly in this section.

A random correction is required, since the PET scanner records all events which occur at the same time within the timing resolution of the detectors.

Therefore, the prompt events include true events and background events (scatter and random events), which do not represent the real distribution of the injected activity [23-26]. Different methods have been introduced for correction of the random events of which the use of an additional coincident technique with a delayed time window is the most common one [27].

Since a positron annihilation event can only be detected if the two emitted 511 keV gamma rays hit the detectors simultaneously and their energies are entirely absorbed, a true coincident event is not registered if one gamma ray is absorbed or scattered by surrounding tissue [21]. Such loss of counts is depending on the habitudes of the surrounding tissue (body). To measure and correct the body attenuation an external gamma ray point source (for example gallium-68 or cesium-137), which is integrated in the PET scanner, rotates around the body and generates a transmission shadow profile of the object of study [28]. During the image reconstruction, the emission data and the according attenuation data are combined, resulting in images which are corrected for the body attenuation.

After the correction for random events and body attenuation, the last data do still contain scatter events. Several algorithms and methods for scatter correction have be introduced [25, 26, 29, 30]. One way to minimize the scatter events, is to use a transmission attenuation map in combination with an initial estimated filtered back projection image of the emission data to compute the scatter distribution [31].

1.1.1.5 Data processing and reconstruction

All the tracked counts of each detector at any given time over the entire scanning period are stored in a special file called list-mode file. Since this list mode file is a huge file which requires a lot of memory capacity, some scanners transform the list-mode data simultaneously to the data acquisition into the sinogram and then delete the according part of the list-mode file. The scanner which was used for this study was programmed to store all events in the list-mode file and keep this file.

Over the time of data acquisition, all detected coincident events are stored into data arrays referring to their space coordinates, which include the distance from the centre, the trans-axial angle and the axial angle of the LOR, delivering a four-dimensional histogram. The histogram that bins all the coincident events in space is referred to as sinogram [21]. Even if techniques and algorithms for the reconstruction of the four-dimensional sinogram exists, the most of them are too computationally intensive preventing their use in clinical imaging. Therefore, the transformation of the four dimensional sinogram into a certain stack of two dimensional sinograms, called rebinning is often used [32, 33]. The Fourier rebinning algorithm is known to preserve the three-dimensional representation of the original data for a broad spectrum of axial angles [32]. After the rebinning process, each slice can be reconstructed independently, enabling the use of two-dimensional reconstruction algorithms and thus the performance of the reconstruction in a shorter time [34]. Before the reconstruction can begin the raw data must be corrected (random correction, calibration data is added, death time loss correction, decay correction, attenuation correction, scatter correction and smoothing).

Different methods exist for the image reconstruction, of which a form of conventional filtered back-projection (FBP) algorithm is most often used [35]. However, this conventional FBP, which only involves a single back-projection step, is known to be prone to artefacts in tissue with low count density. Therefore, multiple projection and back-projection may be performed using iterative reconstruction algorithms to achieve an optimal image estimate [35]. The maximum-likelihood expectation-maximization method is a widely used iterative algorithm [36]. In this method, an image-estimate first is projected and subsequently compared to the sinogram data to compute scaling factors. Afterwards the image is back projected into a sinogram with the new scaling factors to produce a more accurate image estimate. This process repeated for a certain number of iterations so that at the end a final image estimate is achieved [36]. It is also possible to compute the scaling factors from ordered subsets of the sinogram, which allows a faster reconstruction. This ordered-subsets

expectation-maximization (OSEM) algorithms is most commonly used in clinical settings and is also used in the here presented study [37].

1.1.2 Gated cardiac PET

Today, PET is an established imaging technique for specific examinations of the heart including myocardial perfusion and viability imaging [38, 39]. However, cardiac imaging is complicated by respiratory and contraction-induced heart motions, which are needed to be reduced [40]. In order to do so, the PET data need to be acquired in a gated mode. The use of ECG-gated PET data acquisition offers not only the opportunity to minimize imaging artefacts that are caused by cardiac motion, but also allows to assess images of the heart in a specific cardiac phase.

For an ECG-gating a constant ECG signal is needed. Some PET scanners offer the opportunity to apply the ECG signal in the list-mode data [41]. In the ECG signal, one cardiac cycle refers to the time between two detected R-peaks. Therefore, the accurate detection of the R-peaks is the primary aim for ECG-gated PET data acquisition. After the determination of the R-R interval, which is intrinsic to one heartbeat, and its inclusion into the list mode file, one heart cycle can be split into a user-defined equal length number of frames (for example eight or 16 frames per cardiac cycle) [42]. The data of ECG-gated PET is binned accordingly to the phase it correlates to within the cardiac cycle, meaning that for each frame a sinogram is reconstructed separately. An increasing number of frames per cardiac cycle comes along with a higher number of reconstructed sinograms and images and thereby with a prolonged total reconstruction time [43]. One more problem, that needs to be considered is that with an increasing number of frames, the count density of each frames lowers. To produce high quality ECG-gated images, a higher injection dose must be administered or the scan time must be prolonged to increase the number of counts per frame (see ***Figure 3***) [43]. ***Figure 3*** demonstrates, that the image quality is decreasing with the number of gates per cardiac cycle. The image quality with only four gates is superior to the quality of the images of the

reconstruction with 16 gates per cycle, which is possible to see at the less sharp delineation of the LV myocardial wall. But a reconstruction with a higher number of gates enables a more exact determination of the myocardial wall movement and the volume changes throughout the cardiac cycle and thereby the calculation of a more accurate time-volume curve.

In general, there exist two different approaches for cardiac ECG-gating: prospective and retrospective ECG-gating [44]. For prospective gating, a certain number of previous R-R intervals is measured to calculate the average R-R interval time with a certain tolerance (usually 10 to 20%). Based on this average R-R interval duration the following cardiac cycles are separated [20]. For retrospective gating, each R-R interval is recorded and afterwards separated in frames. Moreover, different techniques have been introduced to reduce the influence of heart rate (HR) variability during the data acquisition referred to as bad beat rejection, which discard cardiac cycles from the acquisition if their length is outside of certain limits [45].

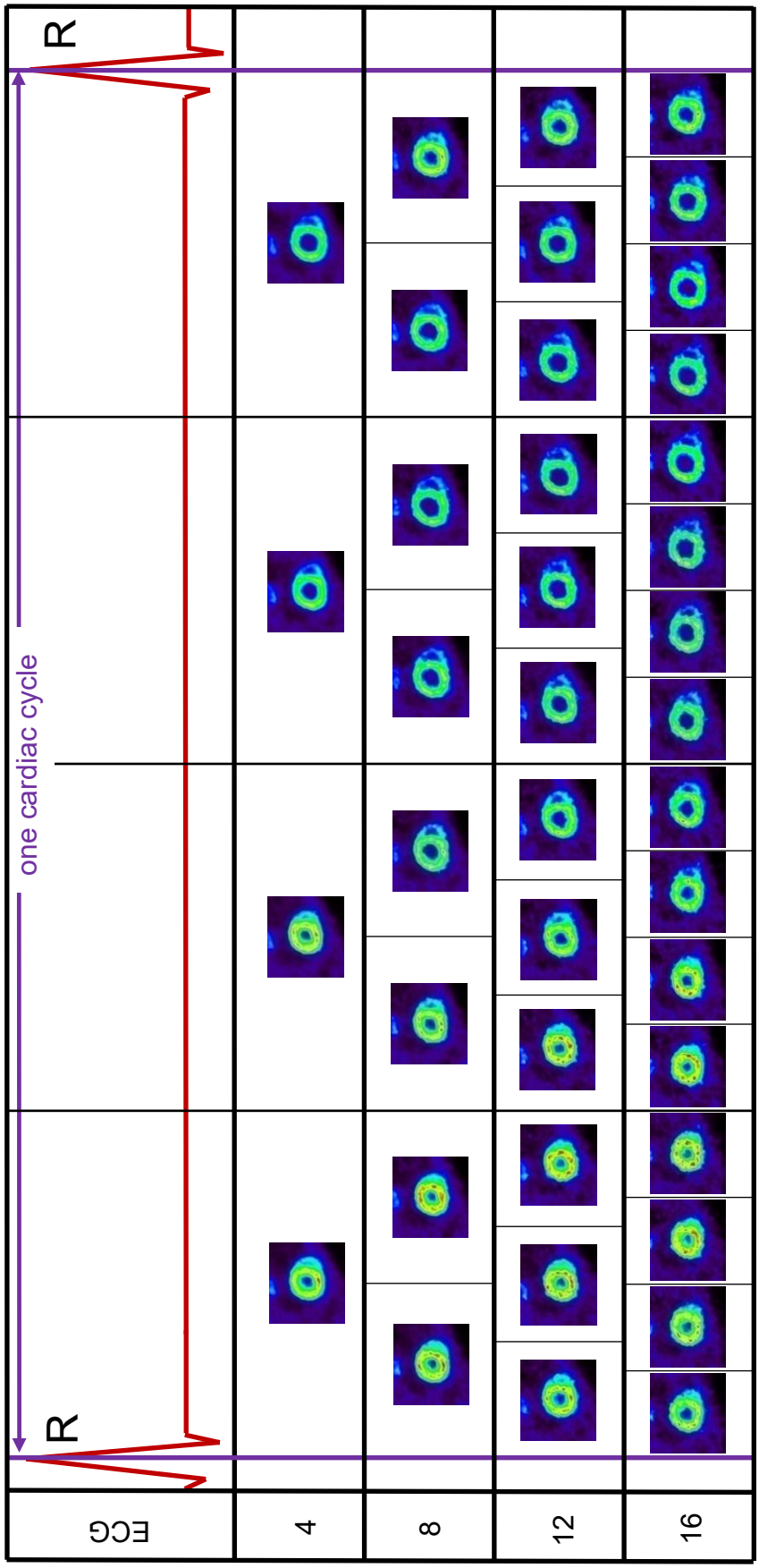

Figure 3 Schematic image of the ECG-gated PET data acquisition with different numbers of gates.

This scheme was generated by using the program Powerpoint 2016 (Microsoft Office 365 ProPlus). This scheme shows short axis slices of the same mid-ventricular part of the same ZL control rat from each gate of the cardiac cycle of the different reconstructions generated by AMIDE. The four reconstructions have been with four, eight, twelve and 16 bins (from top to bottom). The short axis slices have been ordered according to the schematic ECG signal which demonstrates one RR interval (violet arrows) and thereby one cardiac cycle.

1.1.3 ^{18}F-FDG as tracer

Cardiac ^{18}F-FDG PET imaging is a useful method for the assessment of myocardial viability [46]. The base of the ^{18}F-FDG PET is a trapping mechanism of the glucose analogue ^{18}F-FDG, which is taken up by cardiomyocytes through glucose transporters (GLUT 1 and 4) and subsequently phosphorylated by the intracellular enzyme hexokinase 2 (see **Figure 4**) [47, 48]. After this phosphorylation step, ^{18}F-FDG-phosphate cannot be further metabolized in cardiomyocytes, since the 2-hydroxyl group is missing, and cannot leave the cell before radioactive decay. As consequence, ^{18}F-FDG-phosphate is trapped in cells and its distribution is a good reflection of the glucose metabolism of the cells.

Figure 4 Hexokinase reaction of ^{18}F-FDG.

This scheme was generated by using the program ChemDraw 16 (PerkinElmer Informatics).

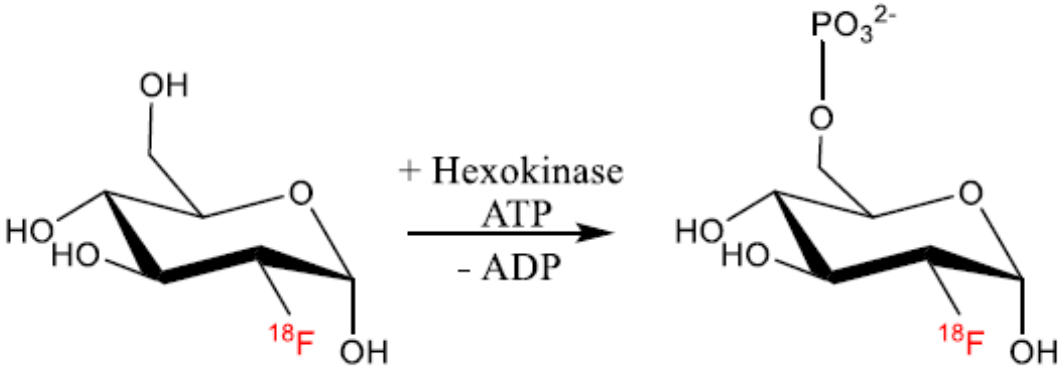

^{18}F-FDG *^{18}F-FDG-Phosphate*

However, myocardial glucose and thereby ^{18}F-FDG uptake depends on several variables [35, 49]. Therefore, protocols have been developed to standardize the metabolic conditions at the time of the study including long fasting periods, glucose administration and pharmacological pre-treatment. Especially, ^{18}F-FDG PET imaging in subjects with diabetes is problematic because of the decrease glucose and ^{18}F-FDG uptake [50, 51].

For this study, the PET scans were performed under hyperinsulinemic-euglycemic clamp conditions. The hyperinsulinemic-euglycemic clamp technique is an established method for assessing the state of insulin resistance

[52, 53]. A high dose insulin infusion is used to completely suppress the hepatic glucose production, so that under steady state conditions no change in the blood glucose concentration can be observed [52-54]. Previous studies have shown, that the hyperinsulinemic-euglycemic clamp protocol produces a significantly higher myocardial ^{18}F-FDG uptake than all other investigated pre-treatment protocols studied [51, 55].

1.1.4 Advantages of cardiac ECG-gated ^{18}F-FDG PET

A great advantage of PET compared to SPECT is the large number of low atomic number elements for which positron emitters exist. This enables the incorporation of such positron emitters into many biological active compounds. The use of these different radionuclide tracers enables the simultaneous evaluation of the perfusion, metabolism, viability or innervation and the function of the LV [12, 18, 56]. Radiotracers that assess sympathetic innervation and myocardial metabolism are important to gain new insights in the pathophysiology of different cardiac diseases and their role in the progression to HF and sudden cardiac death.

Furthermore, PET radiotracers have an extraction fraction that is superior to SPECT tracers [16, 17]. The short half-life of the PET tracers enables the use of shorter imaging protocols and lower radiation exposure but provides more complications in the use of exercise stress imaging.

Moreover, the use of PET enables the in-vivo identification and characterization of alterations in cellular or subcellular level, which permits the association between abnormal function or metabolism of the cardiomyocytes and the occurrence of HF, which cannot be detected by MRI or computed tomography (CT) yet.

1.1.5 PET studies in small animals

Animal research is an urgent step in preclinical science. A lot of new insights into the pathophysiology of many diseases and disorders as well as in the bio-

distribution of new drugs could be generated by combination of experimental animal models, new tracer-molecules and new small animal scanners. Since these scanners require a higher spatial resolution than clinical scanners due to relative volumetric differences in objects of study and thereby in the organs, the scanner design has been modified to improve the spatial resolution [28, 57].

Firstly, the detector crystals are arranged in blocks with a fix array of individual crystals and each of these crystals is connected to one individual channel of a multichannel PMT [28]. These detector units are arranged in a certain number of continuous rings. Furthermore, the new generation of PET scanners use crystal material with a high time resolution like lutetium oxyorthosilicate (LSO) [28, 57]. These new technological advances have led to small animal scanners with an intrinsic resolution of one to two millimetres [28, 57]. Through this high spatial resolution, the examination of even small structures like the myocardial wall of rats and mice is now possible using small animal PET scanners. Never the less, PET studies in small animals are still more challenging and time consuming than studies of human patients as consequence of the required anaesthesia and the prolonged preparation time, but they offer the opportunity to investigate the underlying pathophysiological processes of different diseases and the influence of different treatment strategies in vivo at a subcellular level under standardized conditions.

1.2 **Imaging of cardiac function**

1.2.1 The cardiac cycle

An appreciation of normal cardiac function is necessary for the understanding of the consequences, clinical features and challenges in the imaging of diastolic and systolic disturbances. A correct cardiac cycle is crucial to provide adequate LV filling (input) and LV ejection (output) in rest and during exercise.
The function of the heart depends on its ability to switch between two functional states: a relaxed chamber during diastole that enables the filling of the LV from low pressure and a stiff chamber during systole for the ejection of the stroke volume at arterial pressures. Therefore, the ventricle has two functions: the diastolic filling and the systolic ejection of the blood volume.

1.2.1.1 The systole

The isovolumetric contraction, and thereby the ventricle systole, begins with the closure of the atrioventricular valves. Besides the short phase of isovolumetric contraction during which the pressure in the ventricle increases, a longer ejection period completes the systolic phase, within which the ventricles eject a certain percentage of their end-diastolic volume (EDV). As soon as the pressure in the LV exceeds the pressure in the aorta and the pulmonary arteries, the semilunar valves open and the same blood volume is ejected by both ventricles (stroke volume (SV)). If the pressure in the ventricles falls below the pressure in the subsequent vessels, the semilunar valves close and the systole is finished [58].

1.2.1.2 The diastole

The diastole is defined as the period of the cardiac cycle beginning with the closure of the semilunar valves and ending with the closure of the atrioventricular valves. During this time, the chamber relaxes and refills with blood and the cardiac muscle is perfused [58].
The relaxation is responsible for the ability of the LV to fill and accommodate the venous return without a big increase in the LV pressure. The blood flow into the ventricles has three components, an early flow (E-wave) which is caused by ventricular suction as consequence of the active ventricular relaxation and that

accounts for 65-80% of the volume, a slow passive filling, mentioned as diastasis, whose duration is greatly dependent on the HR and a third one as result of the atrial contraction (A-wave) [59]. The contraction of the atria increases the pressure in each atrium, what forces additional blood volume into the ventricles [3].

1.2.2 Heart failure

HF is a clinical syndrome with diverse aetiologies that appears when the heart is unable to maintain a sufficient blood supply of the organs. It is further characterized by typical symptoms and clinical signs, which are most often caused by functional and/or structural cardiac alterations [60]. Since, the present definition of HF is restricted to stages with apparent clinical symptoms, functional or structural abnormalities in absence of any symptoms are considered as precursors of HF [61]. Subjects with HF can be divided into two broad groups: SHF and DHF [60].

It is crucial to recognize that the terms DHF and SHF refer to two different groups of HF patients distinguished by different features including their pathophysiology, differential LV remodelling and changes in the LV structure [60].

1.2.2.1 Systolic heart failure

SHF is the consequence of a disturbance in the contraction of the myocardium. The most common reasons for SHF are coronary artery disease (CAD), different cardiomyopathies, arterial hypertension and myocarditis [62]. SHF is characterized by a reduced LVEF and therefore also called heart failure with reduced ejection fraction (HFrEF) [60]. An EF between 50 and 70% percent is considered as normal [60]. If the EF falls below 40% and typical symptoms of HF appear, the diagnosis of a HFrEF can be made. Patients that present themselves with a EF between 40 and 49 % and symptoms of HF are separated from the both groups and have a type of HF which is defined by the European Society of Cardiology (ESC) as heart failure with mid-range ejection fraction (HFmrEF) [60].

1.2.2.2 Diastolic heart failure

DHF or heart failure with preserved ejection fraction (HFpEF) is characterized by similar symptoms and clinical signs like SHF but in contrast to SHF, the systolic function is normal and patients show predominant abnormalities in LV diastolic function [60]. The underlying pathophysiology of DHF is based on increased passive stiffness, impaired active relaxation or concentric remodelling of the ventricles, which cause an impaired filling of the ventricles. Accordingly, DHF occurs when the ventricle is unable to fill with an adequate blood volume during diastole at normal pressure resulting in a lack of volume [63].

1.2.2.3 Symptoms and clinical features

The symptoms of HF are often non-specific but can include among others dyspnoea, stenocardia and periphery oedema, due to fluid retention. The presence of symptoms are the basis for the clinical stage classification of HF introduced by the New York Heart Association (NYHA) [64]. Both DHF and SHF can be present with symptoms that occur at rest (NYHA IV), during less-than-ordinary physical activity (NYHA III) or that are present during ordinary physical activity (NYHA II) [64].

In contrast to SHF, which is often presented with a dilated LV, DHF often presents itself with an increased LV wall thickness (LV hypertrophy) and increased left atrial (LA) size, as consequence of the increased filling pressure and further with additional signs of reduced suction capacity or reduced LV filling [6].

1.2.2.4 Diagnosis

The differentiation between SHF and DHF cannot be made at the bedside since a discrimination between diastolic and systolic dysfunction is necessary. Therefore, the support of cardiac imaging techniques is essential. SHF can be diagnosed if the clinical symptoms of HF are present and the LVEF is ≤ 40% [60]. The diagnosis of DHF is more challenging since LVEF remains normal at the beginning of the disease and the symptoms often are non-specific. The ESC published in their guidelines 2016 [60] diagnosis criteria for HFpEF that must be fulfilled, which include:

1.) the presence of signs and/or symptoms of HF
2.) a normal LVEF (≥ 50%)
3.) evidence of abnormal cardiac function and structural alterations which underlie HF and
4.) elevated natriuretic peptide levels.

Since an abnormal cardiac function is often present, even if no symptoms or elevated natriuretic peptide levels can be detected, this isolated alteration of the cardiac function is called DD and must be separated from the diagnosis of DHF.

1.2.3 Diastolic dysfunction

The determination of LV diastolic function should be included in every cardiac examination of any patients with signs for cardiovascular disease, since it has a major impact on functional capacity, symptom status, prognosis and medical treatment in both DHF and SHF [6]. The DD is a functional abnormality characterized by impairment of active myocardial relaxation and/or decreased LV compliance which refers to mechanical abnormalities of the LV during the diastolic phase regardless of whether the LV systolic function is normal or abnormal and whether symptoms are present or not [65].

1.2.3.1 Pathophysiology and clinical features

The diastole is the period of the cardiac cycle during which the cardiomyocytes are unable to generate force and return to their relaxed length and force. DD is present when this process is prolonged, decelerated or incomplete, which can be caused by several underlying mechanisms including coronary insufficiency [66], changes in preload and afterload [67], alterations of the pericardial anatomy (e.g. constrictive pericarditis) [68], metabolic alterations (diabetes, acidosis) [69], different cardiovascular drugs [70], hypoxia [71] and arterial hypertension [66, 72].

A compromised diastolic function can present itself with a variety of signs, ranging from only a minor slowdown of ventricular relaxation, without relevant hemodynamic changes, to the onset of pulmonary venous congestion, as

consequence of the increased intraventricular pressures [3, 73]. Progressive DD is associated with an advanced impairment of LV relaxation, which reduces the peak trans-mitral pressure gradient and thereby the early mitral inflow velocity (E) [74]. The LA pressure remains relatively in range in the early stage of DD [6]. But if the atrial pressure increases in more advanced stages of DD the LA becomes passively enlarged. This enlargement of the LA is therefore a relatively sensitive marker of DD [75]. However, DD is often present in both DHF and SHF, since alterations of the diastolic function do not only influence the diastolic filling of the ventricles but may also have an impact on the ventricular systolic performance [76].

1.2.3.2 Epidemiology

Studies have shown that HFpEF accounts for almost one-half of all HF cases [77]. The overall prevalence of DD has been investigated by different groups and was found to vary from 11,1 to 35% [78, 79].

A significantly higher risk of DD has been reported to be linked to different patient characteristics including increased systolic blood pressure, higher age, serum insulin level, obesity, female gender and increased HR [6, 8, 78, 80, 81]. Of particular importance is that the existence of a DD is an independent predictor of all-cause mortality even after the correction for sex, age and LVEF [6].

1.2.4 Challenges in the assessment of diastolic function

The diastole is a complex process that is influenced by several different factors including HR, age, gender, myocardial stiffness, LV hypertrophy, ischemia, loading conditions and wall coordination of the myocardium, that complicate an accurate determination of the diastolic function. Therefore, the evaluation of the diastolic function requires the assessment of both diastolic and systolic properties of the ventricles and the atria as well as of ventricle-atria interactions [82, 83]. The LVEF and the cardiac output (CO) as major signs for the LV systolic function can be easily calculated from EDV, end-systolic volume (ESV) and the HR, but even if systolic abnormalities are present, the clinical question also concerns the existence of a normal or abnormal diastolic function. The

most accurate evaluation of the diastolic function is the determination of the intra-cardiac pressures, since different cardiac volumes are often in range at the onset of a diastolic impairment.

Moreover, it has been shown that both diastolic and systolic properties differ between age and gender [84-89]. Therefore, a sex and age adjustment may be needed for correct interpretation of diastolic function parameters.

Since variations of the HR affect the diastole rather than the systole, they can profoundly affect the assessment of diastolic parameters, which is particularly relevant in patients having a bundle branch block or observed arrhythmia. Furthermore, abnormalities in the diastolic function may only occur under stress conditions when the HR is increased and the duration of the diastole is shortened [90].

However, the accurate assessment of the LV diastolic and systolic function is indispensable to target the underlying cause of HF and to plan the best treatment strategy for the patients.

1.2.5 Preclinical animal model for diastolic dysfunction

Recent studies have demonstrated a quite high prevalence of HFpEF and further that the conventional treatment strategies for HFrEF do not provide a satisfying outcome in patients with a HFpEF [91-94]. Moreover, different studies have provided evidence, that the cardiac metabolism might play a key role in the development of DD and HFpEF in certain patients [95-97]. Therefore, the evaluation of the dynamic parameters as well as the cardiac metabolism is an urgent need to improve the understanding of the pathophysiology and thus to develop new treatment strategies for this kind of HF.

Different animal models of HFpEF and DD have been proposed. In this study, Zucker Diabetic Fatty (ZDF) rats and healthy littermates Zucker Lean (ZL) rats were examined. ZDF rats have a mutation in the gene of the leptin receptor [98]. As consequence, they develop obesity and insulin resistance at young age and diabetes between eight and ten weeks of age [99, 100]. Later they progressively develop hyperglycaemia which is associated with impaired

pancreatic β-cell function and decreased responsiveness of liver and extrahepatic tissues to insulin and glucose [101]. The rats develop a lot of obesity- and hyperglycaemia-related complications, which are common between male ZDF rats and humans with T2DM [102]. These metabolic alterations also induce the development of a special form of cardiomyopathy referred to as diabetic cardiomyopathy [100, 103, 104]. In early stages this special form of cardiomyopathy presents itself with a DD and a LV hypertrophy [99]. For these reasons, ZDF rats served as model group and the ZL rats as control.

1.2.6 Preclinical assessment of diastolic dysfunction

Currently, the evaluation of the LV diastolic function in small animals is most often carried out using TTE and tissue Doppler. Thereby it was possible to identify disturbances during the diastolic filling of the LV in ZDF rats which was not present in age matched ZL rats [105]. Lum-Naihe et al. used as parameters for the diastolic filling the ratio between the E (early mitral inflow velocity) and the early diastolic mitral annular velocity (e'). This E/e' ratio has been shown to be correlated to increased LV end diastolic pressure, as it occurs in patients with DD [106, 107].

However, like mentioned above, the ECG-gated cardiac PET is a technique, which assesses the metabolic state and the cardiac function under investigator independent conditions simultaneously. Even if, the ability of the ECG-gated PET for the calculation of reliable LV volumes and EF has already been demonstrated in both, rats and mice [9, 10, 103, 108], its ability for the evaluation of the diastolic function in small animals has not been investigated yet.

2 Objectives of the thesis

ECG-gated PET has lately demonstrated promising preclinical and clinical results due to its ability in the accurate assessment of the systolic cardiac function. The major goal of this thesis is to contribute to the improvement of the cardiac evaluation in preclinical research with small animals by means of investigating the applicability of ECG-gated ^{18}F-FDG PET for the determination of global LV function in healthy and diabetic rats, either for gaining new insights in the pathophysiology of functional alterations or either for the development of new treatment strategies for heart diseases. Specific objectives are as follows:

1. To study the morphology of the LV and its phase dependent change throughout cardiac cycle using ECG-gated PET data acquisition under hyperinsulinemic-euglycemic clamp conditions and the AMIDE software in healthy and diabetic rats.
2. To measure the required time for the reconstruction and histogramming process of the list-mode files with different numbers of frames per cardiac cycle.
3. To calculate the LV volumes, diastolic and systolic parameters of the model and control rats through the evaluation of the time/volume curve and its first derivation the time/filling curve using a clinical detection software.
4. To investigate the impact of the number of gates per cardiac cycle on the calculation of the LV volume as well as on the systolic and diastolic function parameters.
5. To compare the calculated parameters for the LV function between the ZDF rats and the ZL rats to identify differences between the two groups.
6. To determine the potential of the ECG-gated ^{18}F-FDG PET for the detection of a DD in diabetic rats compared to the control rats.

3 Material and methods

3.1 Animal model

3.1.1 Biostatistical calculation

The biostatistical calculation has been carried out using Software Sigma Plot 12,5 (Systat Software, Inc.) by Paula Arias Loza (AG Prof. Pelzer). The sample size was calculated to detect a significant difference in E/e' as a marker of the early filling during the diastole as sign of DD. A difference in means of the E/e' ratio of 3,3 in ZL versus ZDF rats with a SD of 1,47 is expected according to Lum-Naihe K. et al. [105]. Sample size calculation of a two groups comparison by T-test with a power of 0,8 and an alpha error of 0,05 results in a need of five animals per group. Since euglycemic clamp is challenging and complicated to perform in small animals, especially in diabetic subjects, three additional ZDF rats and two ZL rats were included in the study to compensate for possible exclusion in consequence of mis injection of the tracer, excessively high blood glucose levels in the diabetic model or un-expected response to the glucose infusion rate, which makes the performance of an euglycemic clamp impossible.

3.1.2 Animal welfare

Animal experimental protocols were approved prior to the beginning of the experiments (Genehmigungszeichen: 55.2-2531.01-120/13) by the regional governmental Commission of Animal Protection (Regierung von Unterfranken Bayern) and conducted in performance according to the Guide for the Care and Use of Laboratory Animals (National Institutes of Health Publication No. 85-23, revised 2010) [109].

3.1.3 Animal handling

For this study eight male ZDF model rats (fa/fa) and seven male ZL control rats were used. The experiments were performed at age of 13 weeks. ZDF and ZL rats were purchased from Charles River Laboratory (Charles River Laboratories, Research Models and Services, Sulzbach, Germany GmbH) and were marked with a chip in their ear. The rats were owned by the study group of Prof. Dr. Pelzer (University of Würzburg).

The rats were housed in groups under standard controlled conditions at twelve-hour light/dark cycle. The well-being, food, water and bedding of the rats was checked daily. The ZL rats received standard diet, whereas the ZDF rats were maintained on special high caloric food (Purina 5008) as recommended by the supplier. Both groups received water and diet ad libitum during the study. The weight was measured every day. All rats were fasted for ten hours before the experiments started.

Figure 5 Comparison of the phenotype of a ZL rat (left) and a ZDF rat (right).

This image shows the phenotype of a ZL control rat and a ZDF model rat at the age of ten weeks: left -> ZL rat, right -> ZDF rat with mutation of the leptin receptor. The ZDF rat has developed a obesit phenotype at the age of ten weeks, whereas the ZL rat has a slim body.

These photographies were taken and provided by Paura Arias-Loza (Group Pelzer, University of Würzburg).

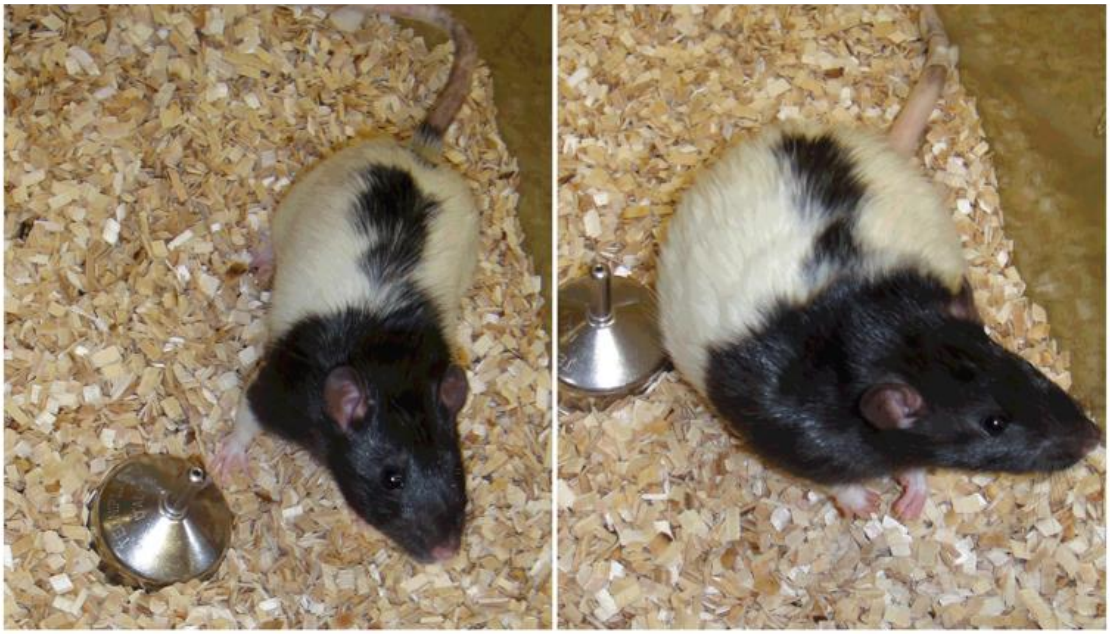

3.2 **Dedicated small-animal PET system**

PET studies were performed using a ring type, high resolution PET system (Inveon micro PET, Siemens Medical Solutions Inc.) intended for small animal imaging studies. Briefly, the system is based on 25,600 LSO crystals with dimension of 1.5 x 1.5 x 10 mm arranged in detector modules containing 20 x 20 crystals. Each LSO block is coupled to a PMT over a tapered multiple-

element light guide. The detector modules are arranged in four rings of 16 blocks (total 64) and each module is placed in time coincidence with opposite modules leading to a crystal ring diameter of 161 mm. This design results in a trans-axial FOV of 10.0 cm and an axial FOV of 12.7 cm. This scanner is equipped with a ^{57}Co retractable rotating point source to acquire transmission data, which is needed to perform attenuation correction.

Figure 6 Siemens Inveon small animal PET system.

These images show the PET scanner which was used for the experiments and is located at the “Zentrum für experimentelle Medizin” University Hospital of Würzburg.

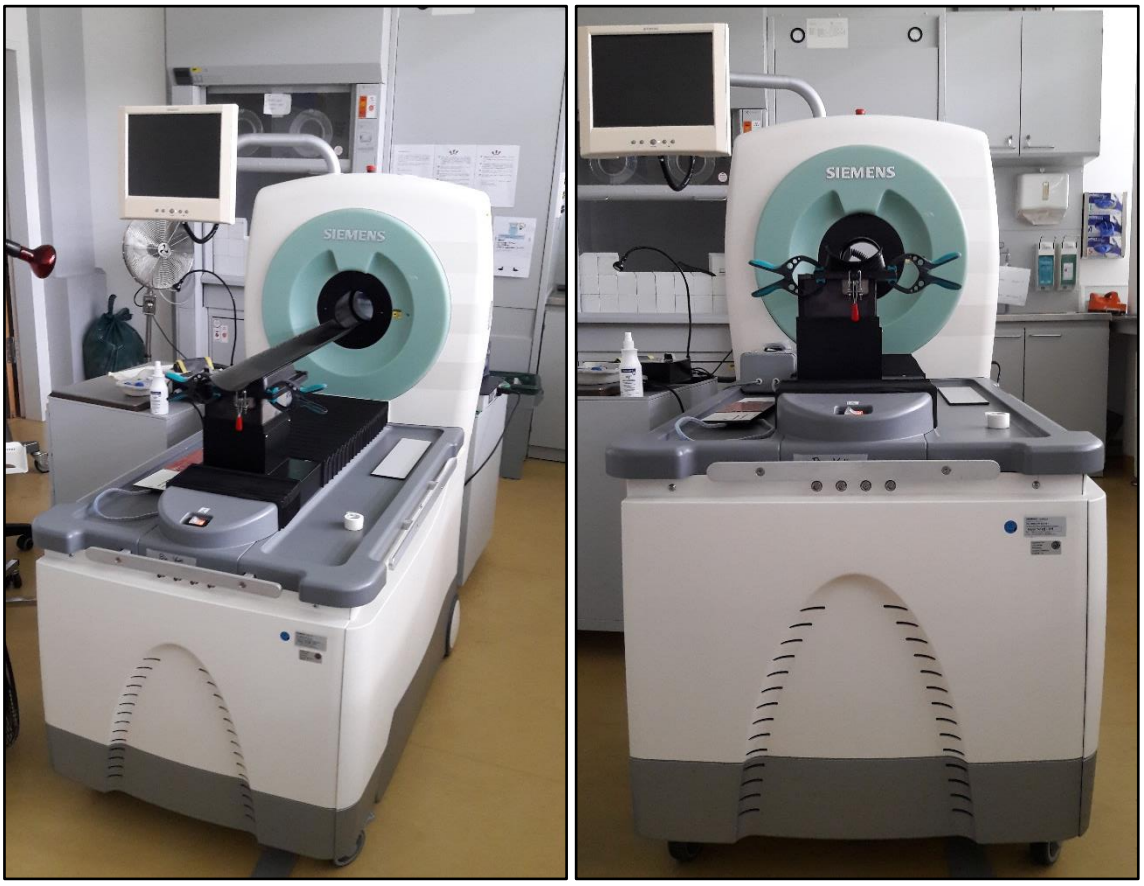

3.3 **Tracer production**

The tracer ^{18}F-FDG was synthesized in the department of radiochemistry at the department of nuclear medicine in Würzburg with a 16 MeV Cyclotron (GE PETtrace T; GE Healthcare, Milwaukee, USA), using GE FASTlab methodology according to the manufacturer’s instructions [110]. The ^{18}F-FDG was analysed

by high performance liquid chromatography at the end of synthesis to confirm radiochemical identity and purity (greater than 95%).

3.4 **Calculation of insulin amount**

The desired insulin concentration was 12 IU/ml so 2.4 ml of the original solution with concentration of 100 IU/ml were mixed with 17.6 ml isotone saline.

$$\text{Volume of orignial solution}$$

$$= \frac{\text{desired concentration } \times \text{final volume}}{\text{Insulin concentration original}}$$

$$= \frac{\frac{12\text{IU}}{\text{ml}} \times 20\text{ml}}{\frac{100\text{IU}}{\text{ml}}}$$

$$= 2.4 \text{ ml}$$

For each animal, the amount of insulin and the volume infusion rate were calculated.

The desired insulin infusion rate was 240 mU/kg/min (bolus) and 12 mU/kg/min (during clamp).

$$\text{Amount of insulin infused (bolus)(mU/min)}$$

$$= \frac{\text{infusion rate desired (mU/kg/min)} \times \text{body weight}}{\frac{1000\text{g}}{\text{ml}}}$$

$$= \frac{240\text{IU} \times \text{body weight}}{\frac{1000\text{g}}{\text{ml}}}$$

$$\text{Amount of insulin infused (clamp)(mU/min)}$$

$$= \frac{\text{infusion rate desired (mU/kg/min)} \times \text{body weight}}{\frac{1000\text{g}}{\text{ml}}}$$

$$= \frac{12\text{IU} \times \text{body weight}}{\frac{1000\text{g}}{\text{ml}}}$$

$$\text{Volume infusion rate} = \text{amount of insulin} \times \text{inverted insulin concentration}$$
$$= \text{amount of insulin} \times \frac{1\text{ml}}{12\text{mU}}$$

3.5 **Experimental protocols**

Hyperinsulinemic-euglycemic clamp was performed to stimulate cardiac glucose uptake and to evaluate systemic and cardiac insulin sensitivity.

The weight of the rats was measure before the experiments were started to calculate the dose of insulin. The used Insulin was Insuman Rapid 100 IE/ml (Sanofy aventis). Both, the glucose and insulin solution were administered with infusion systems.

The anaesthesia was performed in the same way in all animals. The rats were anaesthetized with 4-5% isoflurane (CP-Pharma) via an induction chamber and maintained anaesthetized throughout the whole scanning procedure using 2-3% isoflurane and 0,5 l/min O^2 via spontaneous breathing.

After testing the depth of anaesthesia by using the between-toe-reflex, the rats were placed on a heated plate with the temperature of 37 degrees Celsius. The noses of the rats were put in a tube which was connected to the vaporizer. A crème (Bepanthen, BAYER AG) was put on the eyes of the rats to protect them from drying out.

On the heated plate the skin over the lateral tail veins was disinfected with Cutasept F (BODE Chemie GmbH) for one minute. Afterwards an injection system was placed in the tail vein (Optiva i.v. Catheter Radiopaque, Smith Medical). The position of the injection system was checked by injecting 0.1 ml of isotone saline. When there was a tail oedema, the system was removed, the bleeding was stopped and a new one was placed. Two injection systems were placed in each rat. The injection systems were connected to syringes in which solutions were prepared in advance. In one syringe was insulin 12IU/ml and in the other one 50% glucose solution. The solutions were infused using syringe pumps (Pump 11 Elite, Harvard Apparatus). Glucose infusion rate were

adjusted to keep blood glucose level in range. The glucose clearance (M-value, µmol/min/kg) were calculated by glucose infusion rate.

Blood samples were collected from hind paw before and during the hyperinsulinemic-euglycemic clamp every three minutes to measure blood glucose level. The blood glucose was determined by blood glucose control system (Freestyle mini, Abbott Diabetes Care Inc.) and according test stripes (Freestyle, Abbott Diabetes Care Inc.) every three minutes in mmol/L starting after the correct placement of the injection systems.

The insulin bolus injection was initiated at the infusion rate of 240 mU/kg/min and given for 20 minutes. Afterwards the dose was reduced during the clamp to 12 mU/kg/min and the blood glucose level were measured at least over twelve minutes to adjust the glucose injection rate so that the blood glucose levels were stable between 70 and 100 mg/ml. If the fluctuations of the blood glucose level in the twelve minutes' time window were too big, the measurement and adjustment of the glucose injection were extended until the blood-glucose level became stable.

As soon as the glucose level was stable the rats were placed on the carrying system of the PET scanner. Under the rats, the pressure-sensor for the detection of respiratory movement was installed. The three ECG electrode-sensors were stuck in the skin of the rats. Two on shoulders height and one lower. The position of the ECG electrodes was checked by the ECG signal quality. For holding up the body temperature, a heating lamp was installed 80 cm away from the head of the animals.

3.6 **PET imaging**

3.6.1 Animal PET protocol

The timetable of the animal preparation is shown in **Figure 7**. The ^{18}F-FDG solution was pulled up in a syringe and the activity of the solution in syringe was measured with a radioisotope calibrator (CRC-10R, Capintec, Inc.). The animals received a mean ^{18}F-FDG injection dose of 39.4 ± 3.1MBq via tail vein during

hyperinsulinemic-euglycemic clamp (blood glucose level: 70-100 mg/ml) to enhance the cardiac tracer uptake. ^{18}F-FDG was given per bolus injection over 20 seconds after twelve minutes of stable glucose levels. After the injection, the activity remaining in the syringe was measured again, to determine the real injected activity. The HR and the respiratory rate were checked during the whole scan.

Figure 7 Timetable of PET Scan.

This scheme was generated using the program Powerpoint 2016 (Microsoft Office 365 ProPlus).

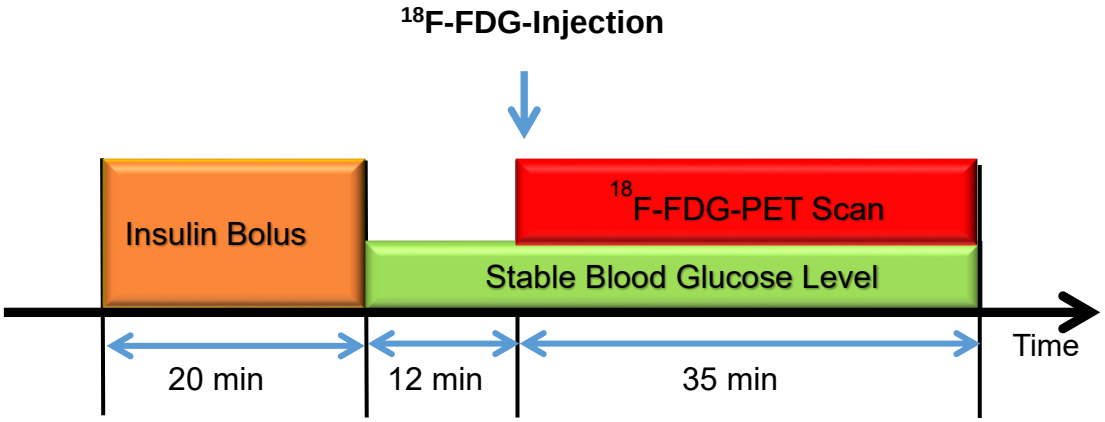

A transmission scan of 13 min with a ^{57}Co rotating source was performed before tracer administration and emission scan to correct the emission images for photon tissue attenuation. ^{18}F decay and dead time correction were also performed for all reconstructed images.

3.6.2 Data processing

The sorting, creation and reconstruction of the scan files were performed with the Inveon Acquisition workplace (Version 1.5.0.28, Siemens medical solutions) on a HP (Hewlett Package) Z820 workstation (HP Inc.). This workstation is equipped with a nVidia k600 graphic board with 1024 megabytes DDR 3, two Intel Xeon E5-2630 v2 processor with each six cores and a working storage of 64 gigabytes. This is mentioned here since the performance of the computer system has great impact on the reconstruction and histogramming-time. The

time which was required for the reconstruction of the images was received from the task list of the Inveon Acquisition workplace.

Images of the rats were acquired at one fixed bed position. List-mode data acquisition enables recording time stamps and gating signals simultaneously, enabling a restoring of the whole data with high flexibility in a short time. The gating signal was added to the list-mode data by feeding the ECG signal from a BioVet small animal system into the Siemens Inveon PET acquisition system (see ***Figure 8***). A gating signal was achieved when the ECG curve passed a manual defined voltage value. All durations of the R-R interval were accepted.

The list mode emission PET acquisition with ECG signal recording was started just after the tracer administration. The list-mode data acquired for 35 min were sorted and histogrammed according to the ECG signals into four, eight, twelve and 16 three-dimensional scan-files for each animal and for each dynamic frame (first from start to 900s, second from 900s to 2100s). The three-dimensional sinograms were reported by Fourier rebinning algorithm (FORE) and reconstructed into two-dimensional images of the whole FOV using two-dimensional ordered subset expectation maximization algorithm with four iterations and 16 subsets. The received two-dimensional pictures were rearranged and cropped in all three-axis using the free available program AMIDE (AMIDE's a Medical Image Data Examiner 1.0.4, GNU General Public License, Version 2) to generate tomographic short axis and long axis images of the heart (see **Figure 9**).

Figure 8 Scheme of the List mode acquisition and data sorting.

This scheme was generated by using Powerpoint 2016 *(Microsoft Office 365 ProPlus).*

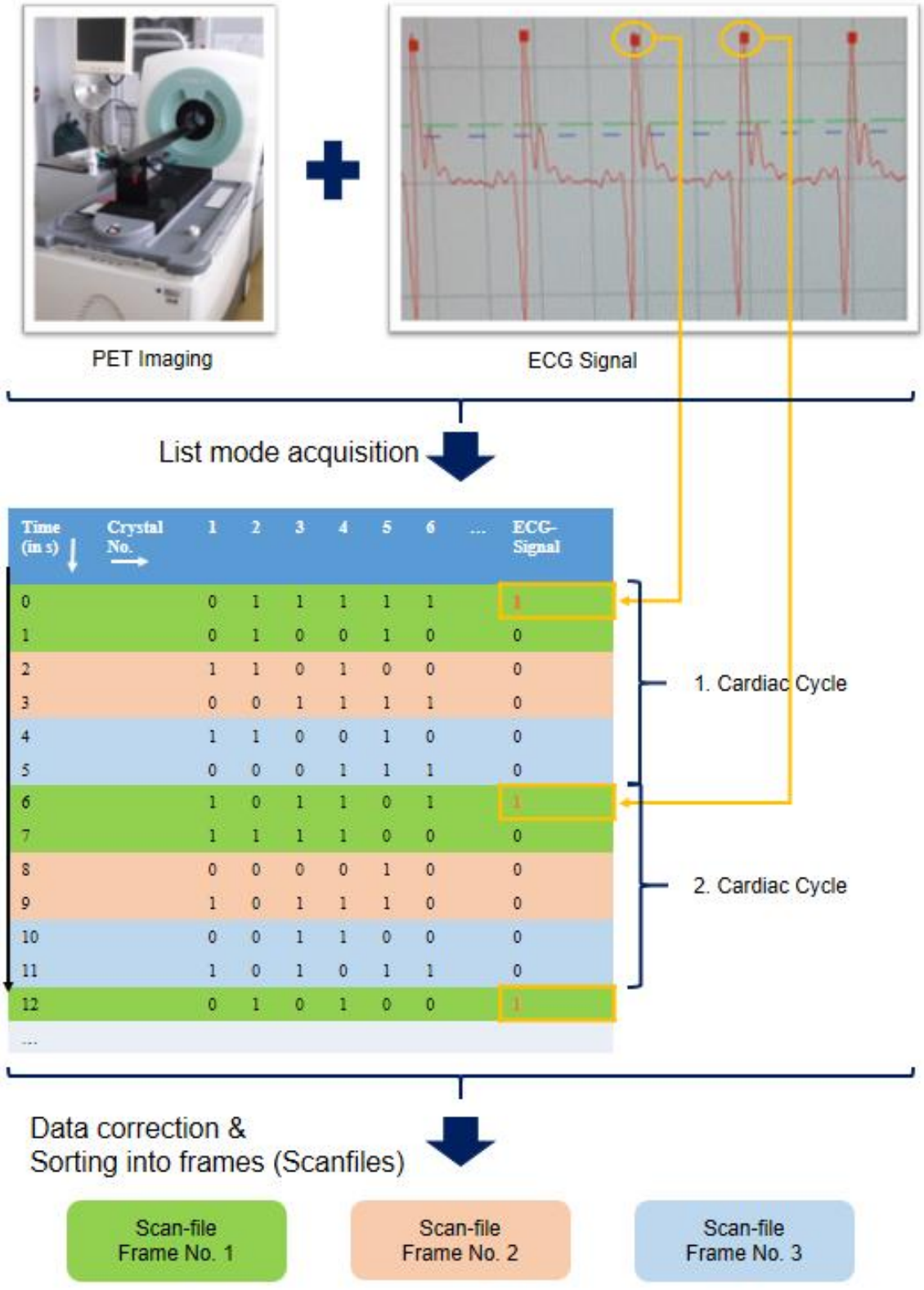

Description **Figure 8**:

This scheme shows how the data from the coincident events registered by the PET and the data from the ECG recording are combined and saved in a list-mode file. The ECG data always registered an event when an R-peak was detected. Based on this recording the list-mode file can easily be reconstructed in a user-defined number of frames (in the present study four, eight, twelve and 16). For each frame a scan-file, which only includes corrected data, is generated, which can be pictured as a sinogram (see **Figure 9**). The next steps of the data processing are shown in **Figure 9**.

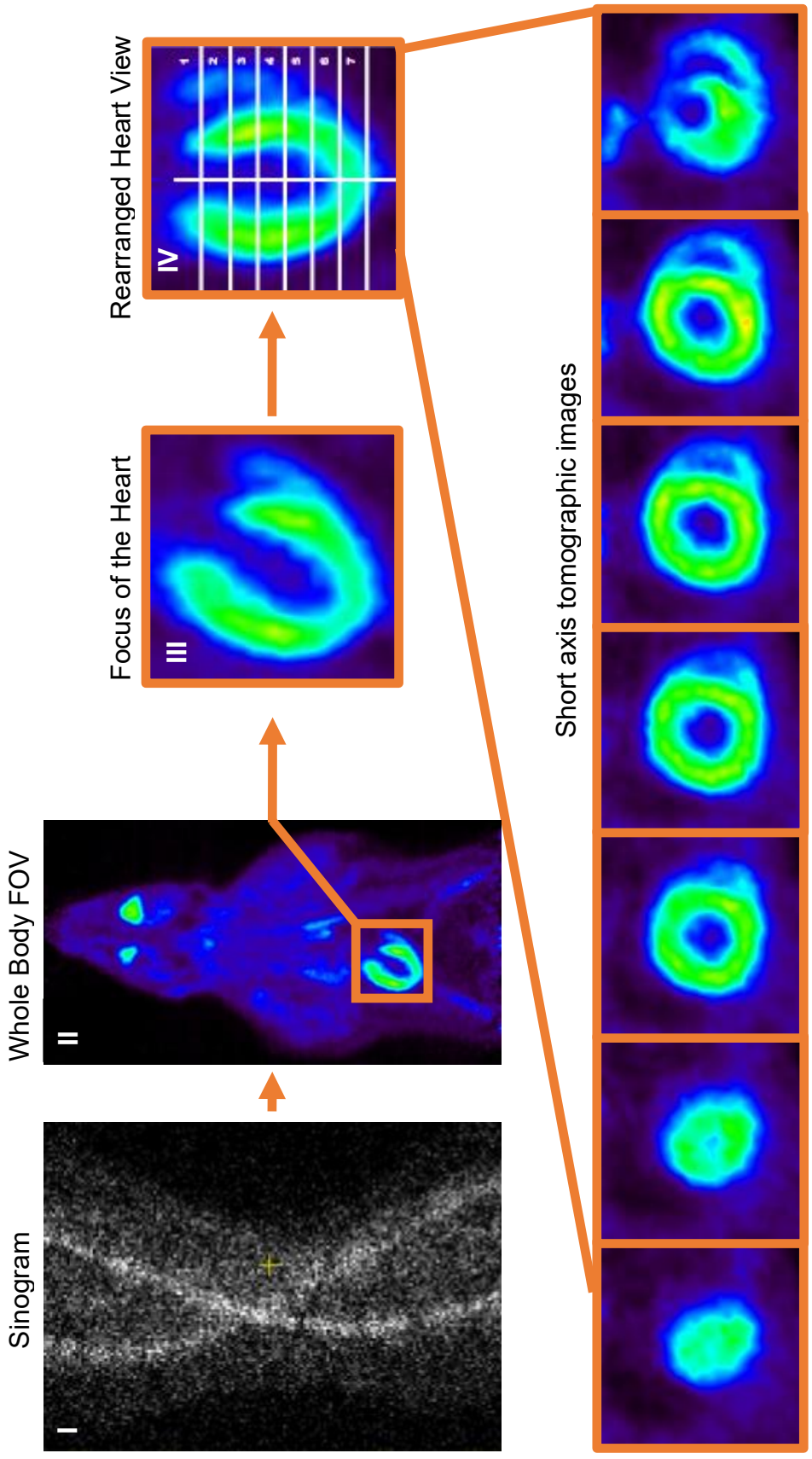

Figure 9 Scheme of the reconstruction and rearrangement steps.

This scheme was generated by using Powerpoint 2016 (Microsoft Office 365 ProPlus).

Description **Figure 9**:

This scheme demonstrates (simplified) the most important steps to receive suitable short axis tomographic images of the LV for the evaluation of the function by HFV. At first, the scan-file data is transferred in an according sinogram (I). These sinograms are reconstructed in images of the whole FOV (II). To get a clear and suitable view of the LV for the edge detection software, it is necessary to rearrange the heart in all three dimensions (III). Next the LV is divided into a certain number of slices to receive short axis tomographic images of the LV (IV). Subsequently the short axis slices were checked if they all show continuous tracer uptake and to confirm that the whole LV is represented.

3.6.3 Left ventricular volume calculation

The calculation of the LV volumes was carried out by a clinical automatic ventricular edge detection software HFV (Heart Function View, Nihon Medi-Physics Co., Ltd) and is here explained in detail. For each gated image, the program HFV automatically defines the heart long axis (HLA) on vertical and horizontal long axis views, the valve plane and defines the ventricular centre, which is located on the HLA, to separate the apical from the mid-ventricular part of the heart. The valve plane is located at the basal onset of tracer accumulation and is a plane perpendicular to the HLA.

The tracer distribution of the LV myocardium of the short axis slices is transformed in coordinates, which allows the calculation of the distances from the inner, mid-myocardial and outer surface of the myocardial wall to the ventricle centre of all short-axis images. The tracer distribution of the apical LV myocardium was expressed in spherical polar coordinates, whereas the tracer distribution of the basal and mid-ventricular myocardium was transformed into circular cylindrical coordinates, assuming a hemispherical shape of the myocardial wall around the apex and a cylindroid shape of the basal and mid-ventricular portions.

The three-dimensional count profile (sphere radially) were created for all short axis images (see **Figure 10, Figure 11, Graph 1**). The maximum point of the count profile was defined as mid-myocardial surface and the crossing of the 75% threshold are defined as inner and outer determination line. Through interpolating by approximation and the determination of the contour point by correcting the extraction point by curve fitting a stable and smoothed contour of the borders was shaped automatically by HFV (see **Figure 12**).

The definition of the inner and outer myocardial border allows the calculation of distances from centre point to the inner and outer surface of the myocardial wall and its time dependent variations. Mathematically, the mid-myocardial surface is represented for every gate in all three dimensions as an elastic surface. The shape of the elastic surface is determined by the distribution of the myocardial activity measured and stored within the PET acquisition data. To calculate accurate values for the LV volumes, the myocardial surface is assumed to have the same properties and react like an elastic membrane.

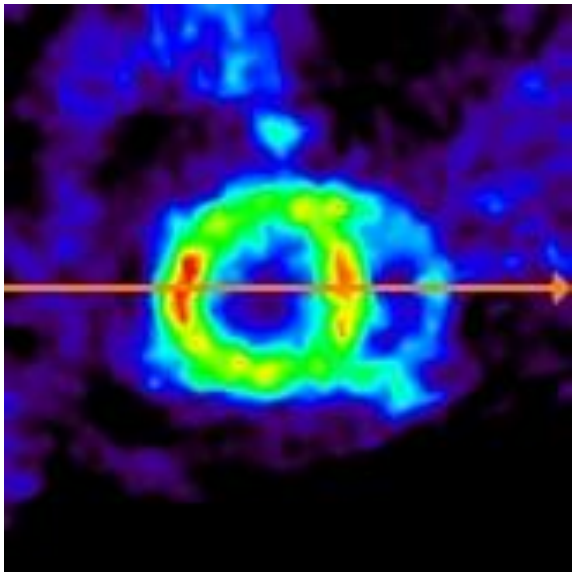

Figure 10 Short-axis image of a ZL rat with vector for line-profile.

Short axis image of the heart of a ZL rat at the mid-ventricular part from AMIDE. It shows the LV and the right ventricle. The orange arrow was set by the programm AMIDE to calculate the corresponding line-profile (count profile) on this line in the direction of the arrow.

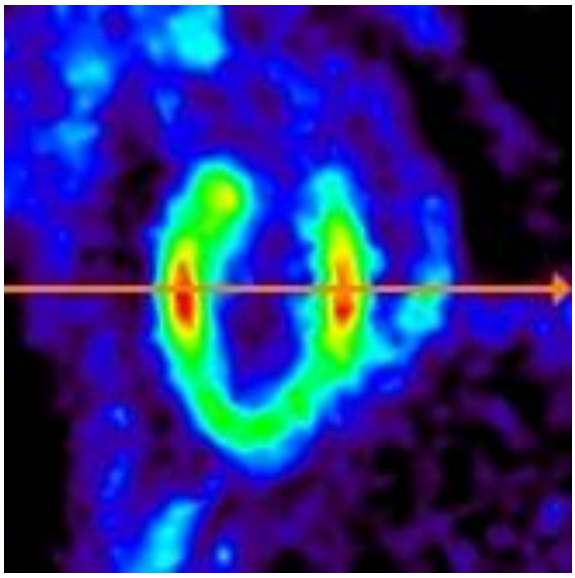

Figure 11 Coronal view of a ZL rat with vector for line-profile.

Corresponding long axis view (coronal) of the heart of the ZL rat from **Figure 10**.

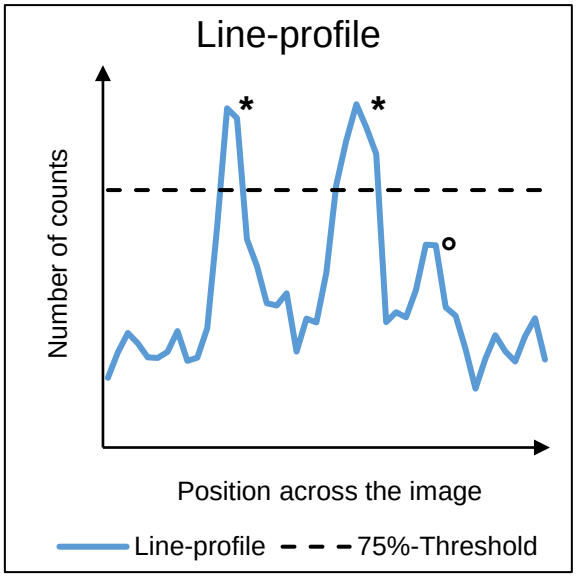

Graph 1 Line-profile of **Figure 10** and **Figure 11**.

Line-profile of the two above shown images derived from AMIDE. The 75 percentage threshold line was added to demonstrate the calculation of the myocardial boarders by HFV. The two big peaks (*) correspond to the LV and the smaller right peak (°) corresponds to the right ventricle.

Figure 12 Determination of the myocardial contour by Heart Function View.

This figure shows a screenshot of the workingplace of the program HFV and an enlarged view of three selected slices. It shows a selection of different cuts through the LV of a representative ZL rat. According to the upper explination HFV detects the myocardial boarder automaticelly by the line-profile curves.

The images have been rearranged by using Powerpoint 2016 (Microsoft Office 365 ProPlus).

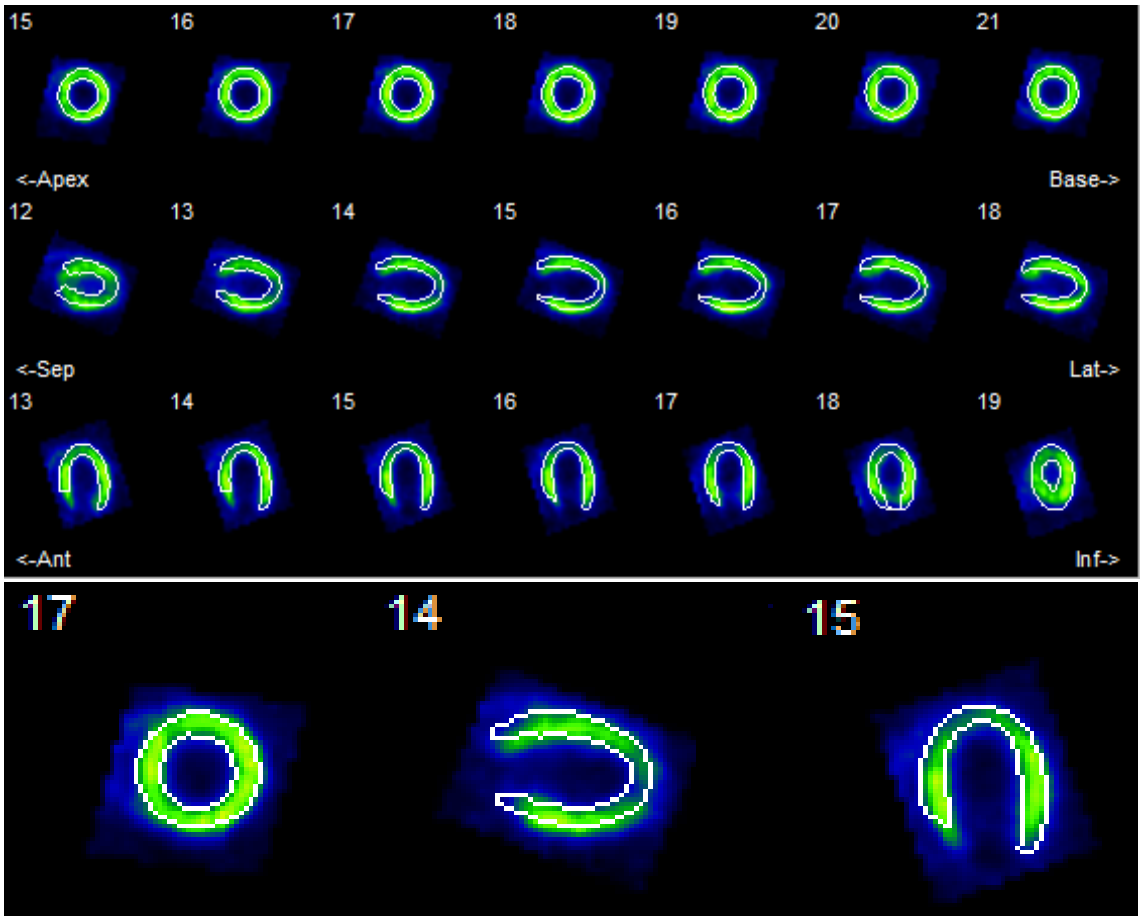

3.7 **Evaluation of left ventricular performance**

The evaluation of the LV data was also carried out by HFV, which was designed for evaluating the LV function from ECG-gated SPECT in human patients. This program enables to provide the systolic and diastolic function parameters by analysing the time-volume curve and its first derivation curve (time-filling curve). To adjust the animal heart size to the detection software for human study, the voxel size of the reconstructed images was magnified by a factor of five. The calculated parameters included EDV, ESV, EF, first-third ejection fraction (1/3 EF), peak filling rate (PFR), first third mean filling rate (1/3 FR), and time to peak filling rate (TPR). All calculated parameters and their meaning are shown in **Table 1**. The LV volume values (EDV, ESV and SV) were calculated from the LV volume/time curve (**Figure 13**) and are reported in microliters (µl). The values for the LVEF are reported as percentages. The PFR, expressed in EDV/s, is the highest detected filling rate during early diastole normalized to the EDV and represents the maximum value of the time-filling curve of the diastole. The TPF, expressed in milliseconds, is the measured time between the end of systole and the detection of the PFR. **Figure 13** shows a representative example of the time-volume and time-filling curve from HFV with explanations. Further parameters such as CO were calculated manually.

The ECG-gated PET was the only modality used for the assessment of the LV volumes, systolic and diastolic function parameters.

Table 1 Parameters from Heart Function View

Parameter	Unit	Meaning
General heart function parameters		
Heart rate (HR)	Beats/ min	Average number of registered R-peaks per minute
R-R duration	ms	Average duration of R-R interval
Frame duration	ms	Average duration of the frames
End-diastole to End-systole	ms	Time from the highest detected volume to the lowest detected volume
Left ventricular volumes		
End-diastolic volume (EDV)	µl	Highest detected volume per cardiac cycle
End-systolic volume (ESV)	µl	Lowest detected volume per cardiac cycle
Stroke volume (SV)	µl	Difference between the highest and lowest detected volumes
Systolic parameters		
Ejection fraction (EF)	% of EDV	Percentage of the SV compared to the EDV
Cardiac output (CO)	µl /min	Volume of blood which is ejected by the heart per minute
Peak ejection rate (PER)	ml/s	Highest detected ejection rate of the left ventricle per second
Time to peak ejection (TPE)	ms	Registered time from the end of diastole to the highest registered ejection
Time to end-systole (TES)	ms	Time from end of diastole to the end of systole
1/3 Ejection fraction (1/3EF)	% of EDV	Percentage of ejected volume compared to EDV, after one third of the duration of the systole
Diastolic parameters		
Peak filling rate (PFR)	ml/s	Highest detected filling rate of the left ventricle per second
1/3 Filling rate (1/3 FR)	ml/s	Ejected volume after one third of the diastole per second
1/3 Filling fraction (1/3FF)	% of EDV	Percentage of intraventricular volume after one third of the diastole compared to EDV
Time to peak filling (TPF)	ms	Registered time from the end of systole to the detection of the PFR
Time to peak filling / R-R duration (TPF cor.)	ms	Time to peak filling in relation to the total duration of the cardiac cycle

Figure 13 Left ventricular volume curve and left ventricular filling curve.

This figure shows the average calculated LV time-volume curve (upper curve) and its first deviation the time-filling curve (lower curve) of a representative ZL rat from HFV. The orange, green and blue arrows and writing were added afterwards by using PowerPoint, to visualize how the different parameters were calculated from the curves. For the evaluation, the systole and diastole, both were separated in three parts of identical duration. The orange arrows are the systolic parameters and the green arrows are the diastolic parameters.

The curves have been generated by the program HFV and were modified by using the program Powerpoint 2016 (Microsoft Office 365 ProPlus).

EDV = end-diastolic volume; ESV = end-systolic volume; SV = stroke volume; TPE = time to peak ejection; TES = time to end systole; 1/3ER = first third ejection rate, PER = peak ejection rate; PFR = peak filling rate; 1/3FR = first third filling rate; TPF = time to peak filling.

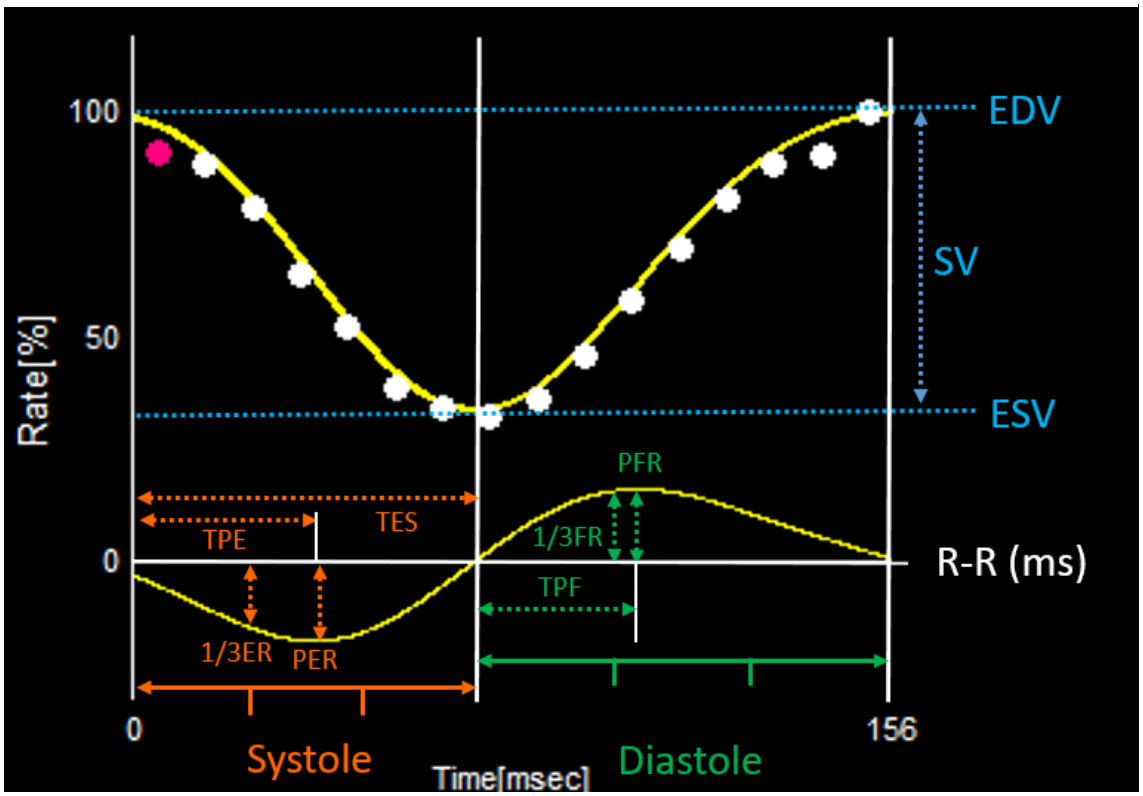

3.8 **Ex-vivo data collection**

Immediately after the ECG-gated ^{18}F-FDG PET acquisition, the animals were euthanized by decapitation. The hearts were excised, collected.

3.9 **Statistics**

The statistical assessment was carried out by means of Microsoft Excel 2016 (MSO 32-bit software package). All data are expressed as a mean ± standard deviation (SD). To assess the difference in values between the diabetic model ZDF rats and the ZL control rats, a two-tailed Student's t-test was performed. A significant group difference was assumed at a p-value below 0.05.

4 Results

As consequence of an insufficient ECG signal, ECG-gating could not be performed in two rats of the model group and thus no valuable heart function data could be received for these animals. In addition, sufficient images could not be derived in consequence of low count density in one animal of the control group, which was caused by an insufficient myocardial FDG uptake. Therefore, these three animals were excluded from the following evaluation.

For the comparison of the LV volumes, systolic and diastolic parameters between the ZDF and the ZL rats, only the reconstruction with 16 gates per cardiac cycle was used.

4.1 Animal characteristics

The body weight of the ZL rats was 289.8 ± 14.7g and of the ZDF rats 382.0 ± 54.6g. At the time of the PET scan, the weight of the ZDF rats was slightly higher than the weight of the ZL rats ($P < 0.01$). The increased body weight of the ZDF rats indicate that ZDF rats have developed obesity at the time point of PET. The blood glucose levels were assessed continuously during the experiment. The fasting blood glucose level was significantly higher in the model group (239.0 ± 77.8 mg/dl) compared to the control group (114.0 ± 14.8 mg/dl) ($P < 0.01$). The M-values, calculated by glucose infusion rate between FDG injection and completion of PET data acquisition, was significantly lower in the ZDF model rats (52.6 ± 30.5 µmol/min/kg) than in the ZL control rats (152.6 ± 27.4 µmol/min/kg) ($P < 0.001$). These changes in the glucose homeostasis reflect systemic insulin resistance in the ZDF model rats and show the development of a manifest diabetes at the timepoint of the experiments. The data are shown in **Table 2**.

4.2 Heart characteristics

The HR of the rats was registered during the whole PET scan (35 min). The ZDF rats showed with 305.7 ± 19.3 beats/min a lower average HR than the ZL rats with 329.7 ± 35.5 beats/min, but this difference did not reach a statistical significance ($P = 0.26$). The mean value of the R-R interval calculated from HFV was also lower in the ZDF rats compared to the ZL rats (ZDF 183.7 ± 19.3 ms

versus ZL 195.4 ± 15.2 ms) (P = 0.27) and the mean frame duration was shorter in the ZDF rats (ZDF 11.5 ± 1.2 ms versus ZL 12.2 ± 0.9 ms) (P = 0.26). The mean SD of the R-R duration was lower in the ZL rats than in the ZDF rats (ZL 3.6 ± 1.1 ms versus ZDF 7.9 ± 7.8 ms) (P = 0.24).

Table 2 Data for animal characteristics and insulin resistance of ZDF model rats and ZL control rats.

Parameter	ZL rats (control)	ZDF rats (model)	ZDF vs. ZL P-value
Body weight (g)	289.8 ± 14.7	382.0 ± 54.6	**< 0.01**
Fasting blood glucose (mg/dl)	239.0 ± 77.8	114.0 ± 14.8	**< 0.01**
Mean clamp glucose (µl/ml)	88.0 ± 16.0	6.8 ± 3.3	**< 0.001**
M-value (µmol/min/kg)	152.6 ± 27.4	52.6 ± 30.5	**< 0.001**

Data are presented as mean values ± SD.

Table 3 Mean left ventricular function parameters of ZL control rats and ZDF model rats.

Parameter	ZL rats(control)	ZDF rats (model)	ZDF vs. ZL P-value
Heart rate (bts/min)	329.7 ± 35.5	308.7 ± 24.1	0.26
R-R (ms)	183.7 ± 19.3	195.4 ± 15.2	0.27
Frame Duration (ms)	11.5 ± 1.2	12.2 ± 0.9	0.26
SD R-R (ms)	3.6 ± 1.1	7.9 ± 7.8	0.24

Data are presented as mean values ± SD.

4.3 **Cardiac images**

The images of the heart are exported from AMIDE and HFV. They represent the number of counts, generate through the decay of Fluorine-18 (^{18}F), and thus the distribution of ^{18}F-FDG in the whole body, encoded in colour. **Figure 14** shows a coronal and a sagittal picture of the whole FOV of a representative ZL rat and further demonstrates a high FDG uptake in the eyes, the brain and the heart of the rat. Lower uptake could be visualized in the muscles and the kidneys (see ***Figure 14***).

For the evaluation of the LV morphology, the whole-body images were rotate and focused on the heart to receive an optimal view of the LV in all three axes (see **Figure 15**). All hearts of both the control and model group showed a continuous FDG uptake of the whole myocardium. No scar could be detected. In some rats, the right ventricle, which shows a distinct lower ^{18}F-FDG uptake as consequence of the thinner myocardial wall, could also be visualized (see **Figure 15**). Accordingly, glucose metabolism assessed by ^{18}F-FDG uptake demonstrated vital myocardium in the whole heart of all ZDF and ZL rats. **Figure 16** shows a representative selection of gated short axis images from apical to the base in a representative ZL control rat at end-systole (ES) and end-diastole (ED). The gated short axis images demonstrate the thickening of the myocardial wall in the systole as result of the contraction and its thinning during diastole in the process of relaxation. The myocardial wall is thickened at the time point of ES and thinned at the point of ED. The intraventricular diameter and thus the intraventricular blood volume are higher at the ED than at ES (compare to **Figure 16**). In **Figure 17** gated short axis images of every gate of the cardiac cycle are shown together with the according time-volume and time-filling curve. This image sequence demonstrates the motion of the LV walls and the LV volume changes during the entire cardiac cycle. Also, the thickening of the LV is demonstrated. ***Figure 18*** shows the three-dimensional reconstruction of the heart at ES and ED of the same control rat like in **Figure 17** out of three different perspectives. The distance between the outer and inner myocardial border is higher during the systole, what demonstrates the contraction and thereby the thickening of the myocardial wall during systole.

Furthermore, the contraction and thereby the reduction of the LV volume in the systole is shown. The intraventricular volume is distinct higher at the time point of ED than at the time-point of ES.

Figure 14 Image of the whole field of view.

Image of the whole FOV of a ZL rat in coronal (A) and in sagittal (B) view derived from the software AMIDE. The heart (*) and the eyes (#) are showing the highest FDG-uptake. Also the muscles (↑) and the kidney (º) are visible.

These images have been generated using AMIDE and modified by using Powerpoint 2016 (Microsoft Office 365 ProPlus).

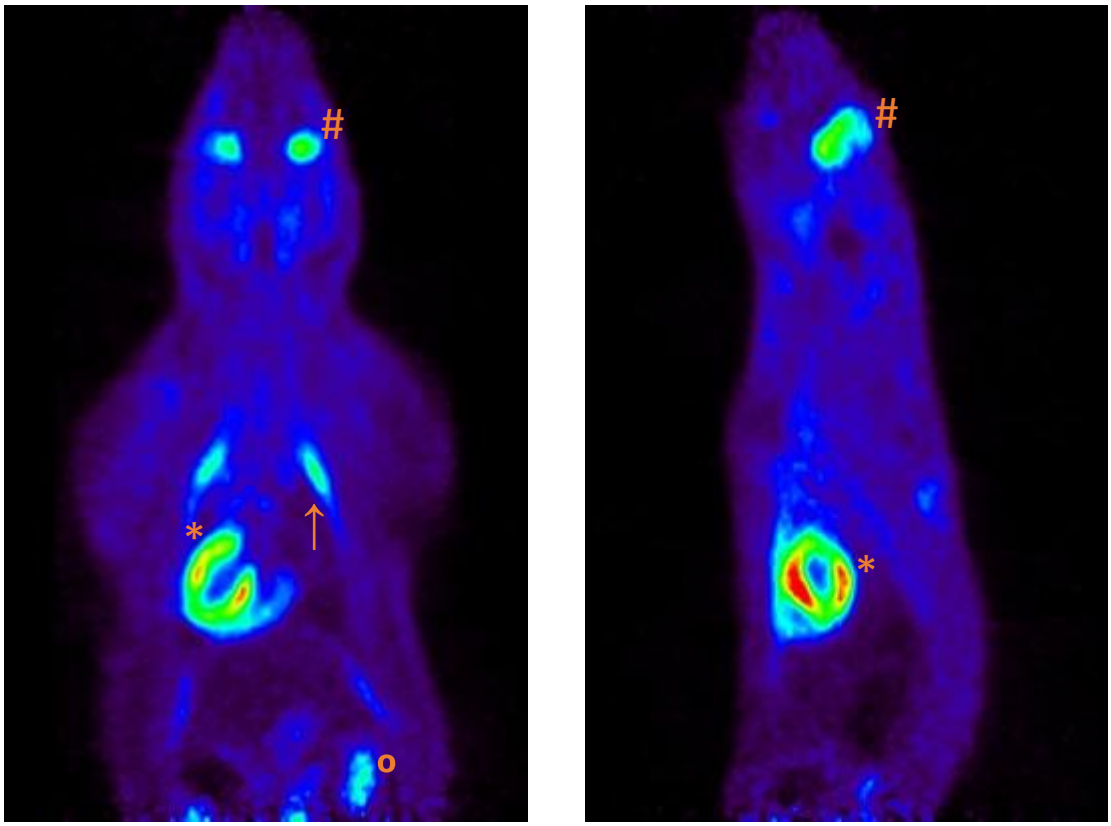

Figure 15 Reconstructed rearranged non gated images of the heart.

Reconstructed non gated PET images of the rotated heart of a ZL rat in sagittal (A) and coronal (B) long axis view and in eight short axis transverse pictures (from the apex C to the base K) exported from AMIDE. The LV (*) is showing a high number of counts and thus a high ^{18}F-FDG uptake in the myocardial wall. The right ventricle (#) is also visible, but shows a distinct lower ^{18}F-FDG uptake, which is caused by its lower wall thickness. The heart apex is marked with a ↑ and the heart base with a ↓ in the long axis images (A+B).
The heart is showing a homogenous ^{18}F-FDG uptake in all images. No scar could be detected.

These images have been generated using AMIDE and modified by using Powerpoint 2016 (Microsoft Office 365 ProPlus).

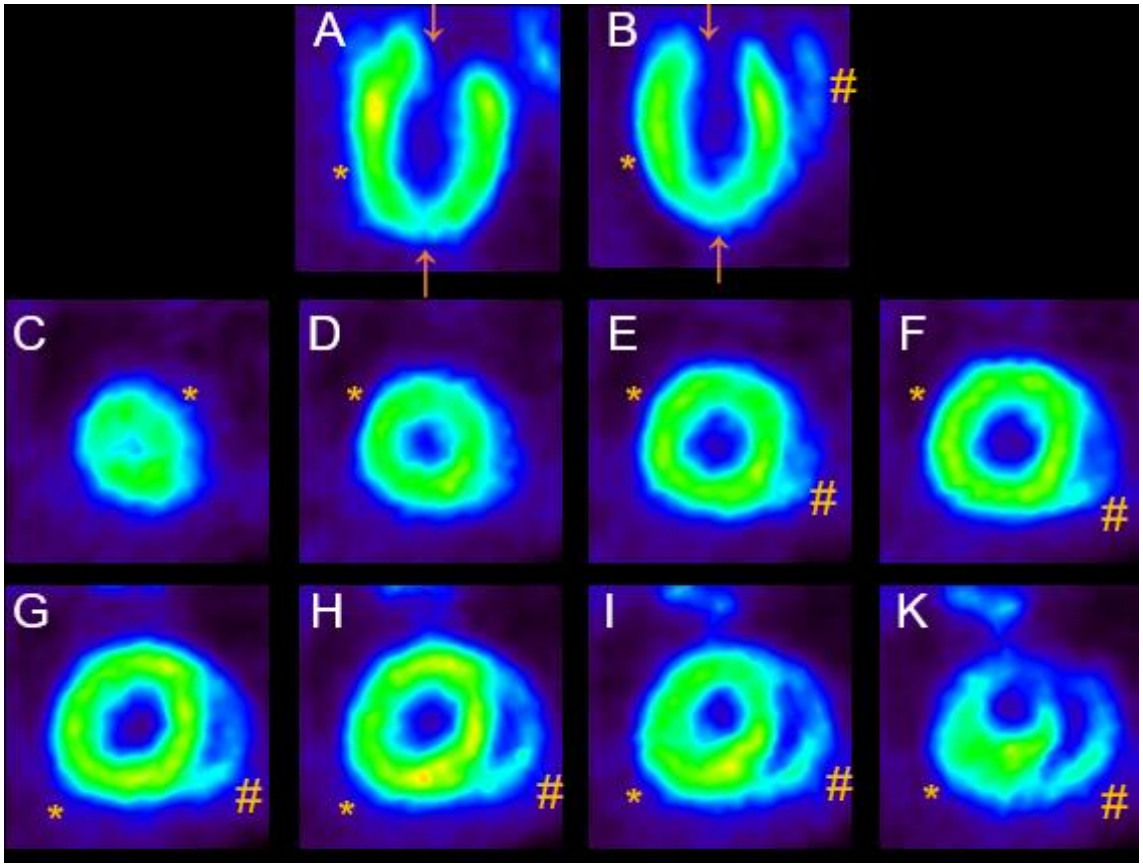

Figure 16 Rearranged gated images of the heart.

Gated images of the heart of a ZL rat during the ES (A-F) and ED (G-L) phase in coronal (A, G) and sagittal (B, H) and in short axis slices (C-F and I-L) at different high of the heart, form close to the apex (C and I) to the base (F and L).

These images have been generated using AMIDE and modified by using Powerpoint 2016 (Microsoft Office 365 ProPlus).

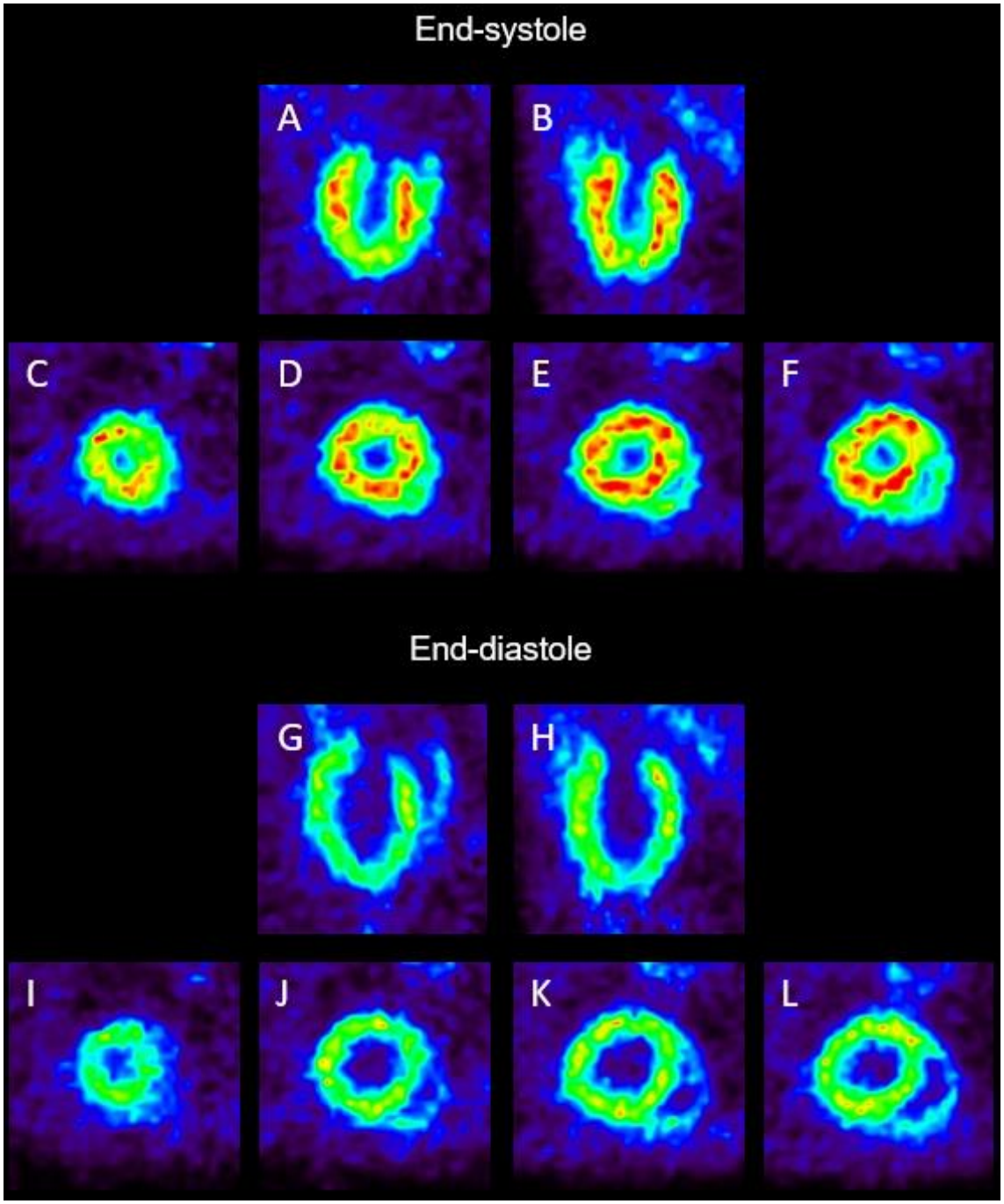

Figure 17 Time-volume curve and Time-filling curve of one ZL rat and the according gated short axis images.

Time-volume curve and its first derivation, the Time-filling curve, of one ZL rat generated by HFV. The points on the curve mark the calculated volumes of each gate. Gated short axis images of the same mid-ventricular part of the heart were generated for each gate by AMIDE. The pictures are ordered according to the Time-volume curve. Picture seven marks the timepoint with the least blood volume in the LV and is the time point of ES. Picture 16 marks the time-point with the highest LV volume and is according the EDV.

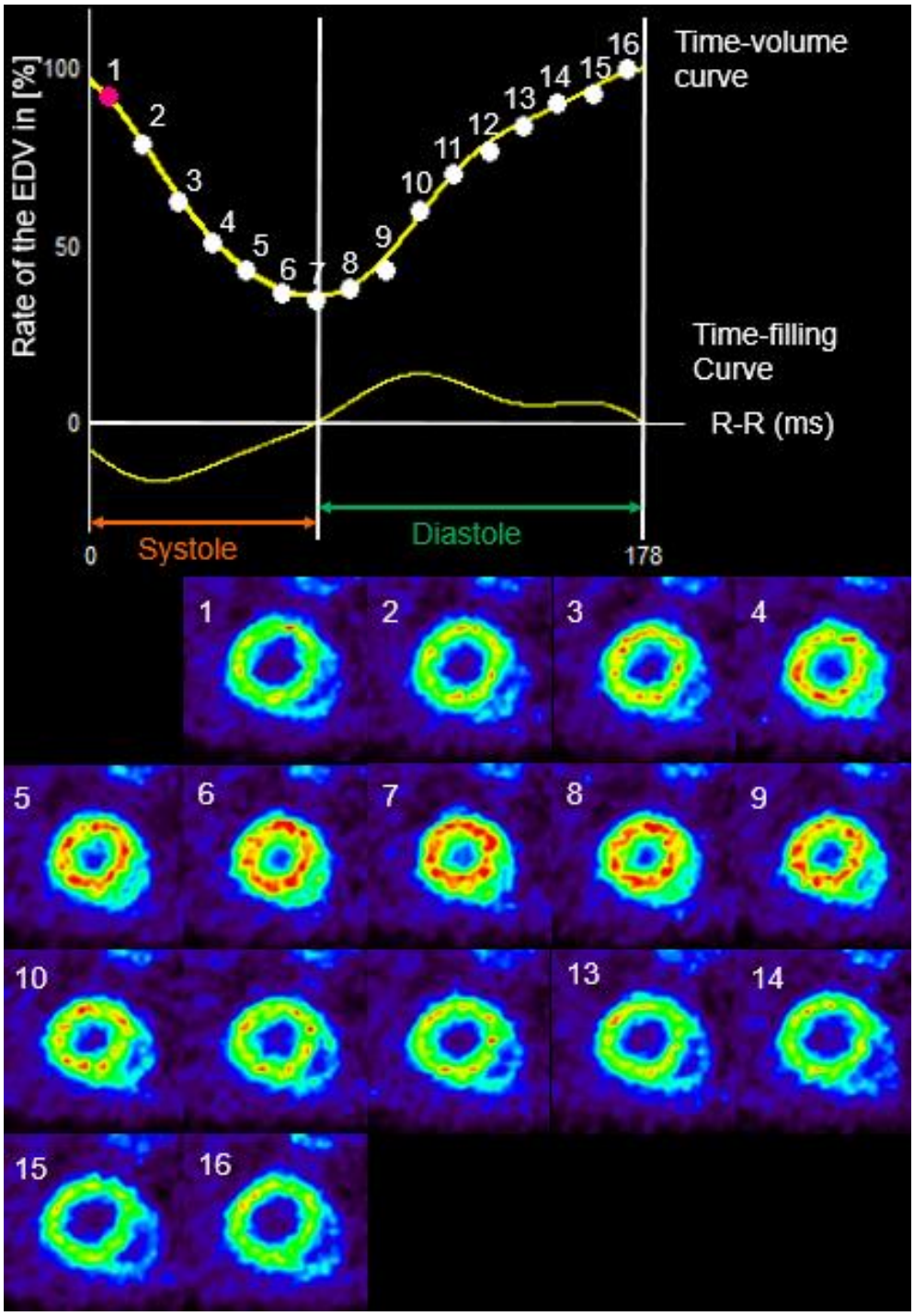

Figure 18 Three-dimensional reconstruction of the left ventricle.

Three-dimensional reconstructed model of the LV of one ZL rat at the time-point of ES (A-C) and ED (D-F), derived from HFV. The LV is shown in anterior (A, D), lateral (B, E) and apex (C, F) view. The net surface is representing the outer border of the LV myocardial wall and the colour surface represents the inner or endocardial border of the myocardium. The volume enclosed by the inner myocardial wall represents the intraventricular blood volume.

Ant. = anterior; lat. = lateral; inf. = inferior; sep. = septal.

These images have been generated using HFV and modified by using Powerpoint 2016 (Microsoft Office 365 ProPlus).

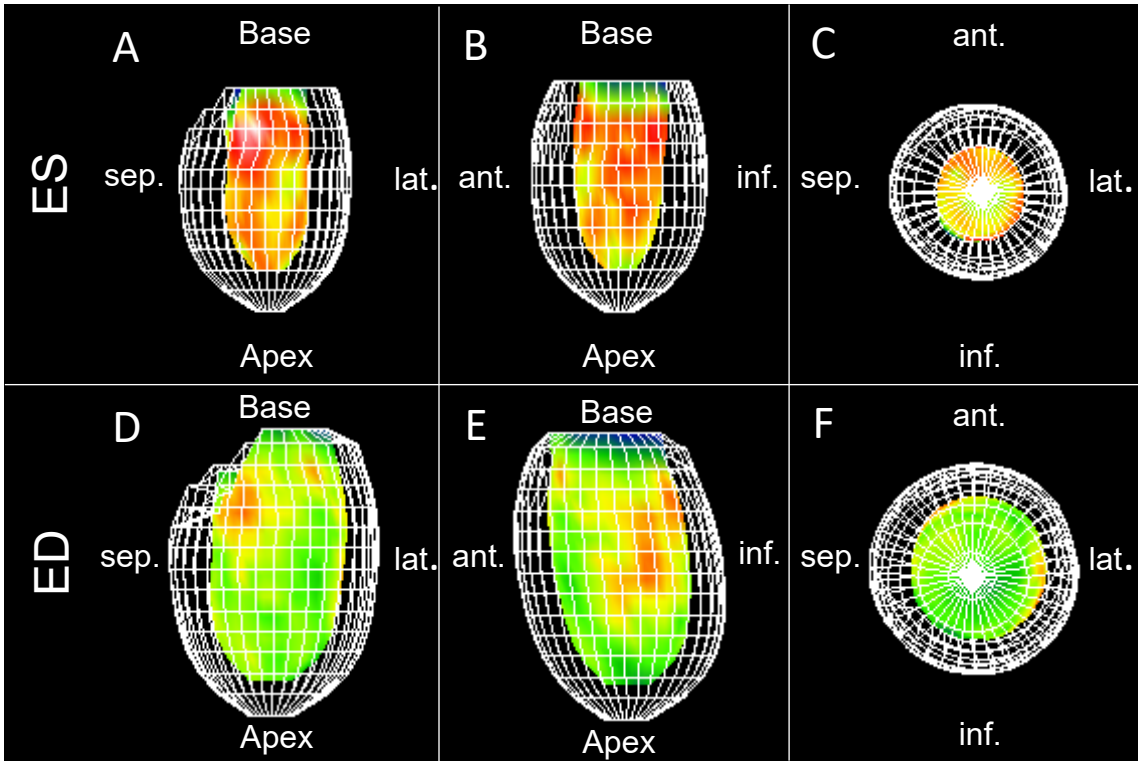

4.4 **Reconstruction and histogramming time**

The average time which was required for reconstruction and histogramming of all rats with different numbers of frames per cardiac cycle is shown in **Graph 2**. In all reconstructions the acquired time for histogramming was higher than the required time for the reconstruction.

The average total time required for histogramming and reconstruction was for 16 bins 52 minutes and 57 seconds (reconstruction time: 47 min and 20 s; histogramming time: 5 min and 37 s), for twelve bins 41 minutes and 27 seconds (reconstruction time: 37 min and 17 s; histogramming time: 4 min and 10 s), for eight bins 27 minutes and 31 seconds (reconstruction time: 24 min and 55 s; histogramming time: 2 min and 36 s) and for four bins 15 minutes and 33 seconds (reconstruction time: 14 min and 15 s; histogramming time: 1 min and 18 s), respectively. The time for reconstruction and histogramming increases with the number of gates per cardiac cycle.

Graph 2 Average image reconstruction and histogramming time.

This graph shows the average time (in hh:mm:ss), which was required to transform the list mode data of the PET scan with ECG recording in histogram files according to the number of bins (blue part of the bars) and to reconstruct these scan-files (sinograms) into an image data (orange part of the bar) of all rats (ZDF and ZL, n=12).

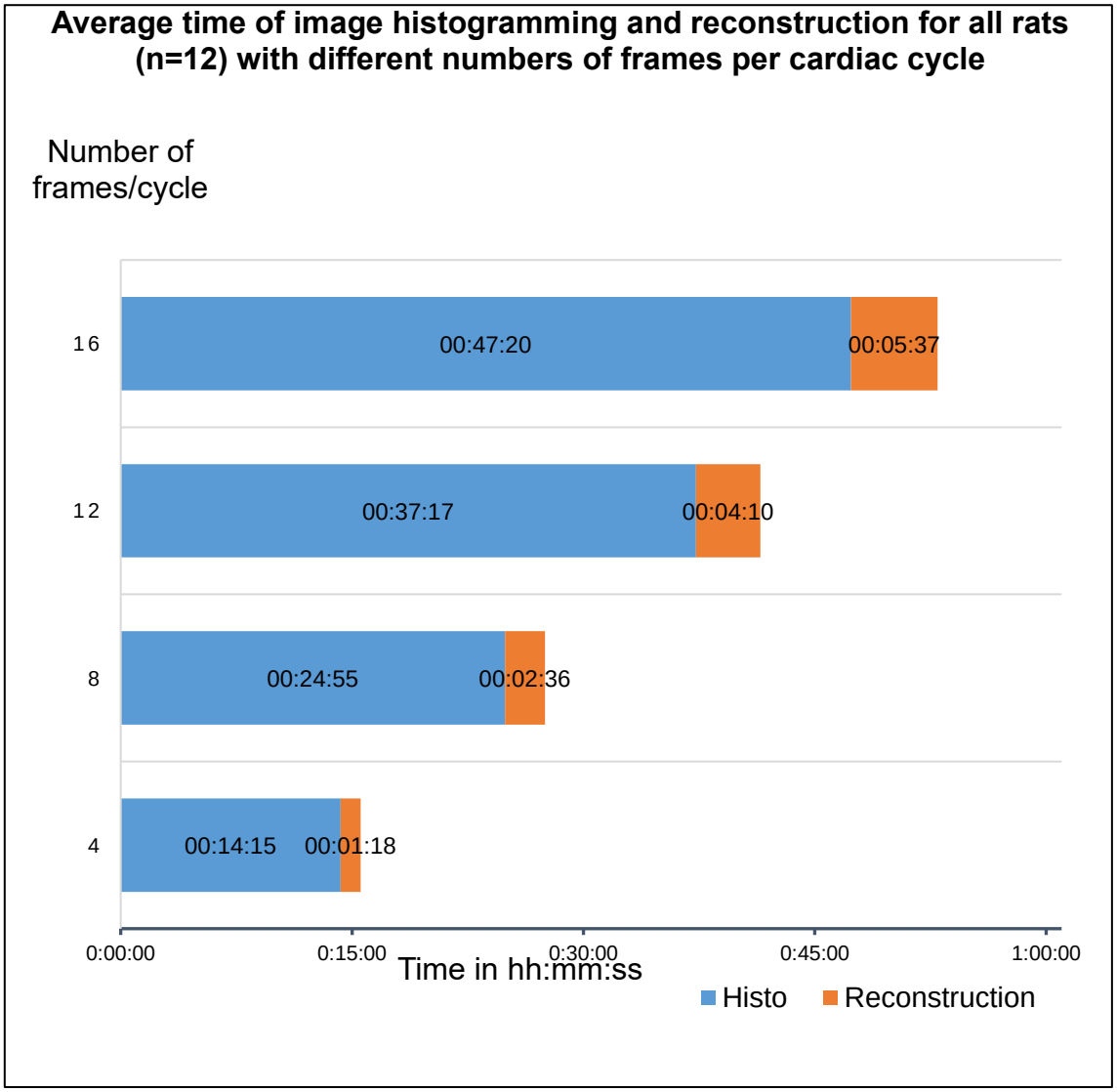

4.5 Influence of gates per cardiac cycle on the LV volumes and function parameters

All values from HFV of each reconstruction of all rats (controls and models) were calculated and compared to the reconstruction with 16 gates per cycle since these data provides the best temporal resolution. All the calculated values are shown in **Table 4** and **Table 5**. The values which differ significantly between the different reconstructions are shown more detailed below.

Short axis and long axis images at different timepoints of the cardiac cycle were acquired and compared to evaluate the difference in the spatial resolution. The spatial resolution of the myocardial wall was higher in the images of the reconstruction with only four images per cardiac cycle than in all the other reconstructions. The images of the reconstructions with 16 gates per cardiac cycle showed the lowest spatial resolution.

Figure 20 shows a selection of transversal and coronal images of a control rat at ES and ED. For all reconstructions, a continuous ^{18}F-FDG uptake in the whole myocardium was detected. It demonstrates that with an increasing number of frames per cardiac cycle the spatial resolution as consequence of the lower count number is decreasing.

The time-volume and time-filling curves of the reconstructions with four, eight, twelve and 16 gates per cardiac cycle were generated and compared (see ***Figure 19***). The calculated intraventricular volumes of the reconstructions with only four gates per cardiac cycle where far of the calculated time-volume curve, which furthermore showed a wavelike course (compare ***Figure 19*****a**). With increasing number of gates per cardiac cycle the time volume curve is becoming smoother. The temporal resolution and thereby the accuracy of the time-volume curve is increasing with the number of gates acquired per cardiac cycle.

Figure 19 Time-volume and time-filling curves of the same ZL rat from HFV, reconstructed with a different number of bins.

This figure shows the time-volume curve and the time-filling curve calculated from HFV of the reconstructions with a) four, b) eight, c) twelve and d) 16 gates per cardiac cycle modified using Powerpoint 2016 (Microsoft Office 365 ProPlus). The white spots are the calculated intraventricular volume of the LV of each gate. The yellow line is the time-volume curve, which was calculated based on the single volume values of each gate. It demonstrates that the curve is more exact or better fitted the more gates per cardiac cycle exist. (EDV = end diastolic volume)

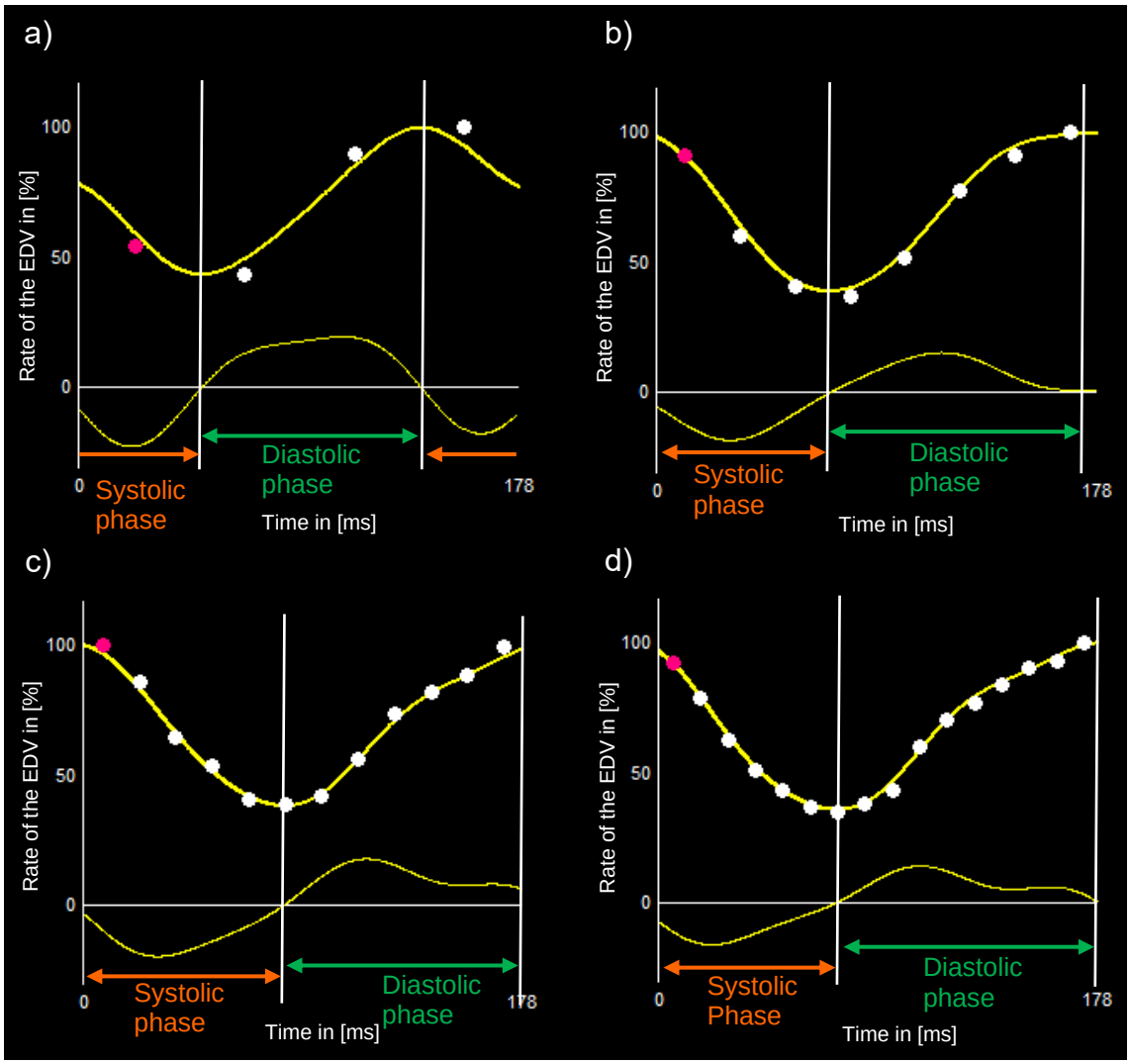

Figure 20 Long- and short axis view at end-systole and end-diastole with different numbers of bins.

This figure shows a short-axis view (transversal) of the mid-ventricular part and a long-axis view (coronal) of the same ZL rat at the ES and ED reconstructed with a different number of gates per cardiac cycle derived from the program AMIDE.

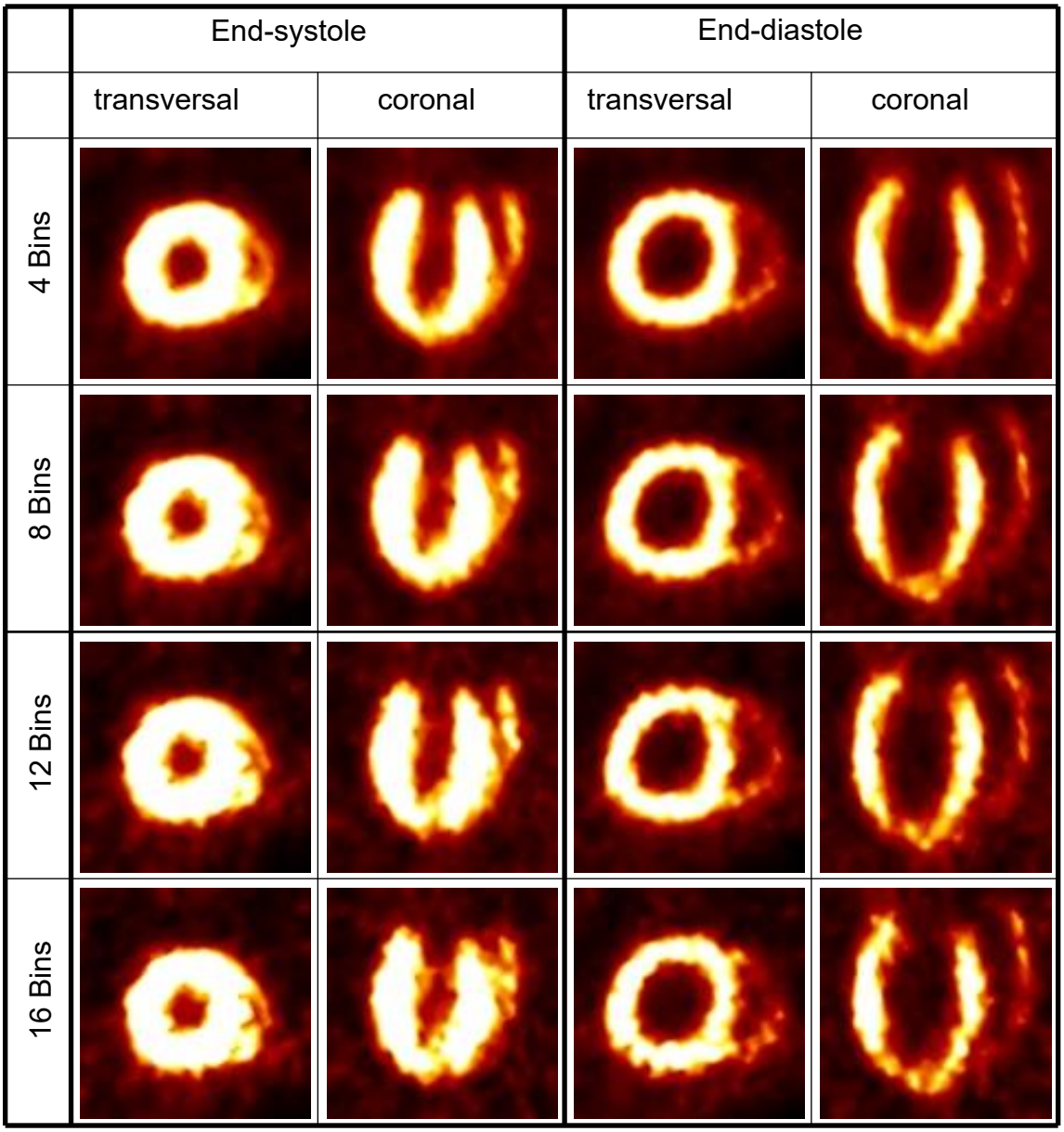

4.5.1 Left ventricular volumes and ejection fraction

The reconstruction with four gates (353.8 ± 57.7µl, $p < 0.01$) and with eight gates (380.3 ± 57.2µl, $p < 0.05$) per cardiac cycle delivered a significant different average EDV than the reconstruction with 16 gates (444.8 ± 75.3µl). No significant differences concerning the average EDV could be found between the reconstruction with twelve gates (398.0 ± 63.1µl, $p = 0.11$) and with 16 gates per cardiac cycle (see **Graph 3**). The average ESV is increasing with the number of gates except from the calculation with only four gates/cycle (see **Graph 4**). No significant differences concerning the average ESV could be found between the reconstructions compared to the reconstruction with 16 gates (four gates: 168.3 ± 35.3µl; $p = 0.67$, eight gates: 156.9 ± 34.5µl; $p = 0.24$, twelve gates: 159.1 ± 35.2µl; $p = 0.31$, 16 gates: 174.6 ± 38.4µl). The average SV is increasing with the number of gates. The comparison with the 16 gates reconstruction revealed that the SV calculated from the reconstruction with four (185.5 ± 31.6µl; $p < 0.01$) and eight (223.5 ± 28.9µl; $p < 0.01$) bins was significantly lower than the SV calculated with 16 gates per cycle (270.2 ± 45.1µl). No significant differences concerning the average SV could be found between the reconstruction with twelve gates and with 16 gates per cardiac cycle (238.9 ± 32.0µl; $p = 0.06$) (see **Graph 5**). The average LVEF is increasing with the number of gates. The comparison revealed that the average LVEF calculated from the reconstruction with four bins (52.7 ± 5.1%; $p < 0.01$) was significantly lower than the EF calculated with 16 gates per cycle (61.0 ± 4.4%). No significant differences concerning the average EF could be found between the reconstruction with eight (59.1 ± 4.3%; $p = 0.30$) and twelve gates (60.4 ± 3.9%; $p = 0.73$) compared with 16 gates per cardiac cycle (see **Graph 6**). All values are shown in **Table 4**.

Table 4 Comparison of the left ventricular volumes between the reconstructions

No. of bins	4	vs 16	8	vs 16	12	vs 16	16
EDV (µl)	353.8 ± 57.7	**p < 0.01**	380.3 ± 57.2	**p < 0.05**	398.0 ± 63.1	p = 0.11	444.8 ± 75.3
ESV (µl)	168.3 ± 35.3	p = 0.68	156.9 ± 34.5	p = 0.24	159.1 ± 35.2	p = 0.31	174.6 ± 38.4
SV (µl)	185.5 ± 31.6	**p < 0.01**	223.5 ± 28.9	**p < 0.01**	238.9 ± 32.0	p = 0.06	270.2 ± 45.1
EF (%)	52.7 ± 5.1	**p < 0.01**	59.1 ± 4.3	p = 0.30	60.4 ± 3.9	p = 0.72	61.0 ± 4.4

Data are presented as mean values ± SD. EDV = end-diastolic volume; ESV = end-systolic volume; SV = stroke volume; EF = ejection fraction.

Graph 3 Average End-diastolic volume of all rats.

This graph shows the average calculated LV EDV from HFV of all rats (controls and models, n = 12) reconstructed with four, eight, twelve and 16 gates per cardiac cycle. The average EDV is increasing with the number of gates. Since the reconstruction with 16 bins provides the best temporal resolution, the differences between the other reconstructions and the one with 16 gates per cycle was made.

(EDV = end-diastolic volume; * = p < 0.05; ** = p < 0.01; ns = non-significant)

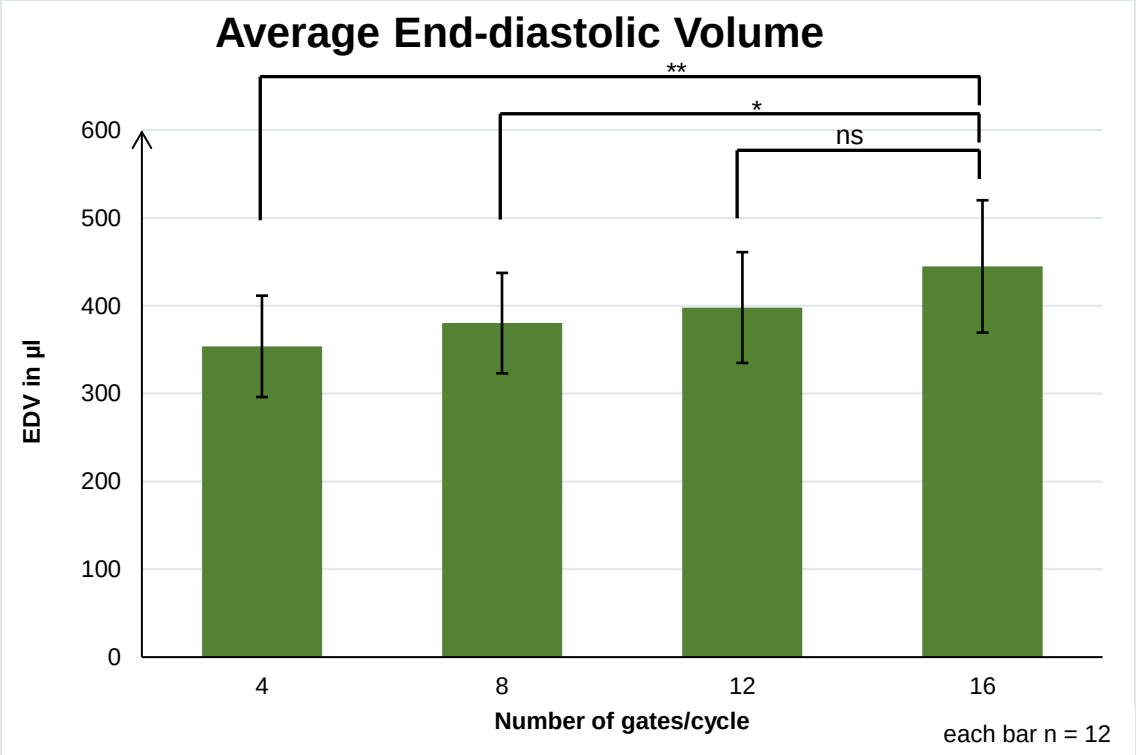

Graph 4 Average End-systolic volume of all rats.

This graph shows the average calculated LV ESV from HFV of all rats (controls and models, n = 12) reconstructed with four, eight, twelve and 16 gates per cardiac cycle. Since the reconstruction with 16 bins provides the best temporal resolution, the differences between the other reconstructions and the one with 16 gates per cycle was made.

(ESV = end-systolic volume ; ns = non-significant)

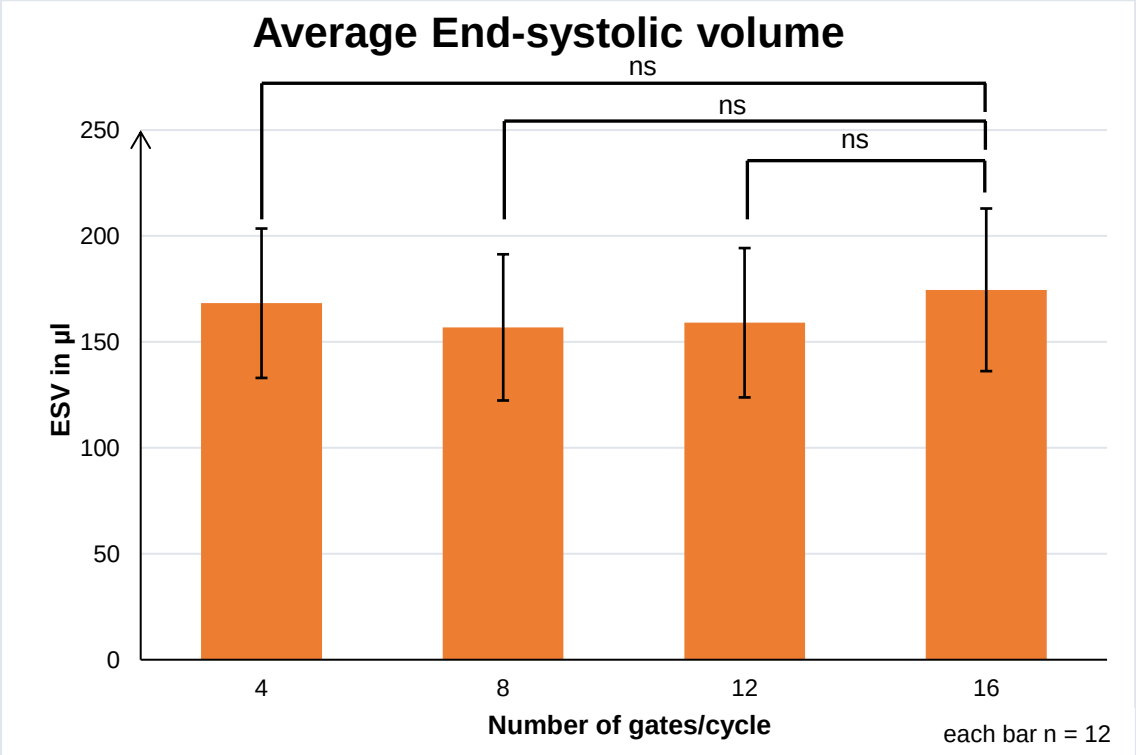

Graph 5 Average Stroke volume of all rats.

This graph shows the average calculated SV from HFV of all rats (controls and models, n = 12) reconstructed with four, eight, twelve and 16 gates per cardiac cycle. Since the reconstruction with 16 bins provides the best temporal resolution, the differences between the other reconstructions and the one with 16 gates per cycle was made.

(SV = stroke volume; ** = p < 0.01; ns = non-significant).

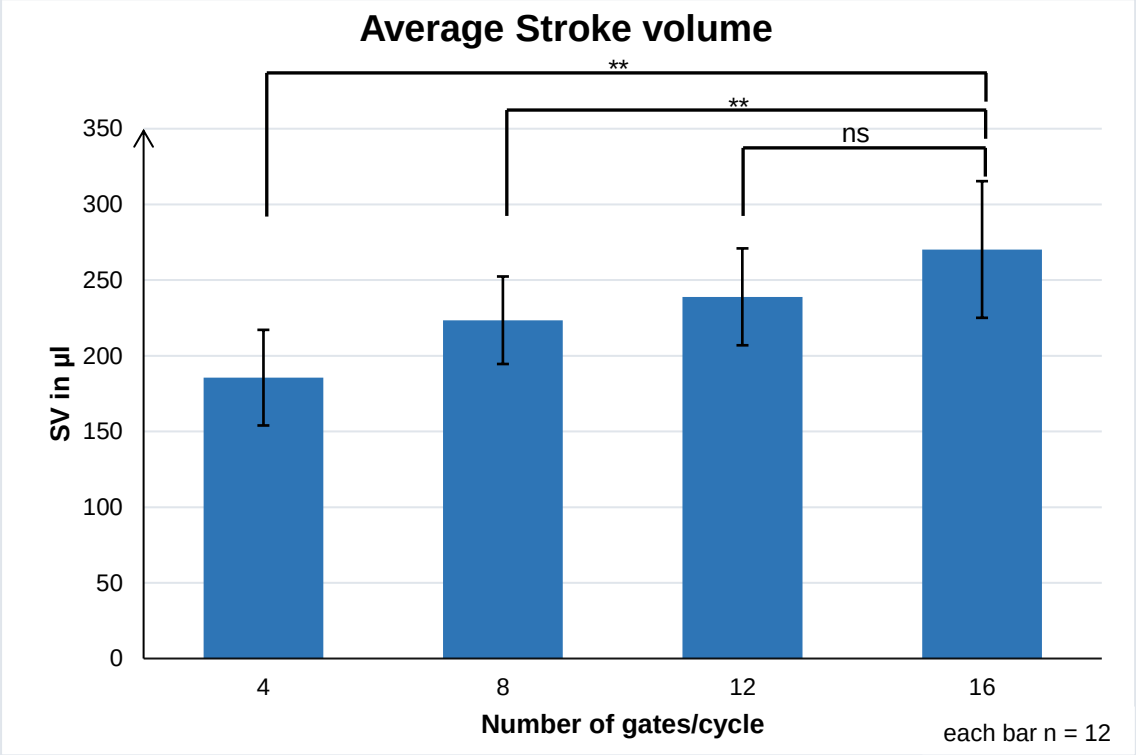

Graph 6 Average Ejection Fraction of all rats.

This graph shows the average calculated LV EF in percent, calculated by HFV of all rats (controls and models, n = 12) reconstructed with four, eight, twelve and 16 gates per cardiac cycle. Since the reconstruction with 16 bins provides the best temporal resolution, the differences between the other reconstructions and the one with 16 gates per cycle was made.

(SV = stroke volume; ** = p < 0.01; ns = non-significant)

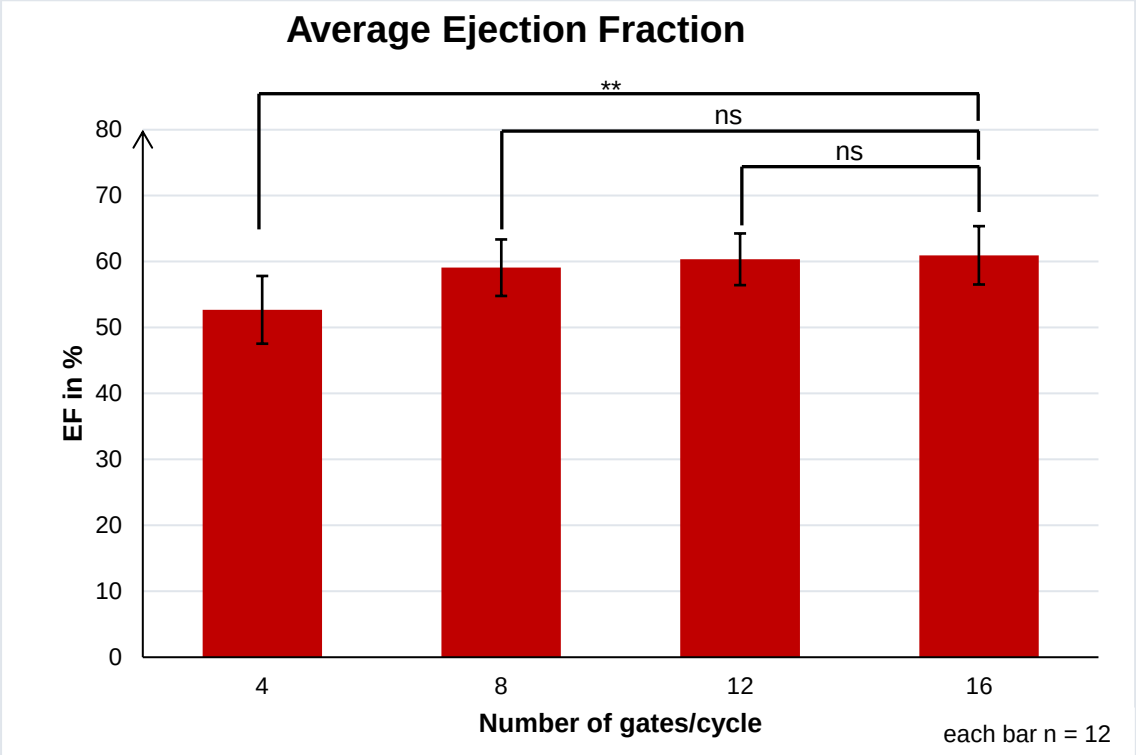

4.5.2 Systolic parameters

The comparison of the systolic parameters between the reconstructions with different numbers of gates per cardiac cycle revealed no significant difference for the 1/3 EF (four bins: 28.6 ± 6.7%; p = 0.08, eight bins: 21.8 ± 3.6%; p = 0.30, twelve bins: 24.2 ± 5.7%; p = 0.92, 16 bins: 23.9 ± 6.3%) and the TPE (four bins: 24.8 ± 5.8ms; p = 0.10, eight bins: 33.0 ± 5.2ms; p = 0.27, twelve bins: 29.6 ± 8.5ms; p = 0.96, 16 bins: 29.8 ± 8.2ms) for all reconstructions compared to the one with 16 gats per cycle. The TES was significantly lower in the reconstruction with four bins (57.9 ± 12.1ms; p < 0.01) than in the reconstruction with 16 bins (80.0 ± 9.1ms). No significant difference for the TES could be demonstrated concerning the reconstructions with eight (75.5 ± 10.0ms; p = 0.26) and twelve bins (77.9 ± 7.6ms; p = 0.55) compared to the one with 16 bins. Also, the PER was significantly lower in the reconstruction with four bins (9.8 ± 1.0ml/s; p< 0.01) than in the reconstruction with 16 bins (11.7 ± 1.4ml/s), but not in the reconstructions with eight (11.6 ± 1.5ml/s; p = 0.84) and twelve bins (11.5 ± 1.3ml/s; p = 0.76). A significant lower 1/3 ER was found in the comparison of the reconstruction with four gates per cardiac cycle (9.4 ± 1.1ml/s; p < 0.01) and 16 gates per cardiac cycle (11.1 ± 1.6ml/s). No significant difference could be shown concerning the 1/3 ER of the reconstructions with eight (10.8 ± 1.7ml/s; p = 0.71) and twelve bins (11.0 ± 1.5 ml/s; p = 0.98) compared to the one with 16 bins. All systolic parameters of the four reconstructions are also shown in **Table 5**.

4.5.3 Diastolic parameters

A significant lower PFR could be detected for the values of the reconstruction with four bins (8.5 ± 0.9ml/s; p < 0.01) compared to the reconstruction with 16 bins (11.2 ± 1.3ml/s). No significant difference could be found between the values of the eight bins (10.7 ± 1.2ml/s; p = 0.84) and twelve bins (10.9 ± 1.0ml/s; p = 0.76) reconstructions when compared to the reconstruction with 16 frames per cardiac cycle (see **Graph 7**). The comparison revealed that the corrected TPF (TPF cor.) calculated from the reconstruction with four (0.34 ± 0.03; p < 0.01) and eight bins (0.24 ± 0.02; p < 0.01) was significantly lower than the TPF (cor.) calculated with 16 gates per cycle (0.20 ± 0.02). No

significant differences concerning the average TPF (cor.) could be found between the reconstruction with twelve gates (0.22 ± 0.03; p = 0.13) and with 16 gates per cardiac cycle (see **Graph 8**). No significant differences could be detected for the 1/3 FF between the values from the four (37.3 ± 7.1%; p = 0.58), eight (35.9 ± 4.5%; p = 0.20) and twelve (37.4 ± 5.7%; p = 0.58) frames reconstruction in comparison to value from the reconstruction with 16 frames per cycle (38.8 ± 6.3%)(see **Graph 9**). Concerning the 1/3 FR, a significant difference could be demonstrated between the reconstruction with four bins (6.9 ± 1.0ml/s; p < 0.01) and 16 bins (11.0 ± 1.4ml/s), but not between the reconstructions with eight (10.1 ± 1.4ml/s; p = 0.13) and twelve bins (10.5 ± 0.8ml/s; p = 0.55) compared to the one with 16 bins. All diastolic parameters of the reconstructions are also shown in **Table 5**.

Table 5 Comparison of the systolic and diastolic parameters between the reconstructions.

No. of bins	4	vs 16	8	vs 16	12	vs 16	16
Systolic parameters							
EDtoES (msec)	93.7 ± 9.5	**p < 0.01**	87.3 ± 11.8	p = 0.30	79.2 ± 6.3	p = 0.17	83.0 ± 7.0
1/3 EF (%)	28.6 ± 6.7	p = 0.08	21.8 ± 3.6	p = 0.30	24.2 ± 5.7	p = 0.92	23.9 ± 6.3
TES (msec)	57.9 ± 12.1	**p < 0.01**	75.5 ± 10.0	p = 0.26	77.9 ± 7.6	p = 0.55	80.0 ± 9.1
PER (ml/sec)	9.8 ± 1.0	**p < 0.01**	11.6 ± 1.5	p = 0.84	11.5 ± 1.3	p = 0.76	11.7 ± 1.4
TPE (msec)	24.8 ± 5.8	p = 0.10	33.0 ± 5.2	p = 0.27	29.6 ± 8.5	p = 0.96	29.8 ± 8.2
1/3 ER (ml/sec)	9.4 ± 1.1	**p < 0.01**	10.8 ± 1.7	p = 0.71	11.0 ± 1.5	p = 0.98	11.1 ± 1.6
Diastolic parameters							
TPF (ms)	63.9 ± 7.5	**p < 0.01**	46.2 ± 6.0	**p < 0.01**	40.3 ± 6.2	p = 0.23	37.7 ± 4.2
TPF/R-R	0.34 ± 0.03	**p < 0.01**	0.24 ± 0.02	**p < 0.01**	0.22 ± 0.03	p = 0.13	0.20 ± 0.02
1/3 FR (ml/s)	6.9 ± 1.0	**p < 0.01**	10.1 ± 1.4	p = 0.13	10.5 ± 0.8	p = 0.38	11.0 ± 1.4
PFR (ml/s)	8.5 ± 0.9	**p < 0.01**	10.7 ± 1.2	p = 0.36	10.9 ± 1.0	p = 0.55	11.2 ± 1.3
1/3 FF (%)	37.3 ± 7.1	p = 0.58	35.9 ± 4.5	p = 0.20	37.4 ± 5.7	p = 0.58	38.8 ± 6.3

Data are presented as mean values ± SD. EDtoES = End-diastole to End-systole ; 1/3EF = 1/3 Ejection fraction; TES = Time to end-systole**;** PER = peak ejection rate; TPE = time to peak ejection; 1/3ER = first third ejection rate; TPF = time to peak filling; 1/3FR = first third filling rate; PFR = peak filling rate; 1/3 FR = 1/3 Filling rate.

Graph 7 Average peak-filling-rate of all rats.

This graph shows the average calculated PFR in ml/s from HFV of all rats (controls and models, n = 12) reconstructed with four, eight, twelve and 16 gates per cardiac cycle. Since the reconstruction in 16 bins provides the best temporal resolution, the differences between the other reconstructions and the one with 16 gates per cycle has been investigated.

(EDV = end-diastolic volume ; ** = p < 0.01; ns = non-significant p > 0.05)

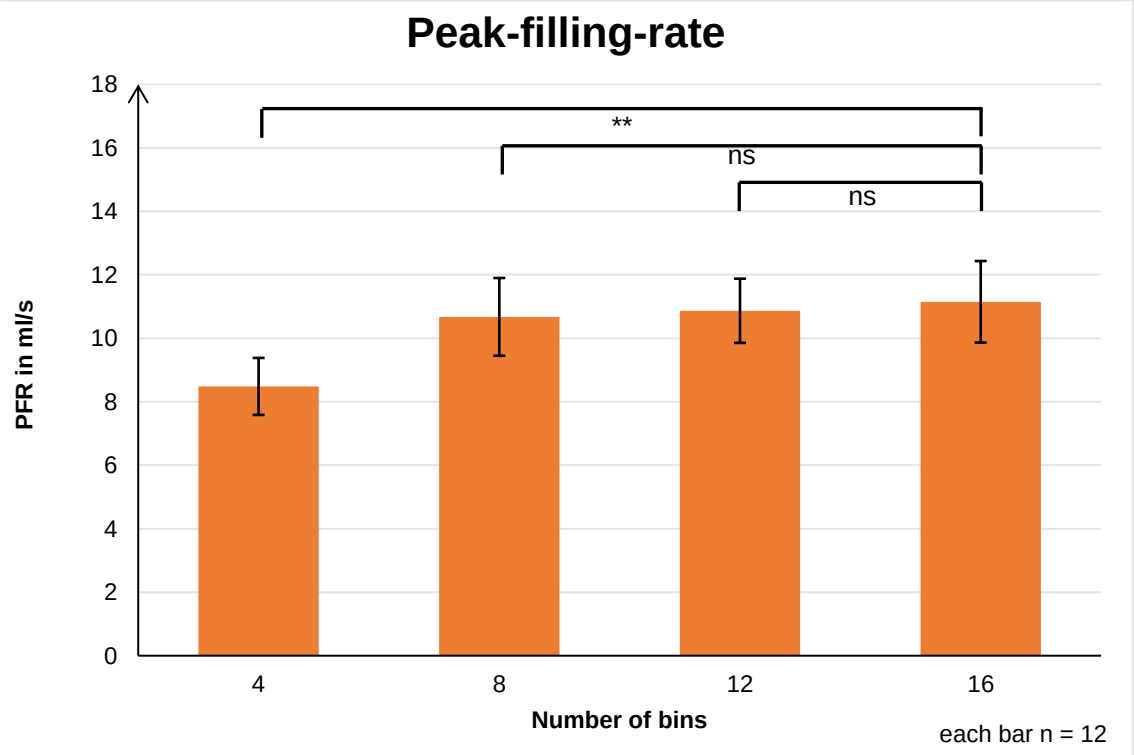

Graph 8 Average corrected time to peak-filling of all rats.

This graph shows the average calculated corrected TPF in ms from HFV of all rats (controls and models, n = 12) reconstructed with four, eight, twelve and 16 gates per cardiac cycle. Since the reconstruction in 16 bins provides the best temporal resolution, the differences between the other reconstructions and the one with 16 gates per cycle was made.

(** = p < 0.01; ns = non-significant p > 0.05)

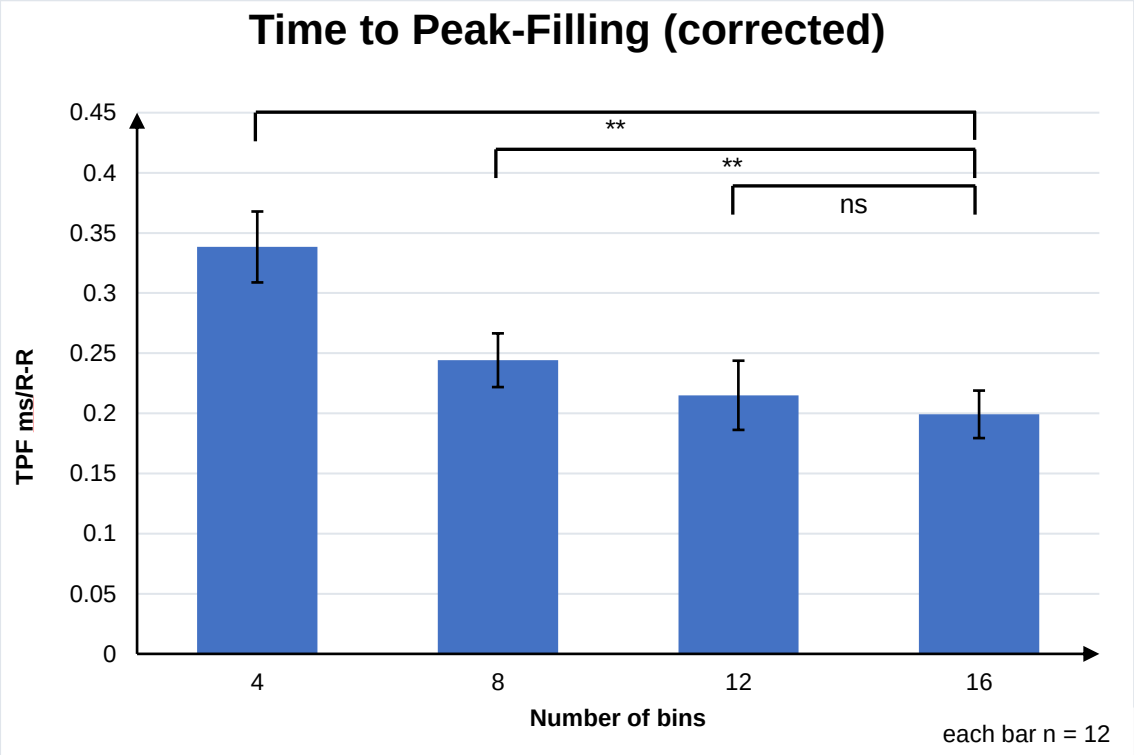

Graph 9 Average one third filling fraction of all rats.

This graph shows the average calculated 1/3FF of the LV in percent of the EDV from HFV of all rats (controls and models, n = 12) reconstructed with four, eight, twelve and 16 gates per cardiac cycle. Since the reconstruction in 16 bins provides the best temporal resolution, the differences between the other reconstructions and the one with 16 gates per cycle was made.

(EDV = end-diastolic volume; ns = non-significant p > 0.05)

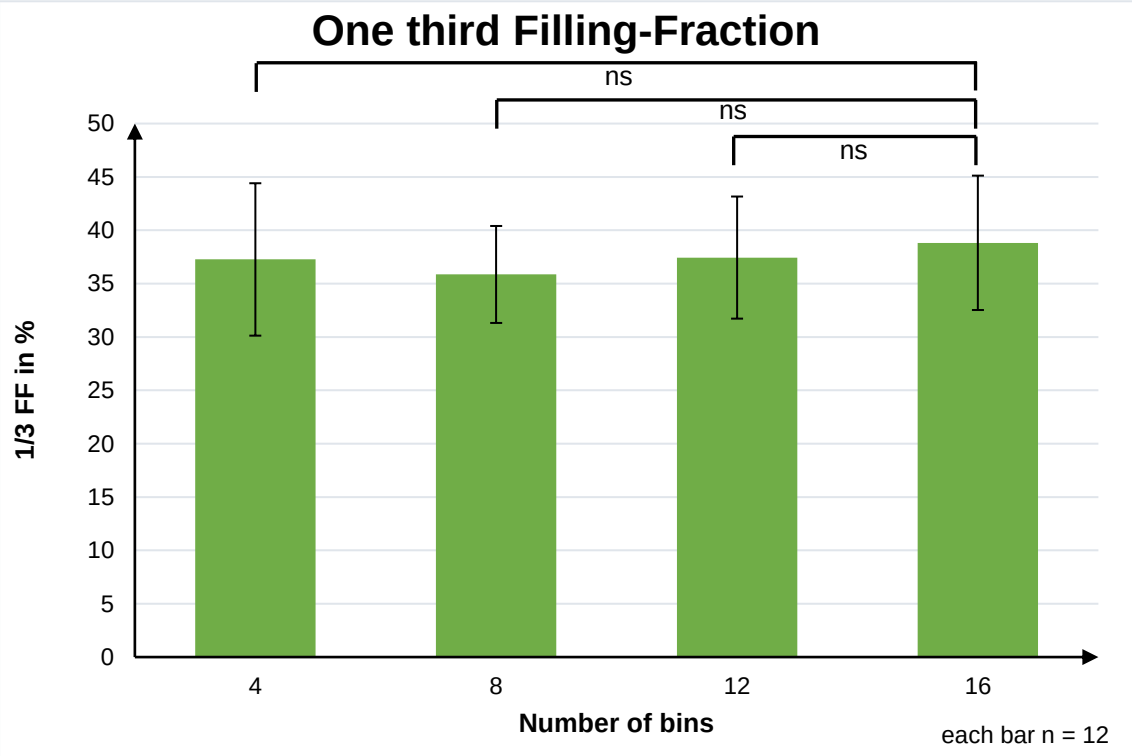

4.6 **Left ventricular volumes comparison**

The LV volumes were calculated by HFV directly from the time/volume curve. Only the values from the reconstruction with 16 bins per cardiac cycle were used for the comparison. The EDV represents the highest detected blood volume in the LV during a heart cycle and thereby the maximum volume of the LV prior to contraction. The mean EDV measured in the ZL rats (410.8 ± 60.3µl) was lower than the average EDV of the ZDF rats (478.8 ± 77.9µl) (P = 0.12) (see **Graph 10**). On the other hand, the ESV represents the lowest volume which could be detected during the cardiac cycle. The average ESV was with 155.1 ± 31.4µl also lower in the ZL rats than in the ZDF rats with 194.1 ± 36.6µl (P = 0.08) (see **Graph 11**). The mean value of the SV, which is the difference between these two values, did only differ a little between the two groups, and was with 255.7 ± 36.4µl in the ZL rats lower than in the ZDF rats with 284.7 ± 51.6µl (P = 0.29). Even if slightly differences between the LV volumes of the ZL and the ZDF rats could be detected, none of these differences reached a statistical significance (compare to **Graph 10**). The volume values are all shown in **Table 6**.

Table 6 Mean Left ventricular volumes of the ZL control rats and the ZDF model rats.

Parameter	ZL rats(control)	ZDF rats (model)	ZDF vs. ZL P-value
EDV (µl)	410.8 ± 60.3	478.8 ± 77.9	0.12
ESV (µl)	155.1 ± 31.4	194.1 ± 36.6	0.08
SV (µl)	255.7 ± 36.4	284.7 ± 51.6	0.29

Data are presented as mean values ± SD. EDV = end diastolic volume; ESV = end systolic volume; SV = stroke volume.

4.7 **Systolic function parameters**

The most common way for estimations of the systolic function is the measurement of the LVEF, which is the fraction of the EDV that is ejected with each beat. The LVEF calculated by HFV from the time-volume curve was 62.5 ± 4.2 % of the EDV in the ZL rats and 59.4 ± 4.5 % in the ZDF rats (P = 0.25). No significant difference could be found between the LVEF of the two groups (compare to **Graph 10**). Also, the 1/3 EF, which is the volume ejected after the first third of the systolic phase in relation to the EDV was nearly the same in the both groups (ZL 23.5 ± 5.3 % versus ZDF 24.4 ± 7.1 %) (P = 0.25) (see **Graph 10**). The normal systolic function in the ZDF rats is further supported by the average value for the CO of the ZDF rats (90917.2 ± 14074.9 µl/min), which was even a little bit higher than the average CO of the ZL rats (85208.1 ± 17511.4 µl/min) (P = 0.90)(see **Graph 10**).

More systolic parameters were calculated by HFV from the time-filling curve. The average duration of the systole (EDtoES) measured by HFV was almost similar in the ZL rats (82.3 ± 9.2ms) and in the ZDF rats (83.7 ± 4.8ms) (P = 0.74), even if the HR was lower in the ZDF rats. The mean PER, referred as the highest detected ejection rate, was with 12.2 ± 1.6ml/s in the ZL rats higher but not significantly higher than in the ZDF rats with 11.1 ± 1.0ml/s (P = 0.16). The average 1/3 ER of the ZL rats was also slightly higher with 11.6 ± 1.4ml/s than the mean value of the ZDF rats with 10.4 ± 1.9ml/s (P = 0.23), but this difference didn’t reach statistical significance. The time from ED till ES is the TES, which was similar in the both groups with 80.4 ± 10.5ms in the ZL rats and 79.2 ± 8.5ms in the ZDF rats. Also, the TPE did not differ significantly between the two groups with 30.1 ± 6.6ms in the ZL rats and 29.8 ± 11.0ms in the ZDF rats (P = 0.95).

In conclusion, no significant difference could be detected for any systolic parameter that has been measured. This shows a normal similar systolic function in both groups. All systolic parameters are shown in **Table 7**.

Table 7 Mean systolic function parameters of the ZL control rats and the ZDF model rats.

Parameter	ZL rats(control)	ZDF rats (model)	ZDF vs. ZL P-value
EDtoES (ms)	82.3 ± 9.2	83.7 ± 4.8	0.74
EF (%)	62.5 ± 4.2	59.4 ± 4.5	0.25
1/3 EF (%)	23.5 ± 5.3	24.4 ± 7.1	0.81
CO (µl/min)	85208.1 ± 17511.4	90917.2 ± 14074.9	0.90
TES (ms)	80.4 ± 10.5	80.3 ± 8.6	0.99
PER (ml/s)	12.2 ± 1.6	11.1 ± 1.0	0.16
TPE (ms)	30.1 ± 6.6	29.8 ± 11.0	0.95
1/3 ER (ml/s)	11.6 ± 1.4	10.4 ± 1.9	0.23

Data are presented as mean values ± SD. EStoED = end-systole to end-diastole; EF = ejection fraction; CO = cardiac output; TES = time to end systole; TPE = time to peak ejection; ER = ejection rate; PER = peak ejection rate

Graph 10 Left ventricular volume and systolic function parameters.

No significant difference could be detected between the ZDF (n = 6) and the ZL rats (n = 6) concerning the EDV (a), ESV (b), stroke volume (c), LVEF (d) and CO (e).

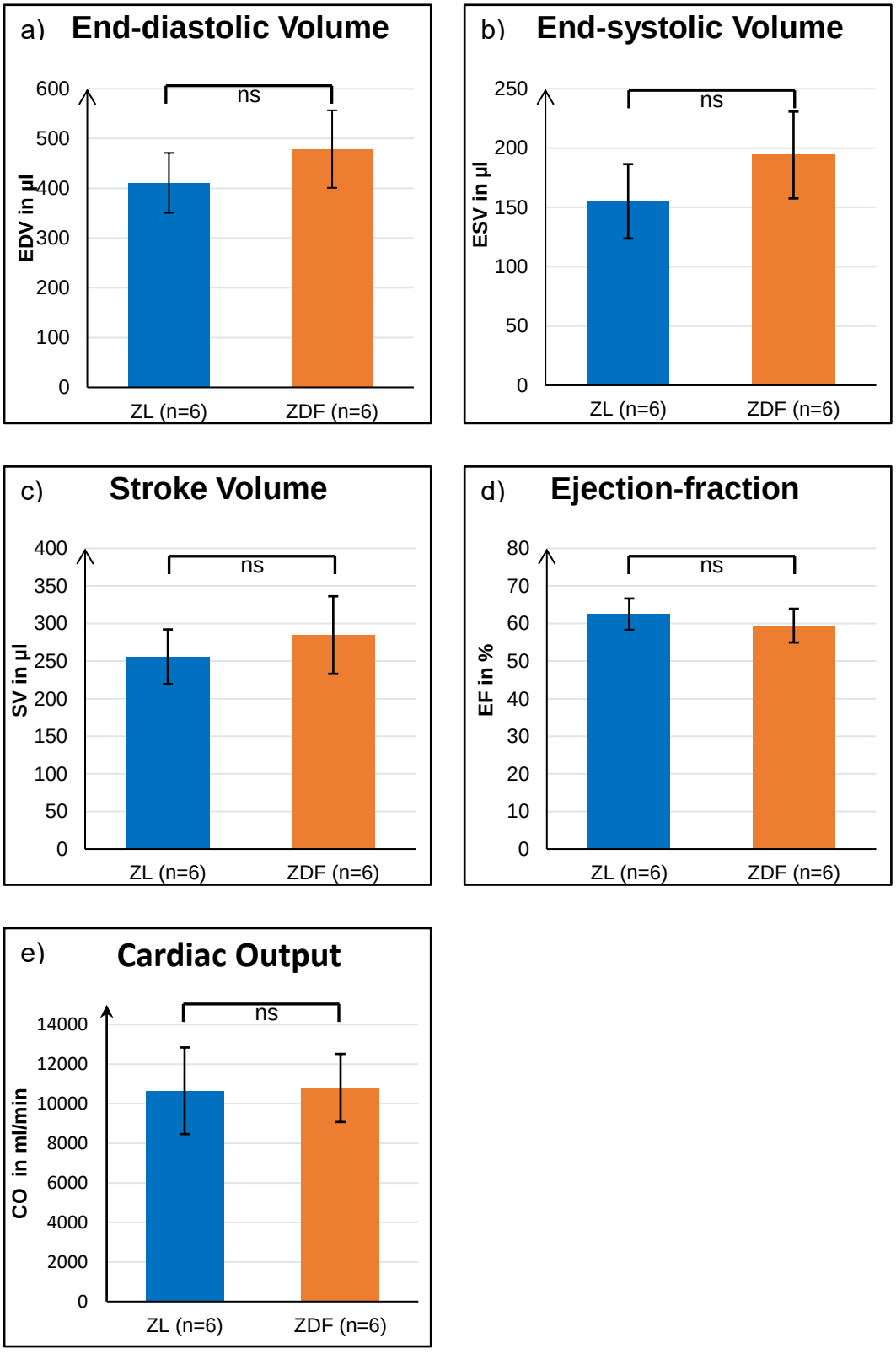

4.8 **Diastolic function parameters**

The diastolic function is characterized by the filling dynamic of the ventricles. The filling parameters were all derived from the time-filling curve calculated by HFV. The average duration of the diastolic phase, calculated by subtracting the EDtoES from the R-R-duration of each rat, was comparable between the two groups with 101.4 ± 14.7ms in the ZL rats and 104.3 ± 9.7ms in the ZDF rats (P = 0.24).

The average percentage volume of the EDV, which has been sucked into the ventricle after the first third of the diastole, the 1/3 FF was nearly the same in both groups with 38.8 ± 3.8% of the EDV in the ZL rats and 38.8 ± 8.6% of the EDV in the ZDF rats (P = 0.99) (see **Graph 11**). The PFR, as highest detectable inflow during the diastole, was always detected during the early filling and was with 12.0 ± 0.8ml/s significantly higher in the ZL rats than in the ZDF rats, which had a mean PFR of 10.2 ± 1.1ml/s (P < 0.01) (see **Graph 11**). Also, the 1/3 FR was significantly lower in the ZDF rats than in the ZL rats (ZL 12.0 ± 0.8ml/sec versus ZDF 9.9 ± 1.3ml/sec) (P < 0.01) (**Graph 11**). The time to the detection of the PFR, the TPF was also significantly longer in the ZDF rats compared to the ZL rats (ZL 35.5 ± 2.6ms versus ZDF 40.2 ± 4.5ms) (P < 0.05). But since the average HR and the average R-R duration were lower in the ZDF rats, a correction for the TPF to the R-R duration was performed to compare this value reasonably between the two groups. After this correction, the TPF corrected was only slightly longer in the ZDF rats and no significant difference could anymore be detected between the TPF of the two groups (0.19 ± 0.01 (ZL) versus 0.21 ± 0.02 (ZDF); p = 0.33) (compare **Graph 11**). These differences are indicating an impaired filling of the LV during the early filling phase. All diastolic parameters are also shown in **Table 8**.

Even if the calculated systolic parameters did not show any statistically significant difference between the two groups, the PFR, which occurs during the first half of the ventricular filling, was significantly lower in the ZDF rats than in the ZL rats. This demonstrated the presence of a diastolic filling abnormality in the ZDF rats, which is not present in the ZL rats, but a comparable systolic function.

Table 8 Mean left ventricular diastolic function parameters of ZL control rats and ZDF model rats.

Parameter	ZL rats(control)	ZDF rats (model)	ZDF vs. ZL P-value
EStoED (ms)	101.4 ± 14.7	104.3 ± 9.7	P = 0.24
TPF (ms)	**35.5 ± 2.6**	**40.2 ± 4.5**	**< 0.05**
TPF cor.	0.19 ± 0.01	0.21 ± 0.02	0.33
1/3 FR (ml/s)	**12.0 ± 0.8**	**9.9 ± 1.3**	**< 0.01**
PFR (ml/s)	**12.0 ± 0.8**	**10.2 ± 1.1**	**< 0.01**
1/3 FF (%)	38.8 ± 3.8	38.8 ± 8.6	0.99

Data are presented as mean values ± SD. Statistically significant parameters are written in fat. EStoED = end-systole to end-diastole; TPF = time to peak filling; 1/3 FR = 1/3 filling rate; PFR = peak filling rate; 1/3FF = 1/3 filling fraction.

Graph 11 Left ventricular diastolic parameters.

These graphs show the average TPF (a), the average TPF cor. (b), the average PFR (c) and the average 1/3 FR (d) of the ZL (n = 6) and the ZDF rats (n = 6).

(EDV = end-diastolic volume, ns = not significant p > 0.05; * = p < 0.05; ** = p < 0.01)

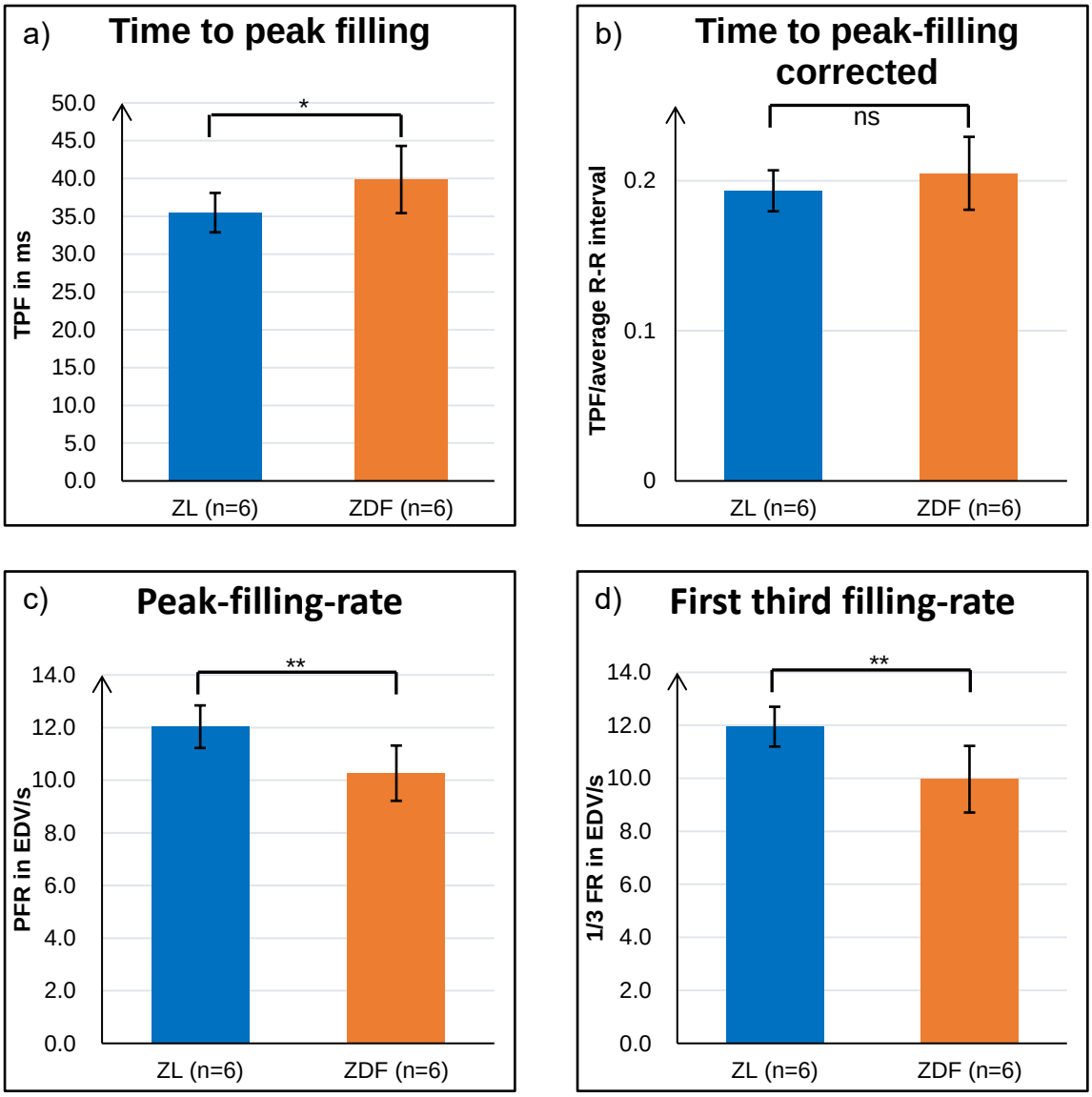

5 Discussion

The imaging and evaluation of small animal hearts is more challenging than the imaging of human hearts, since the imaging of small animals is complicated by the small heart size and the higher HR. Several groups have investigated the utility of the ECG-gated PET in the assessment of LV volumes and EF in humans and found great accordance between the results of ECG-gated PET and the reference method of choice (MRI, ECHO) [10, 111, 112]. But since animal models of different cardiovascular diseases are indispensable to study the effects of therapies and interventions, an accurate determination of the LV volumes, systolic and diastolic parameters of these animal models are of great interest.

The objective of this study was to investigate the applicability of ECG-gated ^{18}F-FDG PET for the assessment of global LV function in healthy control rats and diseased diabetic rats at the age of 13 weeks and further to determine its potential in the detection of a DD in a diabetic rat model. ECG-gated ^{18}F-FDG PET enables an evaluation of both anatomic-functional and molecular characteristics of the heart through a single imaging modality and, moreover, under reproducible physiologic conditions.

Furthermore, the time which is needed for the reconstruction and histogramming process for the different number of utilized frames per cardiac cycle was measured and the impact of the number of frames per cardiac cycle on the calculated systolic and diastolic parameters was investigated.

To the best of our knowledge, the present work is the first which could detect a DD with preserved systolic function in a small animal model by using ECG-gated ^{18}F-FDG PET and the first which compared the influence of the number of bins per cardiac cycle on the values of the diastolic parameters in a small animal model.

5.1 **Methods used**

5.1.1 Animal preparation

The animals in this study had free access to food and water until about ten hours prior to the ^{18}F-FDG injection. Also, the animals underwent hyperinsulinemic-euglycemic clamp procedure to keep the blood glucose level stable (70 to 100mg/ml) during the whole scan to enhance the cardiac ^{18}F-FDG uptake [51, 55] and to standardize the metabolic conditions for all animals. In previous reports by Stegger et al. [9] and Croteau et al [113] the animals did not receive a special treatment except a subcutaneous injection of dextrose to increase the myocardial ^{18}F-FDG uptake. Other investigators performed different pre-treatments including acipimox injection [114], insulin/glucose injection [115] and prolonged fasting [116, 117] and received also a suitable ^{18}F-FDG uptake in the myocardium.

In the here presented study, ^{18}F-FDG PET was performed in a rat model of T2DM, which is a medical condition characterized by impaired glucose metabolism of the cardiomyocytes [13, 118, 119]. Under physiological resting conditions, most energy in the cardiomyocytes derives from the oxidation of long chain-fatty acids and only around 20 to 30% derive from glucose metabolism [15, 120]. As consequence of the peripheral insulin resistance, this percentage gets even smaller in diabetic hearts [100]. The group around van den Brom [100] reported a decreased insulin-mediated myocardial glucose uptake in ZDF rats at eleven weeks of age. This finding demonstrates that ^{18}F-FDG PET imaging is more challenging in diabetic subjects and a special preparation is crucial to receive a sufficient ^{18}F-FDG uptake and good image quality for the border delineation of the myocardial wall. In this study, it could be demonstrated that through a prolonged fasting period of ten hours and the performance of hyperinsulinemic-euglycemic clamp procedure during the PET acquisition the FDG uptake was high enough even for a low ^{18}F-FDG injection dose (39.4 ± 3.1 MBq) to receive good images and to sufficient determine the LV myocardial wall in both diabetic and non-diabetic animal models.

5.1.2 Insulin resistance data

This study showed that ZDF rats develop diabetes at young age (13 weeks). The measured fasting blood glucose at the timepoint of the experiments was significantly higher and the glucose clearance (M-value) was significantly lower in the ZDF model rats than in the ZL controls. This shows that ZDF rats have developed a global insulin resistance. Our findings are in concordance with the reports of different studies, who studied ZDF rats at different age [96, 100, 103, 121].

5.1.3 Use of HFV (Parameters)

In this study, a novel software HFV from Nihon Medi-physics Co. was used to evaluate the LV function from ECG-gated ^{18}F-FDG PET in rats, which was originally designed for the determination of both LV systolic and diastolic function from ECG-gated myocardial perfusion SPECT in humans by analysing the time-volume curve of the LV [122]. Nakae et al. [122] investigated the clinical usefulness of HFV by calculating LV parameters from ECG-gated myocardial perfusion SPECT of 60 patients with HFV and comparing the calculated parameter to those derived from QGS, cardioGRAF and tissue Doppler echocardiographic. They found a good correlation for the LV volumes and EF between HFV, QGS and cardioGRAF, that was clearly significant (HFV and QGS: EDV: R = 0.99; ESV: R = 0.99; EF: R = 0.96; HFV and cardioGRAF: EDV: R = 0.95; ESV: R = 0.96; EF: R = 0.93). Additionally, good correlations were observed between the values of LV EF, EDV and ESV derived from HFV and echocardiography. However, the calculated mean LV volumes and EF differ significantly between these three software solutions.

The diastolic parameters obtained from HFV were compared with those from cardioGRAPF and showed good correlations between the two software. Furthermore, a good correlation between the parameters of tissue Doppler echocardiography (E/e') and PFR calculated by HFV was observed. In conclusion, they showed that HFV is an adequate program for the assessment of diastolic function parameters in human patients.

This study is the first, which shows that HFV is also a useful program for the calculation of the LV diastolic and systolic function parameters in rats. Of course, further studies are required, which compare the parameters from HFV to those from different programs designed for gated imaging and to those from other independent techniques.

5.2 **Reconstruction and histogramming time**

The comparison of the average reconstruction and histogramming time of the reconstructions with different numbers of gates from the list-mode file of the PET scans showed clearly that the average required reconstruction and histogramming time increases with the number of frames.

The required times for the reconstruction step and the histogramming step were measured by the reconstruction software Inveon Acquisition workplace. The most time of the whole process was needed for the historgamming process. The list-mode files were reconstructed with four, eight, twelve and 16 gates per cardiac cycle. Unfortunately, the Inveon Acquisition workplace limited the maximum number of gates per cardiac cycle, so that no reconstruction with more than 16 gates per cardiac cycle were possible. The times increased continuously from four gates (total time 15 min 33 sec) over eight (total time 27 min 31 sec) and twelve (total time 41 min 27 sec) gates to the longest required time with 16 gates per cycle (total time 52 min 57 sec). The measured time clearly depend on the power of the computer system on which the process was performed. In this study, a high-performance workstation of the company Siemens was used (for details see 3.6.2). Of course, systems with a higher performance could shorten this time even more. This data was acquired in this setting to show together with the temporal resolution and their impact on the LV function parameters which number of gates per cardiac cycle are reasonable to receive reliable parameters for the LV function and to perform the scan and the evaluation in a reasonable time.

5.3 **Impact of the number of frames per cardiac cycle on the parameters**

ECG-gated imaging is a technique to assess images of the heart in a specific cardiac phase and to determine specific parameters of the heart function. Therefore, the data are either sorted prospectively during the scan or retrospectively after the completion of the scan. This technique is not only used in PET imaging but also for MRI and CT.

In this study, all the systolic and diastolic parameters were calculated with the use of four, eight, twelve and 16 frames per cardiac cycle, reconstructed retrospectively form the list-mode data, and the corresponding values of each reconstruction were compared to the values of the reconstruction with 16 gates per cycle, since this is the one which provides the highest temporal resolution [43].

5.3.1 Left ventricular volumes and ejection fraction

The use of at least twelve gates per cardiac cycle is recommended to determine the LV volumes sufficiently since the use of only four and eight gates per cycle is leading to a significant underestimation of the EDV and subsequently to mistakes in the determination of the SV and the LVEF.

The list-mode files with the ECG-recording of all rats were reconstructed and histogrammed using the Inveon Acquisition workplace as explained earlier. After the maximatization of the voxel size, the LV parameters were calculated by HFV to compare the assessed LV volumes, systolic and diastolic parameters between the reconstructions. Concerning the LV volumes, a reconstruction with four and eight gates per cardiac cycle results in a significant underestimation of the EDV but no significant overestimation of the ESV. However, the significant underestimation of the EDV is leading to a significant lower calculated SV with four and eight bins. But only the reconstruction with four frames per cycle is leading to a significant underestimation of the LVEF. Since the LV volumes play an important role in the evaluation of the LV function the use of only four or eight frames per cardiac cycle is not recommended. No significant difference could be detected concerning the EDV, ESV, SV or LVEF between the reconstructions with twelve gates per cardiac cycle and 16 gates per cardiac

cycle. Therefore, even a reconstruction with only twelve gates per cycle might be enough to calculate reliable LV volumes and LV EF.

This study is the first to our knowledge which evaluates the influence of the number of gates per cardiac cycle and the value of the LV function parameters from ECG-gated PET in a small animal model. Therefore, corresponding data of other groups for a comparison are lacking. However, ECG-gating is an established tool in the performance of routine myocardial perfusion SPECT [43, 123-125] and myocardial viability PET in human patients to determine the LV volumes and LVEF.

For routine myocardial perfusion SPECT, an acquisition with eight frames per cardiac cycle is most often performed. This low number of frames per cardiac cycle is most often chosen since the acquisition is completed within an adequate time, while the count density is high enough for good image quality. On the other hand, the eight-frame gated acquisition mode only provides a lower temporal resolution. Different studies have shown, that eight-frame data is leading to a overestimated ESV and a underestimated EDV and thus underestimate the LVEF [43, 125]. In the here presented study, an overestimation of the ESV has not been observed. Values for the ESV were even lower in the reconstructions with four, eight and twelve bins. This might derive from the use a different edge detection software in this study and thereby a different way of the heart shape delineation which could have an influence of the ESV. However, a greater number of frames (i.e. 16 or 32) improves the temporal resolution but is also accompanied with a shorter frame duration and thereby with a lower count density of each frame. To provide still an optimal image quality the acquisition should be prolonged, or a higher activity should be injected [43].

Even if the calculation of the LVEF with eight gates per cycle gives an impression of the range of the LVEF, for an accurate determination of the LV volumes and LVEF from ECG-gated myocardial perfusion SPECT a higher frame number than eight is needed. This agrees with the findings of Kumita et al. [43], who measured EDV, ESV and LV EF in 50 patients first using eight

gates/cycle, then 16 gates/cycle and finally 32 gates/cycle. They found an underestimated EDV, an overestimated ESV and a significantly lower LVEF in the eight gates/cycle analysis than for higher frame numbers.

However, PET offers a distinct higher spatial resolution compared to SPECT and can thereby improve the myocardial border determination. Therefore, the gated-PET may measure LV parameters more reliably than gated-SPECT and require less frames [111].

Li Y. et al. [111] performed eight-frame ECG-gated ^{18}F-FDG PET and cardiac MRI on 89 HF patients. LV volumes and EF were calculated from ECG-gated ^{18}F-FDG PET using two different clinical software (QGS and 4D-MSPECT) and compared the results to the values of 25-frame ECG-gated cardiac MRI. Despite the good correlation of LV EDV, ESV and EF between gated-PET and MRI for both programs, only the LV EDV calculated by 4D-SPECT were comparable to the corresponding values measured by MRI. The same tendency was also described by Schaefer W. et al. [10], who evaluated data from gated-^{18}F-FDG PET with also eight frames per cycle and compared it to the results of cardiac MRI from 30 patients with serve CAD.

In conclusion, eight frames might be a reasonable set up to get an impression of the LV volumes and LVEF from ECG-gated PET but does not provide the required temporal resolution for a reliable evaluation of the LVEF.

5.3.2 Left ventricular systolic and diastolic parameters

In addition to the LV volumes, this work also focused on the comparison of the systolic and diastolic parameters, which derive from the time-filling curve calculated by HFV. Since the time-filling curve is the first deviation of the time-volume curve its accuracy is depended on the accuracy of the measured volumes for each gate and of the out of these values calculated time-volume curve. It is simple to recognize that the time-volume and the time-filling curve with four gates per cycle are less exact than the curves of the same rat with 16 gates per cycle (see **Figure 19**).

Therefore, many values of the systolic and diastolic function were significantly different from the values of the reconstruction with 16 gates per cycle. However, only two values (TPF, TPF/(R-R duration) of the reconstruction with eight gates were significantly higher than the corresponding values of the reconstruction with 16 gates and no significant difference concerning the systolic and diastolic values could be detected between the reconstruction with twelve and sixteen gates per cycle.

Since this is the first work and data for a good comparison is lacking, more investigations concerning the influence of the number of bins on the systolic and diastolic parameters is needed, which may also include another method for the calculation of the LV parameters such as cardiac MRI or ECHO, which are well established in the determination of the LV systolic and diastolic function.

Even if no significant difference between the parameters of the diastolic function of the twelve bins and the 16 bins reconstructed images could be found, there were differences, which might become significant in studies with a higher number of animals.

5.4 **Left ventricular performance evaluation and comparison**

5.4.1 LV volumes and systolic function parameters

ECG-gated ^{18}F-FDG PET is a method for the non-invasive measurement of LV volumes and LVEF in experimental small animal models under standardized conditions.

The LV volume parameters and the LVEF are values of great clinical relevance. For example, the group around White et al. [126] revealed that after a myocardial infarction the ESV is one of the most important determinants of survival. Therefore, application of these non-invasive measurements of LV volumes to experimental small animal models is crucial to define normal values, to monitor the development of cardiac diseases and the effect of treatment approaches in experimental animal models.

In this study, no significant difference concerning EDV, ESV and LVEF could be detected between the ZDF rats with an early stage of T2DM and the healthy control group. Also, no significant difference between the systolic parameters calculated from the time-filling curve by HFV of the two groups could be found. The LV volume values obtained from the ECG-gated ^{18}F-FDG PET (16 gates per cycle) of the two groups for EDV, ESV and SV were 410.8 ± 60.3 µl (ZL control), 478.8 ± 77.9 µl (ZDF model), 155.1 ± 31.4 µl (control),194.1 ± 36.6 µl (model), 255.7 ± 36.4 µl (ZDF model) and 284.7 ± 51.6 µl (control). Also, the calculated LVEF did not differ significant between the two groups and was 62.5 ± 4.2 % (control) and 59.4 ± 4.5 % (model). The values for the LVEF are in perfect accordance with the findings of Bousquenaud et al. [114], who performed ECG-gated ^{18}F-FDG PET imaging in 26 Wistar rats of which seven served as control and 19 underwent surgical procedure to induce myocardial infarction. Even if the calculated EDV and ESV of the control group were slightly different than the volume values of the here presented study, the average LVEF value of the control group of Bousquenaud et al. is with 63 ± 7 % perfectly in line with the calculated LVEF of this study.

However, our estimate for the LVEF was higher than the EF (56 ± 3%) Todica et al. [127] have found by using ECG-gated ^{18}F-FDG PET in 7 healthy Sprague-

Dawley rats. They also used ECG-gated ^{18}F-FDG-blood pool imaging, gated ^{68}Ga-albumin blood pool imaging and cardiac MRI (as reference) to determine the LV volumes and EF. Of all these modalities, the correlations with the MRI derived values for the EDV and ESV were best for ECG-gated ^{18}F-FDG PET. Their lower LVEF may be caused by using only eight gates per cardiac cycle, which is attributed to a lower temporal resolution and may have led to an underestimation EDV and an overestimated ESV. Furthermore, they used a clinical MRI scanner for the determination of the LV function, which could only acquire seven slices for the whole heart. This low number of slices may also have had an impact on the calculated LV volumes and thereby on the LVEF. However, in comparison to the LVEF of anesthetized rats in other studies, the values for the LVEF of Todica et al. are at the low end of the range of estimates reported. At the other end of the range are the values of Croteau et al. [113], who also used ECG-gated ^{18}F-FDG PET with 16 gates per cycle for the assessment of the LV volumes and reported an average LVEF of 83 ± 8% in eleven healthy Sprague-Dawley rats. Croteau et al. used TTE as reference method and demonstrated good agreement between the LV volumes and EF in healthy rats. One more study recently used ECG-gated ^{18}F-FDG PET as reference method for the determination of LV volumes in twelve healthy wistar rats [108]. This study of Szymanski et al. also reported a distinct higher LVEF (74.9 ± 10.2%) than the one, which have been found in this work. This variation of the values for the LVEF may derive from the use of different animal models and the different age at which the experiments were performed.

The ability of ECG-gated ^{18}F-FDG PET for the assessment of LV volumes and EF in healthy rats has been demonstrated by different groups. The in the here presented study calculated values for the mean LVEF of both the ZDF and the ZL rats are in the centre span of the published values for LVEF of healthy rats.

However, this is the first study which assessed the LV volumes and EF in an experimental diabetic rat model by using ECG-gated ^{18}F-FDG PET. MRI and echocardiographic studies in experimental T2DM animal models have produced discrepant results on LV volumes and EF. Previous studies reported decreased systolic function (LVEF) in Goto-Kakizaki [128] and ZDF rats [129], but these

results could not be reproduced by other groups [121, 130]. Moreover, there are studies, which show increased LV systolic performance in early stage of T2DM in rats [121, 131]. The presented results of this study, which demonstrate a preserved LV systolic function in ZDF rats are in line with findings of the group of S. Schaefer et al. [103] (EF 51 ± 5 % (ZDF) & 54 ± 3 (ZL)) and Radovits T. et al. [130] (EF 64.8 ± 5.5 % (ZDF) 64.4 ± 4.4 %(ZL)), who performed cardiac catheterization to receive a reliable LV pressure-volume relation in ZDF rats and healthy controls at the age 30 to 37 weeks. Even if a lower LVEF in the ZDF rats than in the ZL controls has been found, this difference did not reach statistical significance (P = 0.08).

This study and several other studies have studied the utility of gated ^{18}F-FDG PET for the determination of LV volumes and EF by using different software packages with or without a reference method (MRI or radionuclide angiography) [9, 10, 111, 127, 132]. But even if ^{18}F-FDG is a well-established tracer for cardiac PET studies, other PET tracers have also been investigated concerning their potential for the evaluation of the LV volumes including ^{13}N-Ammonia (^{13}N-NH_3), [^{15}O]-H_2O and ^{82}Rubidium (^{82}Rb).

^{13}N-NH_3 PET imaging is a common method to assess myocardial blood flow and coronary reserve [133-136], but only a few studies have evaluated the LV function by using ECG-gated ^{13}N-NH_3 PET. Khorsand and colleagues performed ECG-gated ^{13}N-NH_3 PET and ECG-gated ^{18}F-FDG PET as reference method in 27 patients with a history of CAD to determine the LV volumes and EF. They found an excellent agreement of all parameters between the two imaging methods. Also, Okazawa et al. [133] evaluated the LV volumes and EF of six healthy volunteers and 34 patients known to have CAD using ECG-gated ^{13}N-NH_3 PET imaging. Even if the LV volumes were overestimated by ECG-gated ^{13}N-NH_3 PET, the calculated values for the LVEF of the healthy participants has shown good agreement with the values for the LVEF calculated by LV blood pool imaging using C^{15}O PET. However, the LVEF of patients with a perfusion deficit caused by the CAD was significantly underestimated compared to the LVEF from the blood pool imaging.

The group of Rajappan used ECG-gated ^{15}O-CO PET to evaluate LV volumes and EF in nine patients with cardiac MRI as reference method [137]. They found good correlations for ESV and EDV with a trend to underestimate the EDV and thereby to underestimated LVEF. This underestimation may be explained with the use of only eight gates per cardiac cycle. However, they showed that an evaluation of the LV function is possible with the use of ECG-gated ^{15}O-CO PET.

In a study from Chander et al., a comparison of LV EDV, ESV and EF from ECG-gated ^{82}Rb-PET with contrast enhanced CT ventriculography in 24 patients showed that LV function could be assessed from gated ^{82}Rb-PET by using different software products (QGS and CardIQ Physio). Even if the correlations between PET and CT ventriculography yielded good correlation, the comparison revealed that mean values for EDV and LVEF were calculated consistently lower by ^{82}Rb-PET.

Further studies were performed by different groups using ECG-gated ^{13}N-NH_3 PET in patients for the determination of LV volumes and with different reference methods (gated MIBI SPECT [138], gated ^{18}F-FDG PET [39], none [139]). In contrast to all the above mentioned studies, the group of Szymanski et al. investigated the ability of ECG-gated ^{13}N-NH_3 PET for the assessment of the LV volumes in small animals [108]. This study investigated 18 Wistar rats of which six underwent coronary artery ligation to initiate myocardial infarction (MI). ECG-gated ^{18}F-FDG PET was chosen as reference method. Except for the LVEF of the MI group, no significant difference of the LV volumes and EF could be observed, even if both mean values of ESV and EDV were higher and LVEF lower when calculated from ECG-gated ^{13}N-NH_3 PET.

The use of perfusion tracers for the evaluation of the LV function is of great interest, since many patients who underwent cardiac PET have a myocardial infarction in their history. But the above-mentioned approaches are all limited using short live-isotopes (half-life of ^{15}O is 2min, half-life of ^{13}N is 10 min and half-life of ^{82}Rb is 78sec), which requires the availability of an on-site cyclotron and does not allow data sampling with more than eight gates per cycle,

because of the low counts. The low temporal resolution may be the main reason why most of the studies underestimate the LVEF in comparison to the reference method of choice. Therefore, a more exact determination of the LV volumes requires a higher number of gates per cycle. Furthermore, the distribution of the above-mentioned tracers shows the myocardial perfusion, whereas ^{18}F-FDG visualizes the myocardial glucose metabolism. The fact, that hibernating myocardium may show perfusion deficits while the glucose uptake and metabolism is still preserved [133] argues in favour of ^{18}F-FDG instead of perfusion tracers for the evaluation of LV function from ECG-gated PET, because myocardial delineation is complicated by myocardial perfusion deficits [140].

The great advantage of ^{18}F-FDG PET is the evaluation of the myocardial glucose metabolism, which is reported to be impaired in diabetic subjects and related to the development of myocardial dysfunction [100]. Also, further tracers exist including ^{11}C-palmitate, which allow the determination of the myocardial fatty acid metabolism. This supplementary information is of great interest since different studies have reported a relation between the metabolic state of the cardiomyocytes and the cardiac dysfunction [100, 141].

5.4.2 Diastolic function parameters

The here presented data show that the ECG-gated ^{18}F-FDG PET together with an appropriate clinical detection software has the potential to evaluate the diastolic function of diabetic and healthy rats and further can detect even a mild impaired diastolic function.

Any cardiac examination should involve an accurate evaluation of the LV diastolic function, since the presence and severity of a DD may provide important diagnostic and prognostic impacts for patients [142]. DD is a mechanical abnormality of the heart, which is often the earliest detectable sign of a cardiac involvement of different diseases and is also reported to be the earliest detectable sign of diabetic cardiomyopathy in both humans and experimental animal models [11, 69].

ECG-gated ^{18}F-FDG PET has become a regular procedure in patients suffering from ischemic heart disease to differentiate between hibernating myocardium and myocardial scars in patients, who show perfusion deficits in myocardial perfusion imaging. This quantitative technique has not, however, been used to evaluate the LV diastolic function although, in case of hypertension, different cardiomyopathies and ischemic heart disease, myocardial involvement has been detected early through the existence of diastolic abnormities [143-146].

To our knowledge, the present study is the first to validate the ECG-gated ^{18}F-FDG PET-based assessment of LV diastolic function parameters in a rat model. A mild impaired LV diastolic function in the absence of an impaired systolic function in the ZDF rats has been detected, which couldn't be detect in heathy controls. Based on the results of the LV function measurement by the ECG-gated ^{18}F-FDG PET, the predominant dynamic cardiac feature in young ZDF rats suffering from T2DM is a LV DD. In this study, an impaired diastolic filling in the ZDF rats was observed, which could also be found in studies with other determination methods [103, 130].

To evaluate the diastolic function of the rats, different parameters were calculated from the time-filling curve using HFV. The ZDF rats showed significant differences of the diastolic parameters at the age of 13 weeks including lower PFR, lower 1/3 FR and longer TPF compared to their aged matched healthy littermates. Even if the TPF after the correction for the average R-R duration was no longer significant, the decreased filling rates indicate an abnormality of the LV filling, which could not be detected in the ZL control rats. This difference indicates a disturbance during the early filling of the diastole (E-wave). Unfortunately, the program HFV does only calculate the PFR and the 1/3 FR which are both parameters of the early filling so that no investigation of the late filling was possible.

Even if this is the first study which is using ECG-gated ^{18}F-FDG PET for the evaluation of the diastolic function and standard-values are missing many groups have investigated the diastolic function of diabetic animal models by using MRI, ECHO or cardiac catheterization.

In the most studies, TTE combined with Doppler technique has been used for the non-invasive evaluation of the diastolic function. These studies have revealed the presence of a DD in ZDF rats at different ages. Van den Brom et al. [100] determined the systolic and diastolic function in ZDF rats at eleven weeks of age using Doppler echocardiography and reported a prolonged isovolumetric relaxation time, a decreased E-wave and E', which collectively indicates the presence of decreased LV relaxation and filling. These findings indicate an impaired early filling of the LV and are perfectly in line with the decreased PFR which was found in this here presented study. Moreover, the group of Akula [147] has demonstrated an impaired diastolic function in streptozotocin-induced diabetic rats after twelve weeks of diabetes, which was characterized by a decreased E-wave an inversed E/A ratio. In some studies, the inversed E/A ration contributes mostly to an increased A-wave, which indicates a compensation of the impaired passive inflow through an increased atrial contraction [148]. This finding also demonstrates the presence of an abnormal LV filling but could not be confirmed by the results of the present study. However, an impaired PFR in diabetic rats, was also reported by Hoit et al. [149], who performed M-mode echocardiography on seven streptozotocin-induced diabetic rats at different time points and first reported a decreased PFR five weeks after the administration of streptozotocin. These findings are all in line with the decreased PFR which was observed in the 13 weeks old ZDF rats in the here presented study.

These findings were further supported by studies, which evaluated the LV function using LV catheterization. LV catheterization is the most reliable method for the detection of a disturbance in the diastolic filling since it can measure the intraventricular pressure directly. The groups of Schäfer et al. [103] and Radovits et al. [130] evaluated the LV function in ZDF rats at the age of 37 weeks and twelve weeks using LV catheterization. Both reported a significantly impaired LV relaxation in the ZDF rats, whereas the parameters for the LV compliance and the systolic function of the ZDF rats did not differ significantly compared to the healthy littermates. The group of Marsh et al. [150] performed cardiac catheterization in distinct younger ZDF rats (14 weeks) to evaluate the

LV function. Even if they found a significant reduction of the systolic function, the LV diastolic time constant, Tau (τ), was the only diastolic parameter, which did significantly differ between the ZDF rats and the ZL controls. The ZDF rats used by Marsh et al. were only one week older than the ZDF rats in this approach. Therefore, the only mild decreased diastolic function of the ZDF rats from Marsh et al. is in line with the here presented findings. However, the systolic function parameters reported by Marsh et al. differ considerably of those reported by the other groups.

However, LV catheterization and echocardiography are well established methods for the assessment of LV function, but they are also limited to their reproducibility since echocardiography investigations are examiner and position dependent and LV catheterization is an invasive approach. Therefore, the assessment of LV function from examiner independent methods would be favourable.

All the above-mentioned studies have shown a mild impaired diastolic filling in diabetic rats at different ages. Therefore, the here presented findings are in perfect line with the reported results of all these groups and demonstrate the ability and feasibility of ECG-gated ^{18}F-FDG PET for the assessment of both the LV systolic and diastolic function in rats and even allows the detection of a DD in the early stage of diabetes in rats.

5.5 **Perspective**

The determination of the LV systolic and the diastolic function using ECG-gated ^{18}F-FDG PET in a small animal model of diabetes is a method that is first reported in this study. Since, DD is estimated to be present in 20 to 60 percent of all patients with HF [4, 151] and since the occurrence of DD is associated with a higher mortality and morbidity, the accurate assessment of the diastolic function is crucial in all patients with any form of chronic heart disease. However, the evaluation of the diastolic function in ZDF rats, which are a well-established model for T2DM, using ECG-gated ^{18}F-FDG PET is important to visualize the results and molecular changes of new treatment approaches for diabetes related cardiac diseases even if the imaging of the diastolic function in small animals is associated with more effort due to a higher HR and a smaller heart size.

The ECG-gated PET is a cardiac imaging technique which allows the combined measurement of cardiac function and myocardial metabolism at the same time. This is of great interest in evaluating the effectiveness of new treatment strategies and the progress of the cardiac disease in experimental small animal models mimicking different heart diseases especially in animal models of diabetes, since the cardiac dysfunction in early diabetes seems to be closely related to alterations of the myocardial metabolism [11, 119, 147]. The data assessment for the simultaneous evaluation of the myocardial metabolism and the cardiac function is a great advantage of ECG-gated ^{18}F-FDG PET and may save costs and time in the clinical practice.

Diabetes is a chronic disease, which has great influence on the glucose metabolism in the whole body. Therefore, ^{18}F-FDG as glucose analogue is an ideal tracer to detect tissue which has an impaired glucose metabolism as consequence of the periphery insulin resistance. Since not only the glucose metabolism is influenced by diabetes and since alterations of the myocardial metabolism may also play a role in other cardiomyopathies, further studies may be needed which investigate the feasibility of LV function assessment from ECG-gated PET imaging with new tracers, which visualize another metabolic pathway including ^{11}C-palmitate for the fatty acids metabolism [12].

In addition, a new generation of preclinical PET scanners is already on the market with a higher resolution and faster data acquisition. These new techniques may improve the spatial local and global resolution of rodent hearts and may therefore improve the evaluation of the LV function and the understanding of local processes in the myocardium.

In this study, cardiac function has been studied using the program HFV. HFV is a clinical software, that has been originally developed for ECG-gated perfusion SPECT studies in human patients. In this study, it has been demonstrated that HFV can successfully determine both LV systolic and diastolic function parameters in rats, when the data is adapted in advance. Since this is the first study, which uses HFV for the determination of LV function parameters in two small groups of rats, further studies are required with groups of higher numbers and a reference method.

6 Summary

6.1 English version

DD is a cardiac disturbance, which has gained increasing importance in recent years due to its important role in different cardiac disease and cardiomyopathies including ischemic cardiomyopathy, arterial hypertension and diabetic cardiomyopathy.

ECG-gated ^{18}F-FDG PET is an imaging technique, that can distinguish between districts of myocardial viability and myocardial scars and further provides information of great interest on the efficacy of experimental approaches designed to improve the cardiac function and/or myocardial metabolism in experimental small animal models. However, ECG-gated ^{18}F-FDG PET is a technique whose feasibility in the assessment of the LV diastolic function in small animals has not been a subject of study.

In this thesis, the ability of the ECG-gated ^{18}F-FDG PET for the assessment of both the systolic and diastolic function in eight control rats and in seven ZDF rats, which are an experimental animal model mimicking T2DM conditions and diabetic related complications in humans including DCM, has been investigated The ECG-gated ^{18}F-FDG PET imaging was performed under hyperinsulinemic-euglycemic clamping and the data were stored in list mode files and retrospectively reconstructed. The systolic and diastolic parameters were achieved from the time/volume and the time/filling curve calculated from the software HFV. Additionally, the influence of the number of gates per cardiac cycle on the LV volumes and function parameters has been studied.

Hyperinsulinemic-euglycemic clamp procedure and blood glucose measurement did confirm the development of a manifest diabetes in the ZDF rats at the timepoint of the experiments.

Regarding the systolic parameters, no significant difference could be detected between the ZDF and ZL rats. The values for the CO were similar in both groups, which demonstrates a similar LV systolic function in the ZDF and the ZL rats at the age of 13 weeks. Values for the systolic parameters are in good line

with previous PET, MRI and cardiac catheterization-based studies in diabetic rats.

The main finding of this study was that by using in vivo ECG-gated ^{18}F-FDG PET and the software HFV, reliable diastolic parameters could be calculated. Moreover, it was possible to detect the presence of a mild impaired diastolic filling in the ZDF rats in absence of any systolic alteration. This impaired diastolic function in an early stage of diabetes could also be detected by other investigators, who used echocardiography or cardiac catheterization. Therefore, this is the first study showing, that the assessment of the diastolic function in rats can be carried out by ECG-gated ^{18}F-FDG PET imaging.

In conclusion, additionally to calculating LV volumes and LV EF, ECG-gated ^{18}F-FDG PET can evaluate the diastolic function of healthy and diabetic rats and is able to detect a DD in ZDF rats.

6.2 **German version**

Die DD ist eine Störung der Herzdynamik, welche, aufgrund ihrer Beteiligung in verschiedenen Herzerkrankungen und Kardiomyopathien wie der ischämischen Kardiomyopathie, der arteriellen Hypertonie und der diabetischen Kardiomyopathie, in den letzten Jahren zunehmend in das Interessenzentrum der Herzforschung gerückt ist.

Die EKG-getriggerte ^{18}F-FDG PET ist eine Bildgebungsmethode, welche die Unterscheidung von vitalem Myokard und Narben ermöglicht und zusätzlich noch in der Lage ist, wichtige Informationen zu erheben, welche von Bedeutung für die Beurteilung von experimentelle Behandlungen zur Verbesserung der Herzfunktion und/oder des kardialen Stoffwechsels in präklinischen Tiermodellen sind. Trotz dieser Möglichkeiten wurde bisher noch nicht die Fähigkeit der EKG-getriggerten ^{18}F-FDG PET zur Bestimmung der LV diastoischen Funktion in Kleintiermodellen untersucht.

Deshalb wurde in dieser Arbeit das Potential der EKG-getriggerten ^{18}F-FDG PET in Bezug auf die Bestimmung der LV systolischen und diastolischen Funktion in acht Kontrollratten (ZL) und sieben ZDF-Ratten, welche eine experimentelles Tiermodell für T2DM und die damit verbundenen Komplikationen einschließlich der diabetischen Kardiomyopathie sind, untersucht. Die EKG-getriggerte ^{18}F-FDG PET wurde unter der hyperinsulinämischen euglykämischen Klemm Methode durchgeführt, die Daten in „list-mode“ Dateien gespeichert und retrospektiv rekonstruiert. Die Berechnung der LV systolischen und diastolischen Parameter erfolge aus der Zeit-Volumen-Kurve und der Zeit-Füllungs-Kurve durch das Programm HFV. Zudem wurde der Einfluss der pro Rekonstruktion verwendeten „frames“ pro kardialen Zyklus auf die LV Volumina und die linksventrikulären Funktionsparameter untersucht.

Durch die hyperinsulinämische euglykämische Klemm Methode und durch Blutglukose Messungen konnte die Entwicklung eines manifesten Diabetes zum Zeitpunkt der Experimente in den ZDF Ratten nachgewiesen werden.

Es konnte kein signifikanter Unterschied zwischen den systolischen Parametern der ZDF und der ZL Ratten gefunden werden. Der kardiale Auswurf war nahezu identisch in den beiden Gruppen zum Zeitpunkt der Experimente, was eine vergleichbare systolische Funktion in beiden Gruppen demonstriert. Die erhobenen Werte für die systolischen Parameter befinden sich in guter Übereinstimmung mit den Werten der Literatur von vorherigen PET, MRT und Katheter-gestützten Experimenten in diabetischen Rattenmodellen.

Ein wichtiges Ergebnis dieser Arbeit ist die Erhebung von verlässlichen diastolischen Parametern durch den kombinierten Einsatz von EKG-getriggerter ^{18}F-FDG PET und HFV. Zudem war es möglich, eine gestörte diastolische Füllung des LV in den ZDF Ratten nachzuweisen, in Abwesenheit von systolischen Funktionseinschränkungen.

Eine Beeinträchtigung der diastolischen Funktion in der frühen Phase des Diabetes wurde bereits in anderen Rattenstudien mittels Echokardiografie und Katheter basierten Untersuchungen gezeigt. Dennoch ist dies hier die erste Studie, welche demonstriert, dass die Bestimmung der diastolischen Funktion auch mit Hilfe der EKG-getriggerten ^{18}F-FDG PET durchgeführt werden kann.

In Zusammenfassung lässt sich festhalten, das zusätzlich zu der Bestimmung der LV-Volumina und der LVEF durch EKG-getriggerten ^{18}F-FDG PET auch die Bestimmung der diastolischen Funktion in gesunden und diabetischen Ratten möglich ist und dass durch EKG-getriggerten ^{18}F-FDG PET die Identifikation einer DD in ZDF Ratten möglich ist.

8 References

1. Kinehan, P., *from Bioengineering 508 - Physical Aspects of Medical Imaging*, U.o.W.W. Courses, Editor. 2006. p. 26.
2. Christ, M., et al., *Heart failure epidemiology 2000-2013: insights from the German Federal Health Monitoring System.* Eur J Heart Fail, 2016.
3. Zile, M.R., C.F. Baicu, and W.H. Gaasch, *Diastolic heart failure--abnormalities in active relaxation and passive stiffness of the left ventricle.* N Engl J Med, 2004. **350**(19): p. 1953-9.
4. Vasan, R.S., et al., *Congestive heart failure in subjects with normal versus reduced left ventricular ejection fraction: prevalence and mortality in a population-based cohort.* J Am Coll Cardiol, 1999. **33**(7): p. 1948-55.
5. Mosterd, A., et al., *Prevalence of heart failure and left ventricular dysfunction in the general population; The Rotterdam Study.* Eur Heart J, 1999. **20**(6): p. 447-55.
6. Redfield, M.M., et al., *Burden of systolic and diastolic ventricular dysfunction in the community: appreciating the scope of the heart failure epidemic.* JAMA, 2003. **289**(2): p. 194-202.
7. Kane, G.C., et al., *Progression of left ventricular diastolic dysfunction and risk of heart failure.* JAMA, 2011. **306**(8): p. 856-63.
8. Abhayaratna, W.P., et al., *Characteristics of left ventricular diastolic dysfunction in the community: an echocardiographic survey.* Heart, 2006. **92**(9): p. 1259-64.
9. Stegger, L., et al., *Quantification of left ventricular volumes and ejection fraction in mice using PET, compared with MRI.* J Nucl Med, 2009. **50**(1): p. 132-8.
10. Schaefer, W.M., et al., *Validation of an evaluation routine for left ventricular volumes, ejection fraction and wall motion from gated cardiac FDG PET: a comparison with cardiac magnetic resonance imaging.* Eur J Nucl Med Mol Imaging, 2003. **30**(4): p. 545-53.
11. Abe, T., et al., *Left ventricular diastolic dysfunction in type 2 diabetes mellitus model rats.* Am J Physiol Heart Circ Physiol, 2002. **282**(1): p. H138-48.
12. Li, Y., et al., *Determination of Fatty Acid Metabolism with Dynamic [11C]Palmitate Positron Emission Tomography of Mouse Heart In Vivo.* Mol Imaging, 2015. **14**: p. 516-25.
13. Ohtake, T., et al., *Myocardial glucose metabolism in noninsulin-dependent diabetes mellitus patients evaluated by FDG-PET.* J Nucl Med, 1995. **36**(3): p. 456-63.
14. vom Dahl, J., et al., *Myocardial glucose uptake in patients with insulin-dependent diabetes mellitus assessed quantitatively by dynamic positron emission tomography.* Circulation, 1993. **88**(2): p. 395-404.
15. Camici, P., E. Ferrannini, and L.H. Opie, *Myocardial metabolism in ischemic heart disease: basic principles and application to imaging by positron emission tomography.* Prog Cardiovasc Dis, 1989. **32**(3): p. 217-38.
16. Goldstein, R.A., et al., *Myocardial perfusion with rubidium-82. II. Effects of metabolic and pharmacologic interventions.* J Nucl Med, 1983. **24**(10): p. 907-15.
17. Machac, J., et al., *Positron emission tomography myocardial perfusion and glucose metabolism imaging.* J Nucl Cardiol, 2006. **13**(6): p. e121-51.
18. Chen, X., et al., *Radionuclide imaging of neurohormonal system of the heart.* Theranostics, 2015. **5**(6): p. 545-58.
19. Beck, G. and K. Sitte, *β-Emission of Positive Electrons.* Nature, 1934. **133**: p. 722-722.
20. DiFilippo, F.P., *Instrumentation and Principles of Imaging: PET*, in *Cardiac PET and PET/CT Imaging*, M.F. Di Carli and M.J. Lipton, Editors. 2007, Springer New York: New York, NY. p. 3-18.
21. Bailey, D.L., J.S. Karp, and S. Surti, *Physics and Instrumentation in PET*, in *Positron Emission Tomography: Basic Sciences*, D.L. Bailey, et al., Editors. 2005, Springer London: London. p. 13-39.
22. Lewellen, T.K., *Recent developments in PET detector technology.* Phys Med Biol, 2008. **53**(17): p. R287-317.

23. Cranley, K., R. Millar, and T. Bell, *Correction for deadtime losses in a gamma camera/data analysis system.* European Journal of Nuclear Medicine and Molecular Imaging, 1980. **5**(4): p. 377-382.
24. Bergström, M., et al., *Correction for scattered radiation in a ring detector positron camera by integral transformation of the projections.* Journal of computer assisted tomography, 1983. **7**(1): p. 42-50.
25. Hirano, Y., et al., *Monte Carlo estimation of scatter effects on quantitative myocardial blood flow and perfusable tissue fraction using 3D-PET and (15)O-water.* Phys Med Biol, 2012. **57**(22): p. 7481-92.
26. Guerin, B. and G. El Fakhri, *Novel scatter compensation of list-mode PET data using spatial and energy dependent corrections.* IEEE Trans Med Imaging, 2011. **30**(3): p. 759-73.
27. Saha, G.B., *Data Acquisition and Corrections*, in *Basics of PET Imaging: Physics, Chemistry, and Regulations*. 2010, Springer New York: New York, NY. p. 41-69.
28. Constantinescu, C.C. and J. Mukherjee, *Performance evaluation of an Inveon PET preclinical scanner.* Phys Med Biol, 2009. **54**(9): p. 2885-99.
29. Polycarpou, I., et al., *Comparative evaluation of scatter correction in 3D PET using different scatter-level approximations.* Ann Nucl Med, 2011. **25**(9): p. 643-9.
30. Vandervoort, E. and V. Sossi, *An analytical scatter correction for singles-mode transmission data in PET.* IEEE Trans Med Imaging, 2008. **27**(3): p. 402-12.
31. Larsson, S.A., *Gamma camera emission tomography: development and properties of a multi-sectional emission computed tomography system.* Acta Radiol Suppl, 1980. **363**: p. 1-75.
32. Tanaka, E. and Y. Amo, *A Fourier rebinning algorithm incorporating spectral transfer efficiency for 3D PET.* Physics in medicine and biology, 1998. **43**(4): p. 739.
33. Matej, S., et al., *Performance of the Fourier rebinning algorithm for PET with large acceptance angles.* Physics in medicine and biology, 1998. **43**(4): p. 787.
34. Cline, H.E., et al., *Two algorithms for the three-dimensional reconstruction of tomograms.* Medical physics, 1988. **15**(3): p. 320-327.
35. Ramos, C.D., et al., *FDG-PET standardized uptake values in normal anatomical structures using iterative reconstruction segmented attenuation correction and filtered back-projection.* Eur J Nucl Med, 2001. **28**(2): p. 155-64.
36. Shepp, L.A. and Y. Vardi, *Maximum likelihood reconstruction for emission tomography.* IEEE Trans Med Imaging, 1982. **1**(2): p. 113-22.
37. Yao, R., et al., *Performance characteristics of the 3-D OSEM algorithm in the reconstruction of small animal PET images. Ordered-subsets expectation-maximixation.* IEEE Trans Med Imaging, 2000. **19**(8): p. 798-804.
38. Nakajima, K., et al., *Accuracy of ventricular volume and ejection fraction measured by gated myocardial SPECT: comparison of 4 software programs.* J Nucl Med, 2001. **42**(10): p. 1571-8.
39. Khorsand, A., et al., *Gated cardiac 13N-NH3 PET for assessment of left ventricular volumes, mass, and ejection fraction: comparison with electrocardiography-gated 18F-FDG PET.* J Nucl Med, 2005. **46**(12): p. 2009-13.
40. Hubmayr, R.D., et al., *Regional ventilation during spontaneous breathing and mechanical ventilation in dogs.* J Appl Physiol (1985), 1987. **63**(6): p. 2467-75.
41. Livieratos, L., et al., *Respiratory gating of cardiac PET data in list-mode acquisition.* European journal of nuclear medicine and molecular imaging, 2006. **33**(5): p. 584-588.
42. Büther, F., et al., *List mode–driven cardiac and respiratory gating in pet.* Journal of Nuclear Medicine, 2009. **50**(5): p. 674-681.
43. Kumita, S., et al., *Assessment of left ventricular diastolic function with electrocardiography-gated myocardial perfusion SPECT: comparison with multigated equilibrium radionuclide angiography.* J Nucl Cardiol, 2001. **8**(5): p. 568-74.
44. Husmann, L., et al., *Diagnostic accuracy of computed tomography coronary angiography and evaluation of stress-only single-photon emission computed tomography/computed tomography hybrid imaging: comparison of prospective electrocardiogram-triggering vs. retrospective gating.* European heart journal, 2008. **30**(5): p. 600-607.

45. Klein, G., et al., *Real-time system for respiratory-cardiac gating in positron tomography.* IEEE Transactions on Nuclear Science, 1998. **45**(4): p. 2139-2143.
46. Altehoefer, C., et al., *Significance of defect severity in technetium-99m-MIBI SPECT at rest to assess myocardial viability: comparison with fluorine-18-FDG PET.* Journal of nuclear medicine: official publication, Society of Nuclear Medicine, 1994. **35**(4): p. 569-574.
47. Keller, S.R., et al., *Cloning and characterization of a novel insulin-regulated membrane aminopeptidase from Glut4 vesicles.* J Biol Chem, 1995. **270**(40): p. 23612-8.
48. Bell, G.I., et al., *Molecular biology of mammalian glucose transporters.* Diabetes Care, 1990. **13**(3): p. 198-208.
49. Toyama, H., et al., *Evaluation of anesthesia effects on [18 F] FDG uptake in mouse brain and heart using small animal PET.* Nuclear medicine and biology, 2004. **31**(2): p. 251-256.
50. Nielsen, R., et al., *Heart failure patients with prediabetes and newly diagnosed diabetes display abnormalities in myocardial metabolism.* J Nucl Cardiol, 2016.
51. Vitale, G.D., et al., *Myocardial glucose utilization and optimization of (18)F-FDG PET imaging in patients with non-insulin-dependent diabetes mellitus, coronary artery disease, and left ventricular dysfunction.* J Nucl Med, 2001. **42**(12): p. 1730-6.
52. Kim, J.K., *Hyperinsulinemic-euglycemic clamp to assess insulin sensitivity in vivo.* Methods Mol Biol, 2009. **560**: p. 221-38.
53. Straczkowski, M., et al., *Comparison of simple indices of insulin sensitivity using the euglycemic hyperinsulinemic clamp technique.* Med Sci Monit, 2004. **10**(8): p. CR480-4.
54. Tam, C.S., et al., *Defining insulin resistance from hyperinsulinemic-euglycemic clamps.* Diabetes Care, 2012. **35**(7): p. 1605-10.
55. Knuuti, M.J., et al., *Euglycemic hyperinsulinemic clamp and oral glucose load in stimulating myocardial glucose utilization during positron emission tomography.* J Nucl Med, 1992. **33**(7): p. 1255-62.
56. Werner, R.A., et al., *Sympathetic nerve damage and restoration after ischemia-reperfusion injury as assessed by (11)C-hydroxyephedrine.* Eur J Nucl Med Mol Imaging, 2016. **43**(2): p. 312-8.
57. Wang, Y., et al., *Performance evaluation of the GE healthcare eXplore VISTA dual-ring small-animal PET scanner.* Journal of Nuclear Medicine, 2006. **47**(11): p. 1891-1900.
58. Daut, J., *Herzmechanik*, in *Physiologie des Menschen: mit Pathophysiologie*, R.F. Schmidt, F. Lang, and M. Heckmann, Editors. 2011, Springer Berlin Heidelberg: Berlin, Heidelberg. p. 539-564.
59. Miyoshi, H., et al., *Influence of comorbid cardiovascular risk factors on left atrial-left ventricular interaction in asymptomatic patients: clinical application of two-dimensional speckle-tracking echocardiography.* Int Heart J, 2014. **55**(2): p. 138-45.
60. Ponikowski, P., et al., *2016 ESC Guidelines for the diagnosis and treatment of acute and chronic heart failure: The Task Force for the diagnosis and treatment of acute and chronic heart failure of the European Society of Cardiology (ESC). Developed with the special contribution of the Heart Failure Association (HFA) of the ESC.* Eur J Heart Fail, 2016.
61. He, J., et al., *Risk factors for congestive heart failure in US men and women: NHANES I epidemiologic follow-up study.* Archives of internal medicine, 2001. **161**(7): p. 996-1002.
62. Jessup, M., et al., *2009 focused update: ACCF/AHA Guidelines for the Diagnosis and Management of Heart Failure in Adults: a report of the American College of Cardiology Foundation/American Heart Association Task Force on Practice Guidelines: developed in collaboration with the International Society for Heart and Lung Transplantation.* Circulation, 2009. **119**(14): p. 1977-2016.
63. Kitzman, D.W., et al., *Pathophysiological characterization of isolated diastolic heart failure in comparison to systolic heart failure.* Jama, 2002. **288**(17): p. 2144-2150.
64. Little, B.C., *The Criteria Committee of the New York Heart Association. Nomenclature and Criteria for Diagnosis of Diseases of the Heart and Great Vessels. 9th ed*. 1994, Boston, Mass. 253–256.

65. Zile, M.R. and D.L. Brutsaert, *New concepts in diastolic dysfunction and diastolic heart failure: Part I: diagnosis, prognosis, and measurements of diastolic function.* Circulation, 2002. **105**(11): p. 1387-93.
66. Mitu, F. and M. Mitu, *[Clinical aspects of the left ventricular diastolic dysfunction at patients with coronary heart disease].* Rev Med Chir Soc Med Nat Iasi, 2001. **105**(4): p. 733-9.
67. McCabe, C., et al., *Right ventricular dysfunction in chronic thromboembolic obstruction of the pulmonary artery: a pressure-volume study using the conductance catheter.* J Appl Physiol (1985), 2014. **116**(4): p. 355-63.
68. Senni, M., et al., *Left ventricular systolic and diastolic function after pericardiectomy in patients with constrictive pericarditis: Doppler echocardiographic findings and correlation with clinical status.* J Am Coll Cardiol, 1999. **33**(5): p. 1182-8.
69. Poirier, P., et al., *Diastolic dysfunction in normotensive men with well-controlled type 2 diabetes: importance of maneuvers in echocardiographic screening for preclinical diabetic cardiomyopathy.* Diabetes Care, 2001. **24**(1): p. 5-10.
70. Lim, S., et al., *PLCdelta1 protein rescues ischemia-reperfused heart by the regulation of calcium homeostasis.* Mol Ther, 2014. **22**(6): p. 1110-21.
71. Pandit, A., et al., *Ia diastolic dysfunction: an echocardiographic grade.* Echocardiography, 2015. **32**(1): p. 56-63.
72. Palmiero, P., et al., *Left ventricular diastolic function in hypertension: methodological considerations and clinical implications.* J Clin Med Res, 2015. **7**(3): p. 137-44.
73. Wan, S.H., M.W. Vogel, and H.H. Chen, *Pre-clinical diastolic dysfunction.* J Am Coll Cardiol, 2014. **63**(5): p. 407-16.
74. Paulus, W.J., et al., *How to diagnose diastolic heart failure: a consensus statement on the diagnosis of heart failure with normal left ventricular ejection fraction by the Heart Failure and Echocardiography Associations of the European Society of Cardiology.* Eur Heart J, 2007. **28**(20): p. 2539-50.
75. Douglas, P.S., *The left atrium: a biomarker of chronic diastolic dysfunction and cardiovascular disease risk.* J Am Coll Cardiol, 2003. **42**(7): p. 1206-7.
76. Quiroz, R., et al., *Comparison of characteristics and outcomes of patients with heart failure preserved ejection fraction versus reduced left ventricular ejection fraction in an urban cohort.* Am J Cardiol, 2014. **113**(4): p. 691-6.
77. Hogg, K., K. Swedberg, and J. McMurray, *Heart failure with preserved left ventricular systolic function; epidemiology, clinical characteristics, and prognosis.* J Am Coll Cardiol, 2004. **43**(3): p. 317-27.
78. Kuznetsova, T., et al., *Prevalence of left ventricular diastolic dysfunction in a general population.* Circ Heart Fail, 2009. **2**(2): p. 105-12.
79. Fischer, M., *Prevalence of left ventricular diastolic dysfunction in the community Results from a Doppler echocardiographic-based survey of a population sample.* European Heart Journal, 2003. **24**(4): p. 320-328.
80. Mureddu, G.F., et al., *Prevalence of preclinical and clinical heart failure in the elderly. A population-based study in Central Italy.* Eur J Heart Fail, 2012. **14**(7): p. 718-29.
81. Lam, C.S., et al., *Cardiac dysfunction and noncardiac dysfunction as precursors of heart failure with reduced and preserved ejection fraction in the community.* Circulation, 2011. **124**(1): p. 24-30.
82. Hoit, B.D., *Left atrial size and function: role in prognosis.* J Am Coll Cardiol, 2014. **63**(6): p. 493-505.
83. Bowman, A.W. and S.J. Kovacs, *Left atrial conduit volume is generated by deviation from the constant-volume state of the left heart: a combined MRI-echocardiographic study.* Am J Physiol Heart Circ Physiol, 2004. **286**(6): p. H2416-24.
84. Stork, T., et al., *Age-related hemodynamic changes during diastole: a combined M-mode and Doppler echo study.* Int J Card Imaging, 1990. **6**(1): p. 23-30.
85. Miller, T.R., et al., *Left ventricular diastolic filling and its association with age.* Am J Cardiol, 1986. **58**(6): p. 531-5.

86. Iskandrian, A.S. and A.H. Hakki, *Age-related changes in left ventricular diastolic performance.* Am Heart J, 1986. **112**(1): p. 75-8.
87. Sharir, T., et al., *Incremental prognostic value of post-stress left ventricular ejection fraction and volume by gated myocardial perfusion single photon emission computed tomography.* Circulation, 1999. **100**(10): p. 1035-42.
88. Sharir, T., et al., *Prognostic value of poststress left ventricular volume and ejection fraction by gated myocardial perfusion SPECT in women and men: gender-related differences in normal limits and outcomes.* J Nucl Cardiol, 2006. **13**(4): p. 495-506.
89. Lomsky, M., et al., *Normal limits for left ventricular ejection fraction and volumes determined by gated single photon emission computed tomography--a comparison between two quantification methods.* Clin Physiol Funct Imaging, 2008. **28**(3): p. 169-73.
90. Morikawa, M., et al., *Sustained left ventricular diastolic dysfunction after exercise in patients with dilated cardiomyopathy.* Heart, 1998. **80**(3): p. 263-9.
91. Pitt, B., et al., *Spironolactone for heart failure with preserved ejection fraction.* N Engl J Med, 2014. **370**(15): p. 1383-92.
92. Ahmed, A., et al., *Effects of digoxin on morbidity and mortality in diastolic heart failure: the ancillary digitalis investigation group trial.* Circulation, 2006. **114**(5): p. 397-403.
93. Hernandez, A.F., et al., *Clinical effectiveness of beta-blockers in heart failure: findings from the OPTIMIZE-HF (Organized Program to Initiate Lifesaving Treatment in Hospitalized Patients with Heart Failure) Registry.* J Am Coll Cardiol, 2009. **53**(2): p. 184-92.
94. Massie, B.M., et al., *Irbesartan in patients with heart failure and preserved ejection fraction.* N Engl J Med, 2008. **359**(23): p. 2456-67.
95. Iribarren, C., et al., *Glycemic control and heart failure among adult patients with diabetes.* Circulation, 2001. **103**(22): p. 2668-73.
96. Sharma, S., et al., *Intramyocardial lipid accumulation in the failing human heart resembles the lipotoxic rat heart.* FASEB J, 2004. **18**(14): p. 1692-700.
97. Luptak, I., et al., *Decreased contractile and metabolic reserve in peroxisome proliferator-activated receptor-alpha-null hearts can be rescued by increasing glucose transport and utilization.* Circulation, 2005. **112**(15): p. 2339-46.
98. Phillips, M.S., et al., *Leptin receptor missense mutation in the fatty Zucker rat.* Nat Genet, 1996. **13**(1): p. 18-9.
99. Daniels, A., et al., *Long-term severe diabetes only leads to mild cardiac diastolic dysfunction in Zucker diabetic fatty rats.* Eur J Heart Fail, 2012. **14**(2): p. 193-201.
100. van den Brom, C.E., et al., *Altered myocardial substrate metabolism is associated with myocardial dysfunction in early diabetic cardiomyopathy in rats: studies using positron emission tomography.* Cardiovasc Diabetol, 2009. **8**: p. 39.
101. Leonard, B.L., et al., *Insulin resistance in the Zucker diabetic fatty rat: a metabolic characterisation of obese and lean phenotypes.* Acta Diabetol, 2005. **42**(4): p. 162-70.
102. Corsetti, J.P., et al., *Effect of dietary fat on the development of non-insulin dependent diabetes mellitus in obese Zucker diabetic fatty male and female rats.* Atherosclerosis, 2000. **148**(2): p. 231-41.
103. Schafer, S., et al., *Impaired left ventricular relaxation in type 2 diabetic rats is related to myocardial accumulation of N(epsilon)-(carboxymethyl) lysine.* Eur J Heart Fail, 2006. **8**(1): p. 2-6.
104. van den Brom, C.E., et al., *Diabetic cardiomyopathy in Zucker diabetic fatty rats: the forgotten right ventricle.* Cardiovasc Diabetol, 2010. **9**: p. 25.
105. Lum-Naihe, K., et al., *Cardiovascular disease progression in female Zucker Diabetic Fatty rats occurs via unique mechanisms compared to males.* Scientific Reports, 2017. **7**(1): p. 17823.
106. Nagueh, S.F., et al., *Doppler tissue imaging: a noninvasive technique for evaluation of left ventricular relaxation and estimation of filling pressures.* J Am Coll Cardiol, 1997. **30**(6): p. 1527-33.

107. Sharp, A.S., et al., *Tissue Doppler E/E' ratio is a powerful predictor of primary cardiac events in a hypertensive population: an ASCOT substudy.* European heart journal, 2010. **31**(6): p. 747-752.
108. Szymanski, M.K., et al., *Use of gated 13N-NH3 micro-PET to examine left ventricular function in rats.* Nucl Med Biol, 2012. **39**(5): p. 724-9.
109. Council, N.R., *Guide for the care and use of laboratory animals*. 2010: National Academies Press.
110. Long, J.Z., M.S. Jacobson, and J.C. Hung, *Comparison of FASTlab 18F-FDG production using phosphate and citrate buffer cassettes.* J Nucl Med Technol, 2013. **41**(1): p. 32-4.
111. Li, Y., et al., *Gated F-18 FDG PET for assessment of left ventricular volumes and ejection fraction using QGS and 4D-MSPECT in patients with heart failure: a comparison with cardiac MRI.* PLoS One, 2014. **9**(1): p. e80227.
112. Khorsand, A., et al., *Assessment of left ventricular volumes, ejection fraction and mass. Comparison of model-based analysis of ECG-gated ((9)(9)m)Tc-SPECT and (1)(8)F-FDG-PET.* Nuklearmedizin, 2011. **50**(1): p. 9-14.
113. Croteau, E., et al., *Quantitative gated PET for the assessment of left ventricular function in small animals.* J Nucl Med, 2003. **44**(10): p. 1655-61.
114. Bousquenaud, M., et al., *Acipimox-enhanced (1)(8)F-fluorodeoxyglucose positron emission tomography for characterizing and predicting early remodeling in the rat infarct model.* Int J Cardiovasc Imaging, 2012. **28**(6): p. 1407-15.
115. Higuchi, T., et al., *Characterization of normal and infarcted rat myocardium using a combination of small-animal PET and clinical MRI.* J Nucl Med, 2007. **48**(2): p. 288-94.
116. Garcia, M.J., J.D. Thomas, and A.L. Klein, *New Doppler echocardiographic applications for the study of diastolic function.* J Am Coll Cardiol, 1998. **32**(4): p. 865-75.
117. Thomas, D., et al., *Noninvasive assessment of myocardial viability in a small animal model: comparison of MRI, SPECT, and PET.* Magn Reson Med, 2008. **59**(2): p. 252-9.
118. Kessler, G. and J. Friedman, *Metabolism of fatty acids and glucose.* Circulation, 1998. **98**(13): p. 1351.
119. Belke, D.D., et al., *Altered metabolism causes cardiac dysfunction in perfused hearts from diabetic (db/db) mice.* Am J Physiol Endocrinol Metab, 2000. **279**(5): p. E1104-13.
120. Bing, R.J., et al., *Metabolic studies on the human heart in vivo. I. Studies on carbohydrate metabolism of the human heart.* Am J Med, 1953. **15**(3): p. 284-96.
121. Fredersdorf, S., et al., *Myocardial hypertrophy and enhanced left ventricular contractility in Zucker diabetic fatty rats.* Cardiovasc Pathol, 2004. **13**(1): p. 11-9.
122. Nakae, I., et al., *Clinical usefulness of a novel program "Heart Function View" for evaluating cardiac function from gated myocardial perfusion SPECT.* Ann Nucl Med, 2014. **28**(8): p. 812-23.
123. Akincioglu, C., et al., *Assessment of diastolic function using 16-frame 99mTc-sestamibi gated myocardial perfusion SPECT: normal values.* J Nucl Med, 2005. **46**(7): p. 1102-8.
124. Faber, T.L., et al., *Left ventricular function and perfusion from gated SPECT perfusion images: an integrated method.* J Nucl Med, 1999. **40**(4): p. 650-9.
125. Germano, G., et al., *Automatic quantification of ejection fraction from gated myocardial perfusion SPECT.* J Nucl Med, 1995. **36**(11): p. 2138-47.
126. White, H.D., et al., *Left ventricular end-systolic volume as the major determinant of survival after recovery from myocardial infarction.* Circulation, 1987. **76**(1): p. 44-51.
127. Todica, A., et al., *Positron emission tomography in the assessment of left ventricular function in healthy rats: a comparison of four imaging methods.* J Nucl Cardiol, 2013. **20**(2): p. 262-74.
128. Iltis, I., et al., *Defective myocardial blood flow and altered function of the left ventricle in type 2 diabetic rats: a noninvasive in vivo study using perfusion and cine magnetic resonance imaging.* Invest Radiol, 2005. **40**(1): p. 19-26.
129. Zhou, Y.T., et al., *Lipotoxic heart disease in obese rats: implications for human obesity.* Proc Natl Acad Sci U S A, 2000. **97**(4): p. 1784-9.

130. Radovits, T., et al., *Comparative investigation of the left ventricular pressure-volume relationship in rat models of type 1 and type 2 diabetes mellitus.* Am J Physiol Heart Circ Physiol, 2009. **297**(1): p. H125-33.
131. Alvarez, J.A., et al., *Enhanced left ventricular systolic function early in type 2 diabetic mice: clinical implications.* Diab Vasc Dis Res, 2004. **1**(2): p. 89-94.
132. Porenta, G., et al., *Parameter estimation of cardiac geometry by ECG-gated PET imaging: validation using magnetic resonance imaging and echocardiography.* J Nucl Med, 1995. **36**(6): p. 1123-9.
133. Okazawa, H., et al., *Quantitative evaluation of myocardial blood flow and ejection fraction with a single dose of (13)NH(3) and Gated PET.* J Nucl Med, 2002. **43**(8): p. 999-1005.
134. Choi, Y., et al., *A simplified method for quantification of myocardial blood flow using nitrogen-13-ammonia and dynamic PET.* J Nucl Med, 1993. **34**(3): p. 488-97.
135. Wu, H.M., et al., *Quantification of myocardial blood flow using dynamic nitrogen-13-ammonia PET studies and factor analysis of dynamic structures.* J Nucl Med, 1995. **36**(11): p. 2087-93.
136. DeGrado, T.R., et al., *Estimation of myocardial blood flow for longitudinal studies with 13N-labeled ammonia and positron emission tomography.* J Nucl Cardiol, 1996. **3**(6 Pt 1): p. 494-507.
137. Rajappan, K., et al., *Measurement of ventricular volumes and function: a comparison of gated PET and cardiovascular magnetic resonance.* J Nucl Med, 2002. **43**(6): p. 806-10.
138. Kanayama, S., et al., *Assessment of global and regional left ventricular function by electrocardiographic gated N-13 ammonia positron emission tomography in patients with coronary artery disease.* Circ J, 2005. **69**(2): p. 177-82.
139. Hickey, K.T., et al., *Assessment of cardiac wall motion and ejection fraction with gated PET using N-13 ammonia.* Clin Nucl Med, 2004. **29**(4): p. 243-8.
140. Gerber, B.L., et al., *Myocardial blood flow, glucose uptake, and recruitment of inotropic reserve in chronic left ventricular ischemic dysfunction. Implications for the pathophysiology of chronic myocardial hibernation.* Circulation, 1996. **94**(4): p. 651-9.
141. van der Meer, R.W., et al., *Pioglitazone improves cardiac function and alters myocardial substrate metabolism without affecting cardiac triglyceride accumulation and high-energy phosphate metabolism in patients with well-controlled type 2 diabetes mellitus.* Circulation, 2009. **119**(15): p. 2069-77.
142. Dokainish, H., et al., *Incremental predictive power of B-type natriuretic peptide and tissue Doppler echocardiography in the prognosis of patients with congestive heart failure.* J Am Coll Cardiol, 2005. **45**(8): p. 1223-6.
143. Hess, O.M., et al., *Diastolic function and myocardial structure in patients with myocardial hypertrophy. Special reference to normalized viscoelastic data.* Circulation, 1981. **63**(2): p. 360-71.
144. Inouye, I., et al., *Abnormal left ventricular filling: an early finding in mild to moderate systemic hypertension.* Am J Cardiol, 1984. **53**(1): p. 120-6.
145. Perrone-Filardi, P., et al., *Impaired left ventricular filling and regional diastolic asynchrony at rest in coronary artery disease and relation to exercise-induced myocardial ischemia.* Am J Cardiol, 1991. **67**(5): p. 356-60.
146. Bonow, R.O., et al., *Impaired left ventricular diastolic filling in patients with coronary artery disease: assessment with radionuclide angiography.* Circulation, 1981. **64**(2): p. 315-23.
147. Akula, A., et al., *Biochemical, histological and echocardiographic changes during experimental cardiomyopathy in STZ-induced diabetic rats.* Pharmacol Res, 2003. **48**(5): p. 429-35.
148. Dent, C.L., et al., *Echocardiographic characterization of fundamental mechanisms of abnormal diastolic filling in diabetic rats with a parameterized diastolic filling formalism.* J Am Soc Echocardiogr, 2001. **14**(12): p. 1166-72.
149. Hoit, B.D., et al., *Noninvasive evaluation of cardiac dysfunction by echocardiography in streptozotocin-induced diabetic rats.* J Card Fail, 1999. **5**(4): p. 324-33.

150. Marsh, S.A., et al., *Cardiovascular dysfunction in Zucker obese and Zucker diabetic fatty rats: role of hydronephrosis.* Am J Physiol Heart Circ Physiol, 2007. **293**(1): p. H292-8.
151. Senni, M., et al., *Congestive heart failure in the community: a study of all incident cases in Olmsted County, Minnesota, in 1991.* Circulation, 1998. **98**(21): p. 2282-9.

9 List of Figures

10 List of Tables

11 List of Graphs

12 Abbreviations

1/3 EF	first-third ejection fraction
1/3 ER	first third ejection rate
1/3 FR	first third filling rate
1/3 FF	one third filling fraction
^{13}N-NH_3	^{13}N-Ammonia
^{18}F	fluorine-18
^{18}F-FDG	fluorine-18-2’-Fluoro-2’-deoxy-D-glucose
CAD	coronary artery disease
CO	cardiac output
CT	computed tomography
DD	diastolic dysfunction
DHF	diastolic heart failure
ECG	electrocardiogram
ED	end-diastole
EDtoES	end-diastole to end-systole
EDV	end-diastolic volume
EF	ejection fraction
ES	end-systole
ESC	European Society of Cardiology
ESV	end-systolic volume
FBP	filtered back-projection
FDG	fluoro-2’-deoxy-D-glucose
FOV	field of view
HF	heart failure
HFmrEF	heart failure with mid-range ejection fraction
HFpEF	heart failure with preserved ejection fraction
HFrEF	heart failure with reduced ejection fraction
HFV	heart function view
HLA	heart long axis
HR	heart rate
keV	kiloelectron volts
LA	left atrial
LOR	line of response

LSO	lutetium oxyorthosilicate
LV	left ventricle
LVEF	left ventricular ejection fraction
MRI	magnetic resonance imaging
MRT	Magnetresonanztomographie
NYHA	New York Heart Association
PER	peak ejection rate
PET	positron emission tomography
PFR	peak filling rate
PMT	photomultiplier tube
Rb	rubidium
SD	standard deviation
SHF	systolic heart failure
SPECT	single photon emission tomography
SV	stroke volume
T2DM	type 2 diabetes mellitus
TES	time to end-systole
TPE	time to peak ejection
TPF	time to peak filling rate
TPF cor.	time to peak filling rate corrected
TTE	transthoracic echocardiography
ZDF	Zucker Diabetic Fatty
ZL	Zucker lean

13 List of Publications

Werner RA*, **Eissler C***, Hayakawa N, Arias-Loza P, Wakabayashi H, Javadi MS, Chen X, Shinaji T, Lapa C, Pelzer T, Higuchi T. - **Left Ventricular Diastolic Dysfunction in a Rat Model of Diabetic Cardiomyopathy using ECG-gated ^{18}F-FDG PET**.

* These authors contributed equally to this work.

Werner RA, Chen X, Maya Y, **Eissler C,** Hirano M, Nose N, Wakabayashi H, Lapa C, Javadi MS, Higuchi T. - **The Impact of Ageing on 11C-Hydroxyephedrine Uptake in the Rat Heart.**

14 Acknowledgment

This work emanates from the Department of Nuclear Medicine, faculty of Medicine of the Julius-Maximilians University of Würzburg and the Graduate School of Life Science. This work was founded by a scholarship for the promotion of medical dissertations by the Graduate School of Life Science (GSLS). The head of the department, Prof. Dr. med. A. Buck and the staff and doctors are all acknowledged for providing me the opportunity to train in the field nuclear medicine and carry out this research. At this point I also need to mention Dr. med. R. Werner, who opened the doors for me to the research in nuclear medicine.

I like also to acknowledge that the data presented in this work are coming from experiments, which were conducted in cooperation with the Group of Prof. Dr. Pelzer (Department of Internal Medicine, University Hospital Würzburg).

My sincere gratitude goes to my leading supervisor Prof. Dr. T. Higuchi of the Comprehensive Heart Failure Centre of Würzburg for his patience and support during all the stages of the study. Also, I like to thank him for the introduction to the basic techniques of nuclear cardiology. This theoretical knowledge and the practical expertise have been of great value to me. In addition, I am grateful to him for sharing his scientific knowledge and critical review and gave me a lot of inputs for my thesis work.

Moreover, I am sincerely grateful for the support of Prof. Dr. med. C. Lapa, my co-supervisor at the Department of Nuclear Medicine, University Hospital Würzburg, who introduced me to the clinical field of nuclear medicine, especially the field of new treatment strategies.

It is important to acknowledge that the experiments in this dissertation were conducted in a group of researchers since small animal imaging under this condition is a work which cannot be successfully handled by only one person. In this context, I especially like to thank Paura Arias Lopez (Group of Prof. Pelzer, Department of Internal Medicine, University Hospital of Würzburg), Dr. med. Kobayashi, Dr. med. N. Hayakawa and Dr. med. H. Wakabayashi who guided the experiments with their expertise. Also, I like to thank Lars Mayer, the biotechnical assistant of our group, who supported me anywhere and anytime when I needed him.

Two of the most important people for me during this work were Dr. med. Nobuyuki Hayakawa and Dr. med. Hiroshi Wakabayashi, who have taught me the best methods to handle the animals and the tracers to gain the best results. They supported me all the way through my thesis. Doesn’t matter what I have asked them for (help with the software programs, statistical support or improvements and corrections of my written work), they have found time to show me all this and more. It was a great experience and pleasure to work with you together.

Furthermore, I like to thank T. Shinaji for his support in all question concerning the field of computer technology and reconstruction.

Last but of course not least, I am grateful for the support of my family not only during this work but also during the whole time of medical school. It is important for me to know that you are supporting me all the time.

Finally, I sincerely thank all the people who have supported me during this work and have made it possible in the first place. Thank you all so much!

Danksagung

Diese Arbeit entstammt der Klinik und Poliklinik für Nuklearmedizin des Universitätskrankenhauses der Julius-Maximilians-Universität Würzburg und der Graduierten Schule der Lebenswissenschaften. Die Arbeit wurde durch ein Stipendium zur Förderung der medizinischen Promotion der Graduiertenschule der Lebenswissenschaften (GSLS) gefördert. Dem Leiter der Abteilung Prof. Dr. med. A. Buck und dem ganzen Personal der Abteilung möchte ich danken für die Möglichkeit meine Forschung und Dissertation auf dem Gebiet der Nuklearmedizin durchzuführen zu können. An diesem Punkt ist es besonders wichtig, Dr. med. R. Werner zu erwähnen, der mir die Türen zur Forschung in der Abteilung öffnete und viel organisatorische Arbeit für mich auf sich genommen hat.

Ich möchte hier auch aufzeigen, dass die im Rahmen dieser Arbeit präsentierten Daten aus Experimenten stammen, die in Kooperation mit der Arbeitsgruppe von Prof. Dr. med. Pelzer (Abteilung für Innere Medizin, Universitätsklinik Würzburg) durchgeführt wurden.

Meine besondere Dankbarkeit gilt auch meinem ersten Betreuer Prof. Dr. med. Takahiro Higuchi aus dem Deutschen Zentrum für Herzinsuffizienz in Würzburg für seine Unterstützung und seine Geduld während allen Phasen dieser Arbeit. Besonders wichtig und wertvoll war für mich seine persönlichen Einführungen und Erklärungen über die grundlegenden Techniken der Nuklearkardiologie. Dieses theoretische Wissen und die praktische Erfahrung werden auch in Zukunft noch von großem Wert für mich sein. Zudem danke ich Prof. Higuchi dafür, dass er sein wissenschaftliches Wissen mit mir geteilt hat, meine Arbeit und mich häufig kritisch hinterfragt hat und mir dadurch viele neue Ideen und Blickwinkel für die Arbeit ermöglicht hat.

Außerdem bin ich besonders dankbar für die Unterstützung von Prof. Dr. med. C. Lapa, meinem dritten Betreuer und Leitendem Oberarzt der Nuklearmedizin des Universitätsklinikums Würzburg, da er vor allem mein Wissen und Interesse in dem klinischen Feld der Nuklearmedizin vorangetrieben hat.

Wichtig ist auch aufzuzeigen, dass die Experimente dieser Dissertation in einer Gruppe von Forschern durchgeführt wurden, da die Bildgebung in Kleintieren nicht von einer einzelnen Person erfolgreich durchgeführt werden kann. In diesem

Zusammenhang möchte ich vor allem Paula-Anahi-Arias-Loza (AG Pelzer), Dr. Kobayashi, Dr. med. N. Hayakawa und Dr. med. H. Wakabayashi danken, welche die Experimente mit ihrer Erfahrung geleitet haben. Zudem möchte Ich unserem biotechnischem Assistenten Lars Mayer danken, welcher mich in allen Fragen und Unklarheiten egal wann unterstützt hat.

Zwei der wichtigsten Personen während meiner Forschung waren Dr. med. Nobuyuki Hayakawa und Dr. med. Hiroshi Wakabayashi, welche mir die speziellen Methoden des Umgangs mit Tieren und Tracern beigebracht haben. Sie haben mich auch darüber hinaus über die komplette Dauer meiner Arbeit unterstützt. Ganz egal um was ich sie gebeten habe, ob Hilfe beim Umgang mit Programmen, statistische Probleme oder Verbesserungen meiner schriftlichen Arbeit, sie haben immer Zeit gefunden mir zu helfen. Es war eine großartige Erfahrung mit euch zu arbeiten.

Des Weiteren möchte ich T. Shinaji meinen Dank aussprechen, welcher mir in allen Fragen auf dem Gebiet der Computertechnologie und der Rekonstruktion unter die Arme gegriffen hat.

Zuletzt möchte ich noch sagen, dass ich meiner Familie und vor allem meinen Eltern sehr dankbar bin, nicht nur für die Unterstützung während dieser Arbeit, sondern auch während der gesamten Zeit des Medizinstudiums. Es ist wichtig für mich zu wissen, dass ihr hinter mir steht. Danke.

Zusammenfassend, möchte ich mich noch einmal bei allen Leuten bedanken, auch denen die ich oben nicht persönlich genannt habe, welche mich in irgendeiner Form während dieses Projektes unterstützt haben und es dadurch vermutlich erst möglich gemacht haben. Vielen, vielen Dank!

15 Curriculum Vitae

16 Affidavit

I hereby confirm that my thesis entitled

Assessment of the left ventricular systolic and diastolic function in rats using electrocardiogram-gated cardiac positron emission tomography

is the result of my own work. I did not receive any help or support from commercial consultants. All sources and / or materials applied are listed and specified in the thesis.

Furthermore, I confirm that this thesis has not yet been submitted as part of another examination process neither in identical or similar form.

Place, Date Signature

Eidesstattliche Erklärung

Hiermit erkläre ich an Eides statt, die Dissertation

Bestimmung der linksventrikulären systolischen und diastolischen Funktion in Ratten durch Elektrokardiogramm-getriggerte kardiale Positronen-Emissions-Tomographie

eigenständig, d.h. insbesondere selbstständig und ohne Hilfe eines kommerziellen Promotionsberaters angefertigt und keine anderen als die mir angegebenen Quellen und Hilfsmittel verwendet zu haben.

Ich erkläre außerdem, dass die Dissertation weder in gleicher noch in ähnlicher Form bereits in einem anderen Prüfungsverfahren vorgelegen hat.

Ort, Datum Unterschrift